ON THE FUNCTION OF CALCIUM-REGULATED ALLOSTERIC DEVICES IN SYNAPTIC PLASTICITY

Melanie Isabelle Stefan
Clare College

A Dissertation submitted to the University of Cambridge for the degree of Doctor of Philosophy

European Molecular Biology Laboratory
European Bioinformatics Institute
Wellcome Trust Genome Campus
Hinxton, Cambridge, CB10 1SD
United Kingdom

mstefan@ebi.ac.uk

17.07.2009

Melanie Isabelle Stefan: *On the Function of Calcium-Regulated Allosteric Devices in Synaptic Plasticity,* A Dissertation submitted to the University of Cambridge for the degree of Doctor of Philosophy, © 17.07.2009

Supervisor:
Nicolas Le Novère

Thesis Advisory Committee:
Janet Thornton, EMBL-EBI
Rob Russell, EMBL Heidelberg
Susan Jones, Cambridge University
Stuart Edelstein, University of Geneva

Cambridge, 17.07.2009

To my parents

DECLARATION

This dissertation is my own work and includes nothing which is the outcome of work done in collaboration except as specified in the text. It is not substantially the same as any I have submitted for a degree, diploma or other qualification at any other university; and no part has already been, or is currently being submitted for any degree, diploma or other qualification.

This dissertation does not exceed the specified length limit of 300 single-sided pages of double-spaced text as defined by The Biology Degree Committee.

Cambridge, 17.07.2009

Melanie Isabelle Stefan

SUMMARY: ON THE FUNCTION OF CALCIUM-REGULATED ALLOSTERIC DEVICES IN SYNAPTIC PLASTICITY

Melanie Isabelle Stefan

Some forms of learning and memory are thought to be encoded in activity-dependent changes of synaptic strength, which involve postsynaptic calcium signalling. I study two allosterically regulated proteins involved in this process: calmodulin and calcium/calmodulin-dependent protein kinase II (CaMKII). At high calcium frequencies, the activation of CaMKII via calmodulin results in a long-lasting increase of synaptic activity. At lower calcium frequencies, calmodulin preferentially activates an alternative pathway, leading to a long-lasting decrease of synaptic activity.

I present an allosteric model of calmodulin, based on a biophysical description of the conformational transitions, which explains the function of calmodulin as a calcium-dependent switch in bidirectional synaptic plasticity. It relies on a generalised formulation of the Monod-Wyman-Changeux (MWC) framework and uses conversion equations which relate allosteric models to experimental results on ligand binding. I also define a novel measure for the cooperativity of conformational change and use it to show that ligand depletion, a common phenomenon in biological systems, reduces cooperativity but increases the dynamic range of signal response.

I investigate various aspects of CaMKII function using two stochastic models. The first model combines stochastic modelling and structural information to provide a mechanistic explanation of "calmodulin trapping", the increase in calmodulin affinity upon CaMKII autophosphorylation. I also show that calmodulin binding is not sufficient for CaMKII activation. The second model addresses interactions within the CaMKII dodecamer. I show that a coiled-coil interaction between subunits on adjacent hexameric rings plays a key role in spreading autonomous activity throughout the holoenzyme.

"So long, and thanks for all the fish."
(Douglas Adams)

ACKNOWLEDGEMENTS

First of all, I would like to thank my supervisor, Nicolas Le Novère for his ongoing support and supervision, deep insight into both biology and computation, enthusiasm and willingness to argue. I have been very lucky to have the opportunity to not only do exciting and inspiring research, but also to widen my horizons at courses and conferences.

I am very grateful to Stuart Edelstein for the very productive collaboration on calmodulin and allostery, and to David Marshall for his excellent work in the calmodulin trapping project.

Susan Jones and Janet Thornton have been very helpful as members of my thesis advisory committee and have offered invaluable comments and suggestions on biological aspects of the thesis.

I am especially grateful to everybody who agreed to proof-read parts of this dissertation, there will be chocolate (or equivalent)!

I would also like to thank all members of CompNeur past and present with whom I have had the pleasure to work (and to play table football): Aniiika, Antonia, Arnaud, Camille, Chen, Кристиан, Dagmar, DJ MC Greal, Duncan, Enuo, Lukas, Kathryn, Kedar, Koray, Marine, Mélanie, Michele, Most Handsome, Most Delightful, Nick, Nico, Noriko-san, Ranjita, Renaud and Viji.

The vibrant predocs (and friends) community on campus have kept me company during countless decadent coffee breaks and done a great job at "implementing happiness". Special thanks go to Elin, Dace, Daniel, Daniela & Michael, Heidi, Jörn, Kristen and Simon. I am also grateful for the friendship and support from staff and students at EMBL Heidelberg and at Clare College, Cambridge.

Finally, I would like to thank my friends family for their kindness, encouragement and support over the years: Mauricette and Raimund, my parents, Barbara, my sister, Stephan, my brother, Lisa and Elias, my niece and nephew, and of course Fabian, my Fabian.

CONTENTS

1

INTRODUCTION

1.1 Synaptic plasticity as a paradigm for learning and memory

Scientists have long tried to elucidate the physiological mechanisms underlying learning and memory, but only in the 20^{th} century were researchers able to combine electrophysiology, cell biology, and behavioural studies in order to address this issue (reviewed in Cooper, 2005). A conceptual breakthrough came in the late 1940s when Hebb formulated his neurophysiological postulate:

> When an axon of cell A is near enough to excite a cell B and repeatedly or persistently takes part in firing it, some growth process or metabolic change takes place in one or both cells such that A's efficiency, as one of the cells firing B, is increased (Hebb, 1949) (reviewed in Cooper, 2005).

This postulate was later complemented by Stent, who stated:

> When the presynaptic axon of cell A repeatedly and persistently fails to excite the postsynaptic cell B while cell B is firing under the influence of other presynaptic axons, metabolic change takes place in one or both cells such that A's efficiency, as one of the cells firing B, is decreased (Stent, 1973).

These postulates provide a powerful conceptual model for the processes underlying memory formation, and even if they were formulated in very general terms, they contain assumptions about the conditions that would need to be fulfilled for activity-dependent strengthening of a neural connection (also called a "Hebb process" (Lisman, 1989)) to take place. Cell A needs to *repeatedly or persistently* take part in firing cell B, which amounts to stating that there is an activation threshold of some kind. Stent's postulate implies input-specificity for

activation, since activity of cell A is necessary for the connection to be strengthened. There might be other inputs involved, however, since the postulate only requires that cell A *takes part in firing* cell B. In analogy, there are conditions that need to be fulfilled for the opposite process, a weakening of the synaptic connection (or "Anti-Hebb process" (Lisman, 1989)) to take place, including the activity of cell B without concurrent activity of cell A.

Ever since the formulation of Hebb's postulate, scientists have been looking for neuronal mechanisms that fulfil the properties of a Hebb process (or indeed, of an Anti-Hebb process) (Cooper, 2005).

Bliss and Lømo (1973) found that in hippocampal excitatory pathways, brief trains of high frequency stimulation (HFS) cause an abrupt and sustained increase in the efficiency of synaptic transmission. This mechanism became known as long-term potentiation (LTP) (reviewed in Bliss and Collingridge, 1993). LTP has been characterised as being cooperative, associative, and input-specific (reviewed in Bliss and Collingridge, 1993): It is cooperative in the sense that there is an intensity threshold for induction (reviewed in Bliss and Collingridge, 1993). Associativity means that a "weak" (sub-threshold) input can still be potentiated if it coincides with a strong input to the same region (reviewed in Bliss and Collingridge, 1993; Cooper, 2005; Malenka and Nicoll, 1999). Input-specificity means that inputs which are not active at the time of the tetanus do not contribute to LTP (reviewed in Bliss and Collingridge, 1993). As discussed above, these characteristics are features that a Hebbian learning device would need to display. For this reason, LTP has been regarded as a potential candidate for a Hebb-process (reviewed in Cooper, 2005; Lisman, 1989). Likewise, the decrease in synaptic strength observed if the postsynaptic neuron is active without concurrent activity of the presynaptic neuron (long-term depression (LTD) (Lynch *et al.*, 1977)) has been seen as a model of an Anti-Hebb process (reviewed in Cooper, 2005; Lisman, 1989). As a consequence, bidirectional synaptic plasticity (i. e. the combined phenomena of LTP and LTD) has long been used as a paradigm to study learning and memory (reviewed in Martin *et al.*, 2000).

Although there have been doubts (Shors and Matzel, 1997), a number of studies have indicated a possible link between synaptic plasticity and memory. Knockout mice that cannot express the α iso-

form of CaMKII show deficiencies in both hippocampal LTP (Silva *et al.*, 1992b) and spatial learning (Silva *et al.*, 1992a), showing that CaMKII is involved in both processes. Another protein that has been implicated in both synaptic plasticity and memory is the *N*-methyl-D-aspartate (NMDA) receptor: While NMDA triggers LTP, NMDA receptor antagonists have been shown to inhibit LTP induction (reviewed in Cooper, 2005). Conditional knockout mice lacking subunit 1 of the NMDA receptor (NR1) in CA1 pyramidal cells of the hippocampus show impaired spatial learning (Tsien *et al.*, 1996) and a loss of both LTP and LTD (Tsien *et al.*, 1996). The latter result suggests that NMDA receptors are necessary for bidirectional plasticity, making them a strong candidate for involvement in Hebbian learning (reviewed in Cooper, 2005; Tsien, 2000). Studying learning in rats, Whitlock *et al.* (2006) found that the effects of learning on glutamate receptors mimic those of LTP and that learning partially occludes subsequent LTP induction, concluding that learning induces LTP. These results tie in with the conclusions of a careful review conducted by Martin *et al.* (2000) who suggest that synaptic plasticity is necessary, but not sufficient, for memory formation.

1.2 Calcium regulation of synaptic plasticity

Both LTP and LTD involve calcium signalling. According to a model first proposed by Lisman (1989), the coordinated activity of a pair of neurons leads to a large increase in calcium levels in the postsynaptic neuron and to an increase in synaptic strength, whereas activity of only one of the two neurons results in more moderate postsynaptic calcium levels and, consequently, a reduction in synaptic strength.

The postsynaptic NMDA receptor-dependent signalling pathway provides a molecular basis for such a mechanism (reviewed in Bear and Malenka, 1994): Upon activation of α-amino-3-hydroxy-5-methyl-4-isoxazolepropionic acid (AMPA) receptors by glutamate, the postsynaptic neuron is depolarised, relieving the Mg^{2+} block that inhibits NMDA receptor function under basal conditions (Mayer and Westbrook, 1985, 1987). The resulting calcium influx through the NMDA receptor leads to the activation of CaMKII via calmodulin (Lisman *et al.*, 2002; Schulman and Greengard, 1978a,b). Active CaMKII en-

hances the function of AMPA receptor channels by phosphorylating their GluR1 subunit (Lee *et al.*, 2000). It also mediates an increase of AMPA receptor delivery to the postsynaptic membrane (Hayashi *et al.*, 2000). In contrast, if there is no co-occurrence of AMPA receptor activation and postsynaptic depolarisation, the Mg^{2+} block remains in place and the calcium concentration in the postsynaptic neuron is lower. In this case, calmodulin preferentially activates protein phosphatase 2B, also called calcineurin (PP2B), leading to activation of protein phosphatase 1 (PP1) and a subsequent reduction of CaMKII activity (reviewed in Groth *et al.*, 2003), possibly resulting in LTD.

While many more proteins have been implicated in synaptic plasticity (reviewed in Sanes and Lichtman, 1999), it seems especially promising to study those involved in NMDA receptor-dependent signalling. This thesis therefore focuses on two key members of this signalling pathway: calmodulin and CaMKII.

1.3 The dual role of calmodulin

By preferentially activating CaMKII or PP2B dependent on the amount of calcium present in the postsynaptic neuron, calmodulin acts as an important switch in the induction of postsynaptic plasticity, mediating either LTP or LTD. The ability of calmodulin to act as a calcium sensor relies on the presence of four calcium binding EF-hands (Babu *et al.*, 1988; Chattopadhyaya *et al.*, 1992). However, the ability of calmodulin to differentiate between high and low calcium concentration seems intriguing, given that the efficacy of calmodulin as an activator of both CaMKII and PP2B increases with increasing calcium concentration. In structural terms this corresponds to the existence of two distinct conformations of calmodulin: an inactive, closed form which is predominant in the absence of calcium (Kuboniwa *et al.*, 1995), and an active, open form which is found in the presence of excess calcium (Babu *et al.*, 1985), and which activates both CaMKII and PP2B.

To further complicate the picture, sub-saturated forms of calmodulin have been shown to activate various targets, including CaMKII (Huang *et al.*, 1981; Kincaid and Vaughan, 1986; Shifman *et al.*, 2006). In addition, the affinity of calmodulin for calcium increases upon target binding, providing further evidence for target binding by sub-

saturated forms of calmodulin (Burger *et al.*, 1983; Olwin *et al.*, 1984; Shifman *et al.*, 2006).

These aspects have been neglected by previous models of calmodulin function (Bhalla and Iyengar, 1999; Burger *et al.*, 1984; Crouch and Klee, 1980; Czerlinski, 1984; d'Alcantara *et al.*, 2003; Franks *et al.*, 2001; Huang *et al.*, 1981; Mirzoeva *et al.*, 1999; Naoki *et al.*, 2005; Pifl *et al.*, 1984; Shifman *et al.*, 2006). However, elucidating these properties of calmodulin might be key to understanding its function as a calcium-dependent bidirectional switch in synaptic plasticity.

1.4 CaMKII as a memory device: functional aspects

CaMKII is another important protein involved in NMDA receptor-dependent synaptic plasticity (Silva *et al.*, 1992a,b), and has been shown to act as a detector of calcium frequency (De Koninck and Schulman, 1998).

The CaMKII holoenzyme is dodecameric, organised as a hexamer of dimers (Rosenberg *et al.*, 2005) with the appearance of two stacked rings (Kolodziej *et al.*, 2000). Each subunit can adopt two distinct conformations: An autoinhibited "closed" conformation, in which the active site is bound to the inhibitory helix (Rosenberg *et al.*, 2005), and an active "open" conformation, in which this interaction is disrupted.

Calmodulin stabilises CaMKII activity by binding to the inhibitory helix (Hanley *et al.*, 1988). The open state is further stabilised by autophosphorylation at threonine residue 286 (Thr^{286}) (Payne *et al.*, 1988), which confers calmodulin-independent activity (Hanson *et al.*, 1994). Furthermore, phosphorylation at Thr^{286} increases the apparent affinity of CaMKII for calmodulin. A mechanistic explanation for this phenomenon, called "calmodulin trapping" (Meyer *et al.*, 1992), is yet to be found. In contrast, autophosphorylation at threonine residue 306 (Thr^{306}) decreases calmodulin sensitivity and CaMKII activity (Patton *et al.*, 1990; Colbran, 1993), thus acting as a desensitisation mechanism.

Phosphorylation at Thr^{286} occurs within the holoenzyme (reviewed in Mukherji and Soderling, 1994), but not within one subunit. Instead, one subunit phosphorylates its neighbouring subunit within the same ring (Hanson *et al.*, 1994; Mukherji and Soderling, 1994). Thus, for

phosphorylation at Thr^{286} to happen, two adjacent subunits both have to be open: The "kinase" subunit because it needs to be active, and the "substrate" subunit because the phosphorylation site at Thr^{286}, which is situated at the "hinge" between inhibitory helix and active domain (Rosenberg *et al.*, 2005) needs to be accessible. This requirement is thought to underlie the ability of CaMKII to detect calcium frequency (De Koninck and Schulman, 1998): Imagine a given subunit is phosphorylated at Thr^{286} and hence active. If the interval between subsequent calcium spikes is very long, this subunit will likely be dephosphorylated and close before one of its neighbouring subunit opens. With increasing calcium frequency, however, it becomes more likely that calmodulin facilitates opening of a neighbouring subunit while the subunit in question is still phosphorylated. In this case, the neighbouring subunit can also be phosphorylated, and its activity thus stabilised. Thus, the spread of autophosphorylation and hence, activity across the holoenzyme is more likely if the calcium frequency is high (reviewed in Braun and Schulman, 1995; Hudmon and Schulman, 2002). According to one model (Lisman and Zhabotinsky, 2001; Zhabotinsky, 2000), not only does a ring of CaMKII subunits act as a bistable switch, the state of which depends on both calcium frequency and phosphatase concentration, but so do whole populations of CaMKII. At low calcium frequencies and high phosphatase concentrations, all subunits within one ring are typically closed, because trans-autophosphorylation events are rare in the first place, and if they happen, they can easily be reversed by phosphatase action. At high calcium frequencies and low phosphatase concentrations, all subunits are typically in the open state, because autophosphorylation becomes far more likely, and phosphatase activity saturates. Importantly, the model also predicts that a newly inserted CaMKII ring would adopt the phosphorylation state of the surrounding population, hence providing a mechanism for maintaining CaMKII activity for longer than the time scale of protein turnover (Lisman and Zhabotinsky, 2001).

These models have focused on explaining the spread of activity between adjacent subunits on the same ring. It is, however, not clear, how – or indeed, whether – the activation status can be communicated between the two rings constituting a dodecamer. According to

the structural model of CaMKII proposed by Rosenberg *et al.* (2005), the inhibitory helices of two adjacent subunits on different rings interact through the formation of a coiled-coil. The model suggests that the disruption of the coiled-coil might be necessary for Thr^{286} autophosphorylation to occur, thus providing a possible mechanism of cooperativity between the two rings (Rosenberg *et al.*, 2005).

1.5 Outline of the thesis

This thesis is structured into two parts, focusing on calmodulin and CaMKII, respectively. Each of the part uses a different methodological framework and therefore features its own separate technical introduction and its own conclusion and discussion section.

In the first part, I begin by developing the theoretical framework required for modelling calmodulin, a generalisation of the classical allosteric MWC model (Monod *et al.*, 1965). I then proceed to present a novel model for calmodulin function, which reconciles experimental evidence gathered so far and offers a molecular explanation for the function of calmodulin as a calcium-dependent switch. Finally, I use the generalised MWC framework to investigate the phenomena of cooperativity and ligand depletion.

The second part turns to modelling CaMKII. Combining structural considerations and stochastic modelling, I present two models that investigate different aspects of CaMKII function: The first model studies trapping of calmodulin by CaMKII, the second investigates the nature of interactions and cooperativity within the CaMKII dodecamer.

Part I

ALLOSTERIC MODELLING OF CALMODULIN

2

MODELS OF COOPERATIVITY AND APPLICATIONS TO POSTSYNAPTIC SIGNALLING

2.1 Quantitative descriptions in systems biology

A major pursuit of life sciences research, whether it be physiology, biochemistry or molecular and cellular biology, is the quantitative description of biological processes. It is performed with the following aims in mind: characterising biological systems, measuring (sometimes subtle) effects of perturbations, discriminating between alternative hypotheses, making and testing predictions, and following changes over time.

A biological process can be described in multiple ways, some of which are purely phenomenological, while others are based on a Systems Biology approach. Phenomenological descriptions provide a way of relating input and outcome of a given process, without requiring a detailed knowledge about the nature of the process or possible intermediate steps. Since they provide a direct link between input and output, they can be easily compared to experimental results. On the other hand, Systems Biology favours more mechanistic representations, that aim at exploring how exactly behaviours of systems emerge from intrinsic properties and interactions of elements at a lower level. Using a phenomenological description to build and validate a Systems Biology representation may present challenges: There is often no one-to-one correspondence between parameters pertaining to both descriptions, and while it might be possible to compute phenomenological parameters from a Systems Biology model, the problem is likely to be under-determined in the other direction.

An example of a biological problem for which several types of descriptions co-exist is the binding of ligand to a protein with several binding sites, and the apparent cooperativity often observed in these cases. Calmodulin, with its for binding sites for calcium (Babu *et al.*, 1988; Chattopadhyaya *et al.*, 1992) constitutes an example of such a

protein. Understanding exactly how calmodulin binds to, and is activated by its ligand calcium is key to elucidating the dual role of calmodulin in mediating bi-directional synaptic plasticity. In order to select a suitable framework within which to study calmodulin, it is therefore useful to review existing frameworks that have been developed to describe cooperativity within multi-site proteins.

2.2 A short history of cooperativity

Throughout the 20^{th} century, various frameworks have been developed to describe binding of ligand to a protein with more than one binding site and cooperative effects observed in this context (Wyman and Gill, 1990).

2.2.1 *The Hill framework*

The first description of cooperative binding to a multi-site protein was developed by Hill (1910). Drawing on observations of oxygen binding to hæmoglobin, Hill suggested the following formula for the fractional occupancy $\bar{Y}$ of a protein with several ligand binding sites:

$$\bar{Y} = \frac{K[X]^{n_H}}{1 + K[X]^{n_H}} \tag{2.1}$$

where K denotes an apparent association constant, $[X]$ denotes ligand concentration and n_H is the "Hill coefficient". The Hill plot, obtained by plotting $\log \frac{\bar{Y}}{1-\bar{Y}}$ versus $\log[X]$ is linear, with slope n_H and intercept $\log K$. This means that cooperativity is assumed to be fixed, i. e. it does not change with saturation. It also means that cooperativity is solely a property of ligand molecules, rather than a property of binding sites, which always exhibit the same affinity.

2.2.2 *The Adair-Klotz framework*

Adair (1925) and Klotz (1946) (reviewed in Klotz, 2004) further explored the notion of cooperative binding. According to their framework, cooperativity was no longer fixed, but dependent on saturation:

There were different binding constants describing binding of the first ligand, the second, the third, etc. It is worth noting that these constants do not relate to individual binding sites. They describe *how many* binding sites are occupied, rather than *which ones*. In the earlier formulation by Adair (1925), the fractional occupancy of a protein is given by the following equation:

$$\bar{Y} = \frac{1}{n} \frac{K_I[X] + 2K_{II}[X]^2 + \ldots + nK_n[X]^n}{1 + K_I[X] + K_{II}[X]^2 + \ldots + K_n[X]^n} \tag{2.2}$$

where n denotes the number of binding sites and each K_i is a combined association constant, describing the binding of i ligand molecules. In its later version, by Klotz (1946), these combined association constants are deconvoluted into the products of association constants K_i, each of which describes binding of the i^{th} ligand molecule.

$$\bar{Y} = \frac{1}{n} \frac{K_1[X] + 2K_1K_2[X]^2 + \ldots + n\left(K_1K_2 \ldots K_n\right)[X]^n}{1 + K_1[X] + K_1K_2[X]^2 + \ldots + \left(K_1K_2 \ldots K_n\right)[X]^n} \tag{2.3}$$

This framework – especially in the Klotz formulation – is often used by experimentalists to describe measurements of ligand binding in terms of sequential apparent binding constants.

2.2.3 *The KNF framework*

By the middle of the 20^{th} century, there was an increased interest in models that would not only describe binding curves phenomenologically, but offer an underlying biochemical mechanism. Koshland (1958) and Koshland, Némethy, and Filmer (1966) offered a tentative biochemical explanation of the mechanism described by Adair (1925) and Klotz (1946). The Koshland-Némethy-Filmer (KNF) model assumes that each subunit can exist in one of two conformations: active or inactive. Ligand binding to one subunit would induce an immediate conformational change of that subunit from the inactive to the active conformation, a mechanism described as "induced fit". Cooperativity, according to the KNF model, would arise from interactions between the subunits, the strength of which varies depending on the relative conformations of the subunits involved.

2.2.4 *The MWC framework*

The MWC model for concerted allosteric transitions (Monod *et al.*, 1965) went a step further by exploring cooperativity based on thermodynamics and three-dimensional conformations. It was originally formulated for oligomeric proteins with symmetrically arranged, identical subunits, each of which has one ligand binding site. According to this framework, two (or more) interconvertible conformational states of an allosteric protein coexist in a thermal equilibrium. The ratio between the two states (often termed tense (T) and relaxed (R)) is regulated by the binding of ligands that have different affinities for each of the states. A schema of an MWC-type protein is shown in figure 1 on the facing page.

For instance, in the absence of a ligand, the T state prevails, but as more ligand molecules bind, the R state (which has higher affinity for the ligand) becomes the energetically favoured conformation (see figure 2 on page 16).

The allosteric isomerisation constant L describes the equilibrium between both states when no ligand molecule is bound: $L = \frac{[T_0]}{[R_0]}$. If L is very large, most of the protein exists in the tense state in the absence of ligand. If L is small (close to one), the R state is nearly as populated as the T state. While the Adair-Klotz framework traditionally operates with association constants, the MWC framework has traditionally been described using dissociation constants. The ratio of dissociation constants for the T and R states is described by the constant c: $c = \frac{K_d^R}{K_d^T}$. If $c = 1$, both R and T states have the same ligand affinity and the ligand does not affect isomerisation. The value of c also indicates how much the equilibrium between T and R states changes upon ligand binding: the smaller c, the more the equilibrium shifts towards the R state. According to the MWC model (Monod *et al.*, 1965), fractional occupancy is described as follows:

$$\bar{Y} = \frac{\frac{[X]}{K_d^R}\left(1+\frac{[X]}{K_d^R}\right)^{n-1} + Lc\frac{[X]}{K_d^R}\left(1+c\frac{[X]}{K_d^R}\right)^{n-1}}{\left(1+\frac{[X]}{K_d^R}\right)^{n} + L\left(1+c\frac{[X]}{K_d^R}\right)^{n}} \tag{2.4}$$

with K_d^R, L and c as described in the paragraph above.

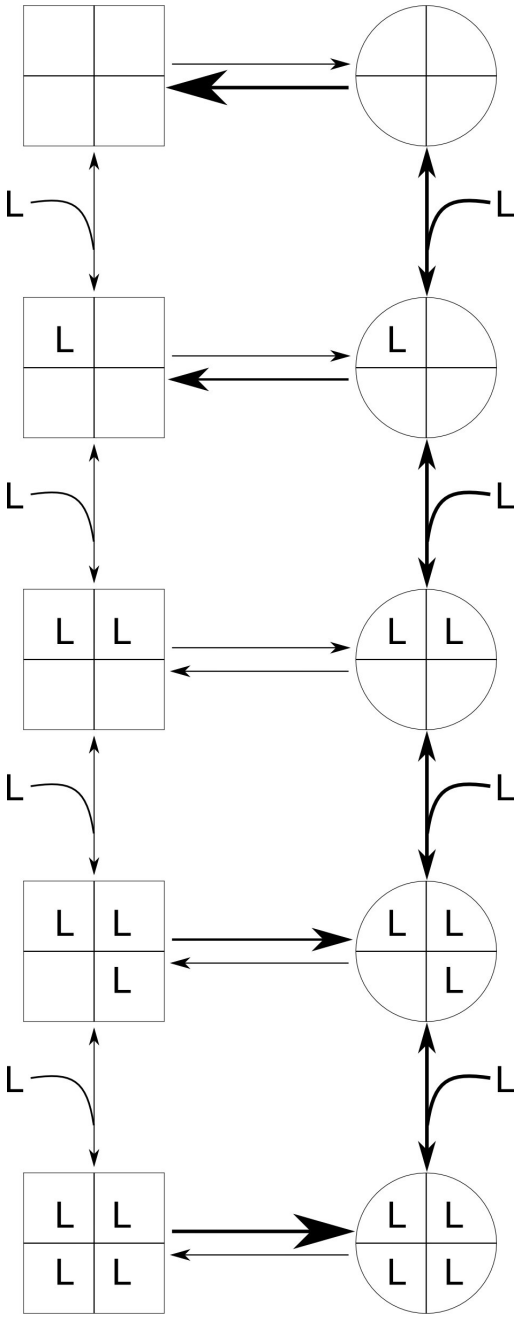

Figure 1: Schematic view of an MWC protein with four subunits. The T state is shown as a square, the *R* state as a circle. In this case, the *R* state has a higher affinity for the ligand *L*; ligand binding thus stabilises the *R* state over the *T* state.

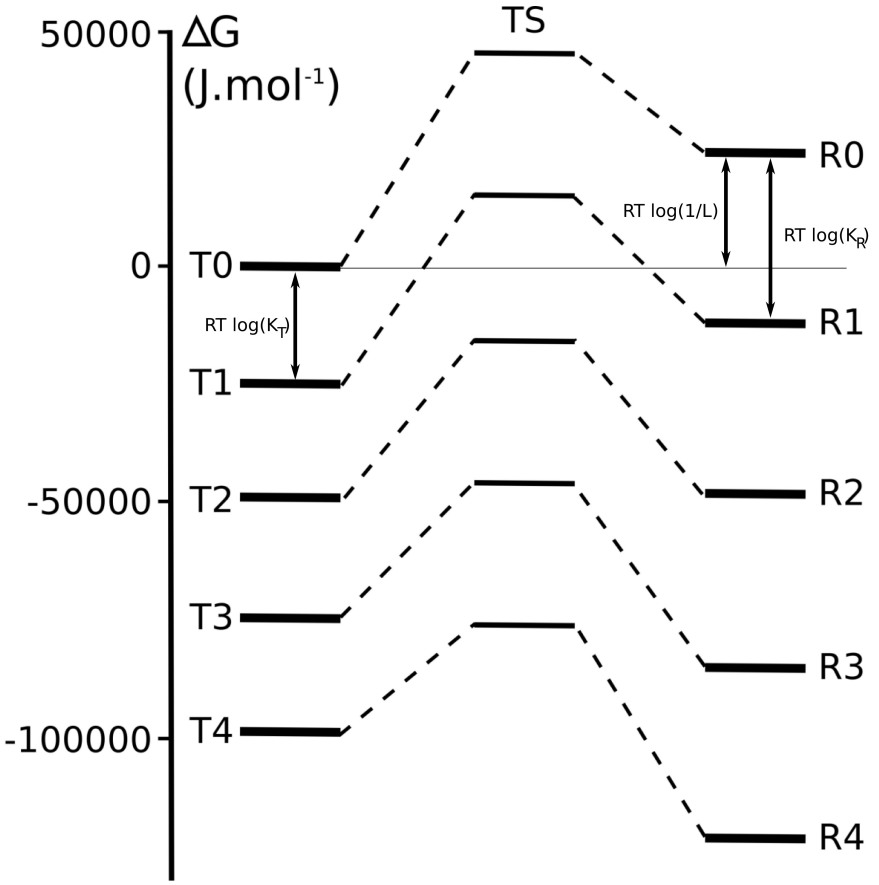

Figure 2: Free energy diagram for an allosteric protein with four binding sites. Energy levels (in J/mol) were computed as in (Edelstein *et al.*, 1996) using the model of calmodulin described later (see Chapter 4 on page 31). Each level of energy represents all the forms carrying the same number of ligand ions. Free energy differences between T state and corresponding R state relate to the allosteric isomerisation constant. Between corresponding T and R states, a hypothetical transition state is depicted based on estimates of rate constants. T state is shown on the left, R state on the right and the transition state in the middle.

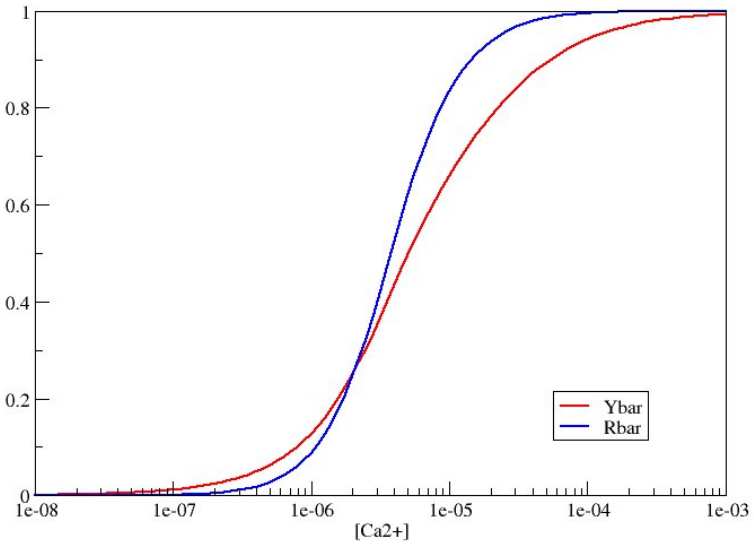

Figure 3: $\bar{Y}$ and $\bar{R}$ for an allosteric protein. Fractional occupancy ($\bar{Y}$) is shown in red; fractional conformational change ($\bar{R}$) in blue. Curves were obtained using the model of calmodulin described later (see Chapter 4 on page 31) with a calmodulin concentration of $2 \times 10^{-7}\, M$.

The degree of conformational change is described by the state function $\bar{R}$, which denotes the fraction of protein present in the R state. As the energy diagram illustrates, $\bar{R}$ increases as more ligand molecules bind. The expression for $\bar{R}$ according to the MWC model (Monod *et al.*, 1965) is:

$$\bar{R} = \frac{\left(1 + \frac{[X]}{K_d^R}\right)^n}{\left(1 + \frac{[X]}{K_d^R}\right)^n + L\left(1 + c\frac{[X]}{K_d^R}\right)^n} \tag{2.5}$$

It is important to note that the curves for $\bar{Y}$ and $\bar{R}$ do not overlap (Rubin and Changeux, 1966), i. e. fractional saturation is not a direct indicator of conformational state (and hence, of activity). This is illustrated in figure 3.

2.3 Contents of the following chapters

In chapter 3 on the next page, I introduce a generalised formulation of the MWC framework for proteins with different groups of binding sites of identical affinity and for proteins with several non-equivalent binding sites. I also present a way of relating the parameters of such a generalised MWC model to the apparent dissociation constants of a corresponding Adair-Klotz model in order to allow for cross-validation of results gained with different methodologies.

This generalised MWC framework is used in chapter 4 on page 31 to develop an allosteric model of calmodulin. The equations for relating MWC models to Adair-Klotz models presented in chapter 3 on the next page are used to validate the model using experimental results that have not been used for parameter determination. The model of calmodulin is compatible with observed properties of calmodulin, including the differential activation of CaMKII and PP2B at different calcium concentrations. It also makes the experimentally testable prediction that open states of calmodulin can exist in the total absence of calcium.

Chapter 5 on page 55 discusses the fact that, while the Hill coefficient is a useful measure for the cooperativity of ligand binding, it cannot be used to describe the cooperativity of conformational change. The chapter therefore introduces an alternative measure for cooperativity, based on the notion of an "equivalent monomer". Using this alternative measure, it is then shown that ligand depletion – a common phenomenon in neuronal signalling – reduces cooperativity *in vivo*, but increases the dynamic range of signal response.

3

EXTENSIONS TO THE MWC FRAMEWORK

3.1 Introduction

The MWC allosteric framework (Monod *et al.*, 1965) was originally developed to describe oligomeric proteins with symmetrically arranged, identical subunits with one binding site each for a given ligand. We introduce a more generalised formulation of the MWC framework for proteins with several groups of ligand binding sites of identical affinities, and for proteins with an arbitrary number of non-equivalent ligand binding sites.

Modellers using either the original or the generalised MWC allosteric framework need ways of comparing the numerical outcomes of their models with experimental results. Indeed, many experiments are not conducted with the notion of alternative conformations in mind, and therefore do not (or cannot) measure relevant microscopic constants and parameters. Instead, experimentalists commonly use the Adair-Klotz approach (Adair, 1925; Klotz, 1946) to describe their experimental data (see chapter 2 on page 11). We propose a way of computing apparent Adair-Klotz constants from microscopic association constants and allosteric parameters of a generalised concerted model with an arbitrary number of non-equivalent ligand binding sites. We apply this framework to compute Adair-Klotz constants for an existing model of hæmoglobin.

3.2 Generalisation of the MWC model

3.2.1 *Fractional occupancy*

As described in chapter 2 on page 11, the fractional occupancy of a protein with ligand according to the classical MWC model (Monod *et al.*, 1965) is:

$$\bar{Y} = \frac{[X]K^R(1+[X]K^R)^{n-1} + Lc[X]K^R(1+c[X]K^R)^{n-1}}{(1+[X]K^R)^n + L(1+c[X]K^R)^n} \tag{3.1}$$

where $[X]$ is the concentration of ligand, K^R (K^T) the association constant for the R (T) state, $c = \frac{K^T}{K^R}$ and L the allosteric isomerisation constant.

The MWC model can be adapted to describe a protein (whether oligomeric or monomeric) with several ligand binding sites possessing different affinities. In this case, microscopic association constants are termed K_i^T and K_i^R, and their ratio is denoted by c_i for the i^{th} binding site. The fractional occupancy is then described as follows:

$$\bar{Y} = \frac{1}{n}\frac{\sum_i \left([X]K_i^R \prod_{j\neq i}(1+[X]K_j^R)\right) + L\sum_i \left(c_i[X]K_i^R \prod_{j\neq i}(1+c_j[X]K_j^R)\right)}{\prod_i(1+[X]K_i^R) + L\prod_i(1+c_i[X]K_i^R)} \tag{3.2}$$

where $1 \leq i \leq n$, $c_i = \frac{K_i^T}{K_i^R}$ and L as described above.

This is equivalent to equation 3.1 if all K_i^R and c_i are the same.

For a protein where binding sites are not all different, but can be grouped into k sets of binding sites of identical affinities, the above equation rewritten as:

$$\bar{Y} = \frac{1}{n}\frac{\sum_i \left(m_i[X]K_i^R(1+[X]K_i^R)^{m_i-1}\prod_{j\neq i}(1+[X]K_j^R)^{m_j}\right) + L\sum_i \left(m_i c_i[X]K_i^R(1+c_i[X]K_i^R)^{m_i-1}\prod_{j\neq i}(1+c_j[X]K_j^R)^{m_j}\right)}{\prod_i(1+[X]K_i^R)^{m_i} + L\prod_i(1+c_i[X]K_i^R)^{m_i}} \tag{3.3}$$

where $1 \leq i \leq k$, m_i denotes the number of binding sites with affinity K_i^R (note that $\sum_i m_i = n$), and L and c_i as described above. This

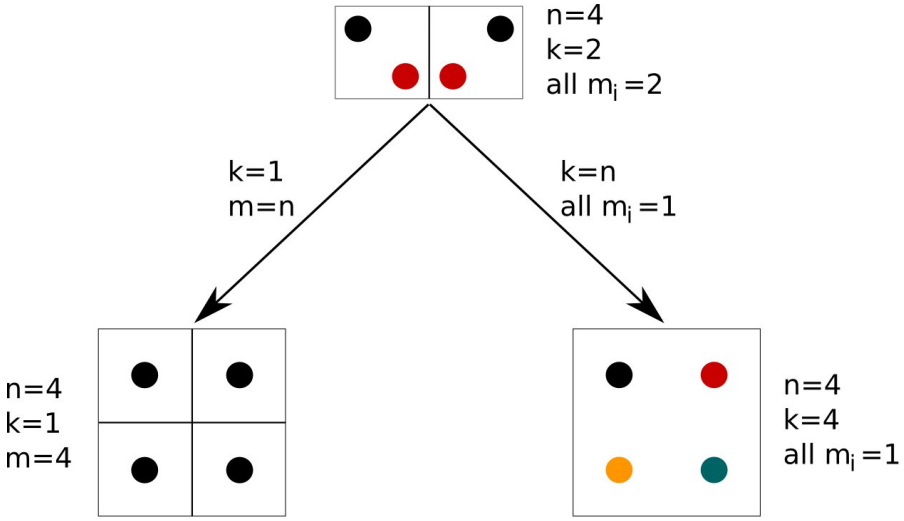

Figure 4: Generalisations of the MWC model. The most general case (top) is a protein with identical subunits containing binding sites with different affinities. There are two special cases of this: In the classical MWC case (bottom left), there is only one binding site per subunit. In the other special case (bottom right), there is only one subunit, i. e. all binding sites have different affinities.

equation reduces to 3.1 on the facing page if $m = n$, and to 3.2 on the preceding page if $m_i = 1$ for all i. The case in which all binding sites are the same, and the case in which all binding sites are different can thus be seen as two extreme cases of this general case, in which binding sites can be divided into groups of same affinity. This is illustrated in figure 4.

3.2.2 *Conformational change*

Similarly, it is possible to develop generalisations of the equation for fractional conformational change ($\bar{R}$), as introduced in chapter 2 on page 11. In the classical MWC model (Monod *et al.*, 1965), this is described by:

$$\bar{R} = \frac{(1 + [X]K^R)^n}{(1 + [X]K^R)^n + L(1 + c[X]K^R)^n} \tag{3.4}$$

In the case of a protein with n different ligand binding sites, the corresponding expression is:

$$\bar{R} = \frac{\prod_i (1 + [X]K_i^R)}{\prod_i (1 + [X]K_i^R) + L \prod_i (1 + c_i[X]K_i^R)} \tag{3.5}$$

When all K_i^R and all c_i are equal, this corresponds to equation 3.4 on the preceding page.

Again, when binding sites are pooled into groups of m_i binding sites that have the same affinity K_i^R (where $\sum_i m_i = n$), then $\bar{R}$ can be written as follows:

$$\bar{R} = \frac{\prod_i (1 + [X]K_i^R)^{m_i}}{\prod_i (1 + [X]K_i^R)^{m_i} + L \prod_i (1 + c_i[X]K_i^R)^{m_i}} \tag{3.6}$$

Introducing the definition $\Omega_i := \frac{1+c_i[X]K_i^R}{1+[X]K_i^R}$, equation 3.6 simplifies to

$$\bar{R} = \frac{1}{1 + L \prod_i \Omega_i^{m_i}} \tag{3.7}$$

Again, if $m = n$, this is equivalent to equation 3.4 on the preceding page, and if $m_i = 1$ for all i, this is equivalent to equation 3.5.

3.3 Obtaining Adair-Klotz constants from microscopic association constants

3.3.1 *Obtaining Adair-Klotz constants from microscopic association constants for a protein with four non-equivalent binding sites*

Consider a protein P with four binding sites for ligand X. The first apparent association constant, K_1 is defined as follows:

$$K_1 = \frac{[P_1]}{[P_0][X]}$$

where $[P_0]$ denotes the concentration of unbound protein, $[P_1]$ the concentration of protein with exactly one ligand molecule bound and $[X]$ the concentration of ligand. Since P is an allosteric protein, it can exist in two different conformations: the high-affinity R conformation and the low-affinity T conformation. If we denote by $[R_i]$ the concentration of protein in the R state bound to i ligand molecules (and analogously for $[T_i]$), we can re-write the above expression as:

$$K_1 = \frac{[R_1] + [T_1]}{([R_0] + [T_0])[X]}$$

Since we treat the four binding sites as non-equivalent, we must discriminate between them. The first ligand molecule binding to the protein in the R state can bind to site A, B, C, or D. If R_A denotes the concentration of protein in the R state bound to exactly one ligand molecule at site A (and analogously for sites B, C, and D, and for the T state), the above equation becomes:

$$K_1 = \frac{([R_A] + [R_B] + [R_C] + [R_D]) + ([T_A] + [T_B] + [T_C] + [T_D])}{([R_0] + [T_0])[X]}$$

The balance between unbound protein in the T and R states is given by the allosteric isomerisation constant, L ($L = \frac{[T_0]}{[R_0]}$). We can use this relationship to derive an equation that links the apparent first association constant K_1 to the microscopic association constants (K_A^R for site A in the R state, and analogously for the other binding sites, and the T state):

$$K_1 = \frac{\left([R_0][X]K_A^R + [R_0][X]K_B^R + [R_0][X]K_C^R + [R_0][X]K_D^R\right) + \left([T_0][X]K_A^T + [T_0][X]K_B^T + [T_0][X]K_C^T + [T_0][X]K_D^T\right)}{([R_0] + [T_0])[X]}$$

Substituting for $[T_0]$ and simplifying, we obtain:

$$K_1 = \frac{K_A^R + K_B^R + K_C^R + K_D^R + L\left(K_A^T + K_B^T + K_C^T + K_D^T\right)}{1 + L} \tag{3.8}$$

Similarly, we can consider the second association constant, K_2.

$$K_2 = \frac{[P_2]}{[P_1][X]}$$

Again, distinguishing between the R and T states and between the four different binding sites, we obtain:

$$K_2 = \frac{[R_{AB}] + [R_{AC}] + [R_{AD}] + [R_{BC}] + [R_{BD}] + [R_{CD}] + [T_{AB}] + [T_{AC}] + [T_{AD}] + [T_{BC}] + [T_{BD}] + [T_{CD}]}{([R_A] + [R_B] + [R_C] + [R_D] + [T_A] + [T_B] + [T_C] + [T_D])[X]}$$

This gives:

$$K_2 = \frac{K_A^R K_B^R + K_A^R K_C^R + K_A^R K_D^R + K_B^R K_C^R + K_B^R K_D^R + K_C^R K_D^R + L\left(K_A^T K_B^T + K_A^T K_C^T + K_A^T K_D^T + K_B^T K_C^T + K_B^T K_D^T + K_C^T K_D^T\right)}{K_A^R + K_B^R + K_C^R + K_D^R + L\left(K_A^T + K_B^T + K_C^T + K_D^T\right)} \tag{3.9}$$

We can apply the same reasoning to the third ligand binding event:

$$K_3 = \frac{[P_3]}{[P_2][X]}$$

which eventually gives:

$$K_3 = \frac{K_A^R K_B^R K_C^R + K_A^R K_B^R K_D^R + K_A^R K_C^R K_D^R + K_B^R K_C^R K_D^R + L\left(K_A^T K_B^T K_C^T + K_A^T K_B^T K_D^T + K_A^T K_C^T K_D^T + K_B^T K_C^T K_D^T\right)}{K_A^R K_B^R + K_A^R K_C^R + K_A^R K_D^R + K_B^R K_C^R + K_B^R K_D^R + K_C^R K_D^R + L\left(K_A^T K_B^T + K_A^T K_C^T + K_A^T K_D^T + K_B^T K_C^T + K_B^T K_D^T + K_C^T K_D^T\right)} \tag{3.10}$$

And similarly for K_4:

$$K_4 = \frac{[P_4]}{[P_3][X]}$$

$$K_4 = \frac{K_A^R K_B^R K_C^R K_D^R + L K_A^T K_B^T K_C^T K_D^T}{K_A^R K_B^R K_C^R + K_A^R K_B^R K_D^R + K_A^R K_C^R K_D^R + K_B^R K_C^R K_D^R + L\left(K_A^T K_B^T K_C^T + K_A^T K_B^T K_D^T + K_A^T K_C^T K_D^T + K_B^T K_C^T K_D^T\right)} \tag{3.11}$$

Note that in the case of four identical binding sites,

$$K_A^R = K_B^R = K_C^R = K_D^R = K^R$$

and

$$K_A^T = K_B^T = K_C^T = K_D^T = K^T$$

and the above expressions reduce to conversion equations for identical binding sites reported by Edelstein (1975).

3.3.2 *Obtaining the i^{th} Adair-Klotz constant from microscopic association constants for a protein with n non-equivalent binding sites*

In general, for a protein with n ligand binding sites, we can express the apparent association constant for the i^{th} binding event by computing the ratio between the concentrations of end products and initial reactants. The equation for the i^{th} apparent association constant thus reads as follows:

$$K_i^n = \frac{[P_i]}{[P_{i-1}][X]}$$

As above, both $[P_{i-1}]$ and $[P_i]$ are sums of protein populations in two different states and with ligand molecules bound to combinations of different binding sites. We can again distinguish between R and T state, which yields:

$$K_i^n = \frac{[R_i] + [T_i]}{([R_{i-1}] + [T_{i-1}])[X]}$$

If we now assume that the n ligand binding sites are, in general, non-equivalent, we must account for the fact that R_i is a collection of protein molecules in the R state with all possible combinations of i out of n ligand binding sites occupied. In other words:

$$R_i = \sum_{\substack{j_1 < j_2 < \cdots < j_i, \\ \text{all } j \in \{1,\ldots,n\}}} R_{j_1 j_2 \ldots j_i} \tag{3.12}$$

Expressing every $R_{j_1 j_2 \ldots j_i}$ in terms of $[R_0]$, $[X]$ and the microscopic association constants, we can write R_i in the following way:

$$[R_i] = [R_0][X]^i \sum_{\substack{j_1 < j_2 < \cdots < j_i, \\ \text{all } j \in \{1,\ldots,n\}}} K_{j_1}^R K_{j_2}^R \ldots K_{j_i}^R \tag{3.13}$$

Introducing the following abbreviations

$$S_i^{nR} := \sum_{\substack{j_1 < j_2 < \cdots < j_i, \\ \text{all } j \in \{1,\ldots,n\}}} K_{j_1}^R K_{j_2}^R \ldots K_{j_i}^R \tag{3.14}$$

$$S_i^{nT} := \sum_{\substack{j_1 < j_2 < \cdots < j_i, \\ \text{all } j \in \{1,\ldots,n\}}} K_{j_1}^T K_{j_2}^T \ldots K_{j_i}^T \tag{3.15}$$

we obtain the expression for K_i^n:

$$K_i^n = \frac{[R_0][X]^i S_i^{nR} + [T_0][X]^i S_i^{nT}}{\left([R_0][X]^{i-1} S_{i-1}^{nR} + [T_0][X]^{i-1} S_{i-1}^{nT}\right)[X]}$$

Using the relationship $[T_0] = L[R_0]$ to eliminate $[X]^i$ and $[R_0]$, this simplifies to:

$$K_i^n = \frac{S_i^{nR} + L S_i^{nT}}{S_{i-1}^{nR} + L S_{i-1}^{nT}} \tag{3.16}$$

with S_i^{nR} and S_i^{nT} as defined above.

If the binding sites can be grouped into k sub-sets that have the same affinity (m_1 binding sites with affinity K_i^R, m_2 binding sites with affinity K_2^R, etc.), the expression for S_i^{nR} can be written as follows:

$$S_i^{nR} := \sum_{\substack{0 \le e_j \le m_j, \\ e_1 + \ldots + e_k = i}} \binom{m_1}{e_1} \left(K_1^R\right)^{e_1} \ldots \binom{m_k}{e_k} \left(K_k^R\right)^{e_k} \tag{3.17}$$

3.4 Applications of the theory

We have studied two proteins with four binding sites each, which constitute extreme cases of the generalised MWC framework: For calmodulin, all binding sites are different, so the protein can be seen as having four sub-groups of binding sites containing one binding site each ($m_1 = m_2 = m_3 = m_4 = 1$). For hæmoglobin, all binding sites are equivalent, so there is only one sub-group of binding sites containing four elements. This section will describe only the hæmoglobin case; the example of calmodulin will be discussed in chapter 4 on page 31.

Hæmoglobin has four identical binding sites for oxygen, and can be described by the classical MWC framework. Thus, the conversion equations are a special case of the equations presented above. They read as follows (Edelstein, 1975):

$$K_1 = 4\frac{K^R + LK^T}{1 + L} \tag{3.18}$$

$$K_2 = \frac{3}{2}\frac{(K^R)^2 + L(K^T)^2}{K^R + LK^T} \tag{3.19}$$

$$K_3 = \frac{2}{3}\frac{(K^R)^3 + L(K^T)^3}{(K^R)^2 + L(K^T)^2} \tag{3.20}$$

$$K_4 = \frac{1}{4}\frac{(K^R)^4 + L(K^T)^4}{(K^R)^3 + L(K^T)^3} \tag{3.21}$$

Yonetani *et al.* (2002) fitted the same data for hæmoglobin binding to oxygen using both the MWC and Adair-Klotz frameworks. This study provides an excellent opportunity to test the validity of the conversion equations presented here: By using the results of their MWC fit and inserting K^R, K^T and L into the equations presented by Edelstein (1975), the Adair-Klotz constants K_1 to K_4 can be determined independently. Table 1 on the next page compares the Adair-Klotz constants thus obtained in this work to the Adair-Klotz constants ob-

	this study	Yonetani *et al.* (2002)
K'_1	7.68×10^{-3}	7.20×10^{-3}
K'_2	0.96×10^{-2}	1.05×10^{-2}
K'_3	1.52×10^{-2}	1.15×10^{-2}
K'_4	2.32×10^{-2}	2.33×10^{-2}

Table 1: Experimental and theoretical determination of Adair-Klotz constants from MWC constants at pH 7.0. Here, $K^R = 3.0 \times 10^{-2}$, $K^T = 7.0 \times 10^{-3}$ and $L = 33$, as obtained by Yonetani *et al.* (2002) by fitting data with an MWC equation. We used these to compute K_1 to K_4 using the equations presented in (Edelstein, 1975) and here compare them to K_1 to K_4 obtained by Yonetani *et al.* (2002) by fitting the same data with an Adair-Klotz equation. Note that Yonetani *et al.* used a slightly modified version of the Adair-Klotz equation (Klotz, 1946); meaning that K_1 for Yonetani *et al.* corresponds to $\frac{1}{4}K_1$ for Klotz, K_2 for Yonetani *et al.* to $\frac{2}{3}K_2$ for Klotz, K_3 for Yonetani *et al.* to $\frac{3}{2}K_3$ for Klotz and K_4 for Yonetani *et al.* to $4K_4$ for Klotz. To allow easier comparability, we used Yonetani's notation for this table and labelled the constants $K'_1, \ldots, K'_4$ to avoid confusion with the original Klotz notation used everywhere else in this study.

tained by Yonetani *et al.* (2002). Both methods yield essentially the same results, slight differences are presumably due to rounding errors and/or to limitations of the data fitting algorithms used, as well as possible over-fitting in the case of the Adair-Klotz framework.

3.5 Discussion and conclusion

The generalised MWC model proposed here opens up new ways of applying the allosteric framework: Not only can it be applied to multimers consisting of identical subunits with one ligand binding site on each, but also to proteins with several binding sites of different affinities for the same ligand, be it multimers with more than one binding sites on each subunit or monomeric proteins containing several binding sites. This framework has been used for an allosteric model of calmodulin (Stefan *et al.*, 2008) (chapter 4 on page 31), and could be useful in the analysis of a wide range of other proteins.

In biology, the same question can be tackled at different levels and with different approaches, often based on different underlying theoretical frameworks. These approaches, however, need to be compara-

ble in order to allow cross-validation and assembly of different types of data into a comprehensive understanding of a given process. Computational modellers need a way of comparing their models with experimental results to assess the validity of their models. In particular, mechanistic models need to be comparable to data or to the phenomenological models describing them. We offer a way of relating intrinsic association constants in allosteric models to Adair-Klotz constants and thus to bridge the gap between generalised allosteric models and experimental observations.

Apart from enabling modellers to validate their models, conversion equations could also help in model construction by providing ways to constrain parameter space and facilitate the estimation of allosteric parameters. This is useful in cases where there is little or no additional experimental evidence that could help with their derivation.

Contributions

A modified version of this chapter has been submitted for publication. I designed the generalised MWC framework and derived the conversion equations. Stuart Edelstein independently derived the conversion equations in order to validate them. Nicolas Le Novère supervised the research. All three of us contributed to the manuscript.

4

ALLOSTERIC MODEL OF CALMODULIN

4.1 Introduction

Calmodulin is a ubiquitous regulatory protein that plays a vital role in mediating bidirectional synaptic plasticity: It preferentially activates CaMKII at high calcium concentrations and PP2B at low calcium concentrations. It remains to be explained, however, how calmodulin performs this dual function.

Calmodulin is a single polypeptide chain of 148 amino acid residues (Watterson *et al.*, 1980), with a dumbbell-like shape (Babu *et al.*, 1988), where each of the lobes contains two calcium binding EF-hands (Babu *et al.*, 1988; Chattopadhyaya *et al.*, 1992). Calmodulin can have two distinct conformations: in the absence of calcium, its EF-hands typically adopt a compact (closed) form which is unable to bind to most targets (Kuboniwa *et al.*, 1995). When bound to four calcium ions, they are found in an open form, which can bind to various target proteins (Babu *et al.*, 1985).

A variety of models for calmodulin activation and action have been used in the past. Each of these models reflects some properties of calmodulin and is reasonably applicable in contexts in which only these properties are relevant. However, none of these models can satisfactorily account for all the observed properties of calmodulin such as cooperativity of calcium binding, different affinities of different calcium binding sites (Crouch and Klee, 1980), activation of targets by unsaturated calmodulin (Huang *et al.*, 1981; Kincaid and Vaughan, 1986; Shifman *et al.*, 2006), and increased affinity for calcium upon binding to targets (Burger *et al.*, 1983; Olwin *et al.*, 1984; Shifman *et al.*, 2006).

We propose an alternative model, based on a biophysical description of the conformational transitions. This generalised allosteric model of calmodulin can reconcile different properties of calmodulin, including differential activation of PP2B and CaMKII, residual acti-

vation of CaMKII at low calcium saturation, differences between the binding sites in terms of calcium affinity and the existence of active and inactive conformations.

4.2 Allosteric model of calmodulin

4.2.1 *Structure of the model*

In this model calmodulin can exist in two different states: the active, open R state and the inactive, closed T state. Each of these states can bind four calcium ions (see figure 5), with calcium affinity being higher for the R state than for the T state.

The four different binding sites are designated *A*, *B*, *C* and *D* (*A* and *B* on the amino-terminal (N-terminal) domain, *C* and *D* on the carboxy-terminal (C-terminal) domain, with no sequential order being implied within the domains). Each of the states and each of the reactions is explicitly modelled, with distinct dissociation constants for each of the sites (see figure 6 on page 34). Target (CaMKII or PP2B) only binds to the R state.

4.2.2 *Parameter determination*

The generalised formula for fractional occupancy of an allosteric protein in the absence of allosteric effectors is given in Chapter 3 on page 19. Versions of this equation were used for parameter determination.

The allosteric isomerisation constant L, the microscopic dissociation constants K_i^R for the R state for each site, and the ratios of R and T state affinity, c_i, for each site cannot be directly obtained from experimental literature. Experimental results do allow us, however, to constrain parameter space and to obtain reasonable estimates. We used calcium binding data in the presence and the absence of an allosteric activator for mutant and wild-type forms of calmodulin.

We introduced the additional assumption that all four c_i values are identical. This is based on the idea that the free energy of transition is spread over the whole molecule. In addition, the published structures of calmodulin (Babu *et al.*, 1985; Kuboniwa *et al.*, 1995) suggest that

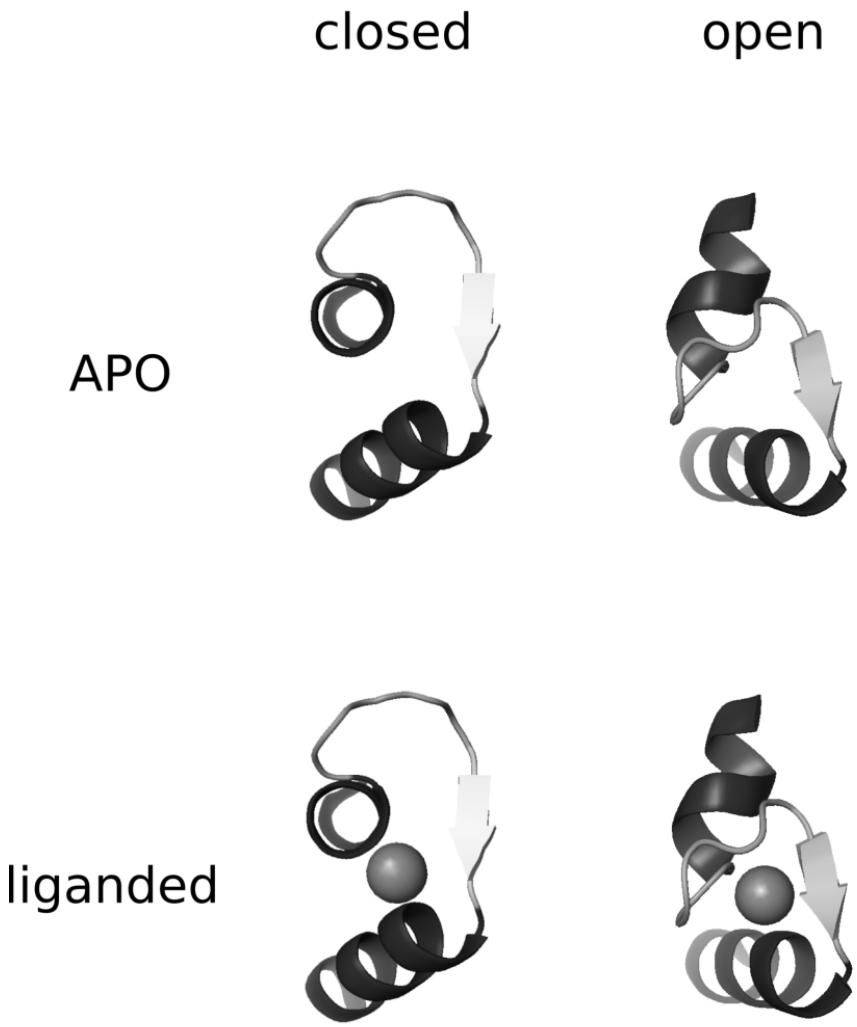

Figure 5: Representative structures of a calmodulin EF-hand as modelled here. Residues 49-75 are shown. The closed *apo* structure is taken from Kuboniwa *et al.* (1995) (PDB: 1CFD). The closed calcium-liganded structure is inferred from Warren *et al.* (2007) (PDB: 2PQ3), using the position of Zn^{2+}. The open structures come from Babu *et al.* (1988) (PDB: 3CLN).

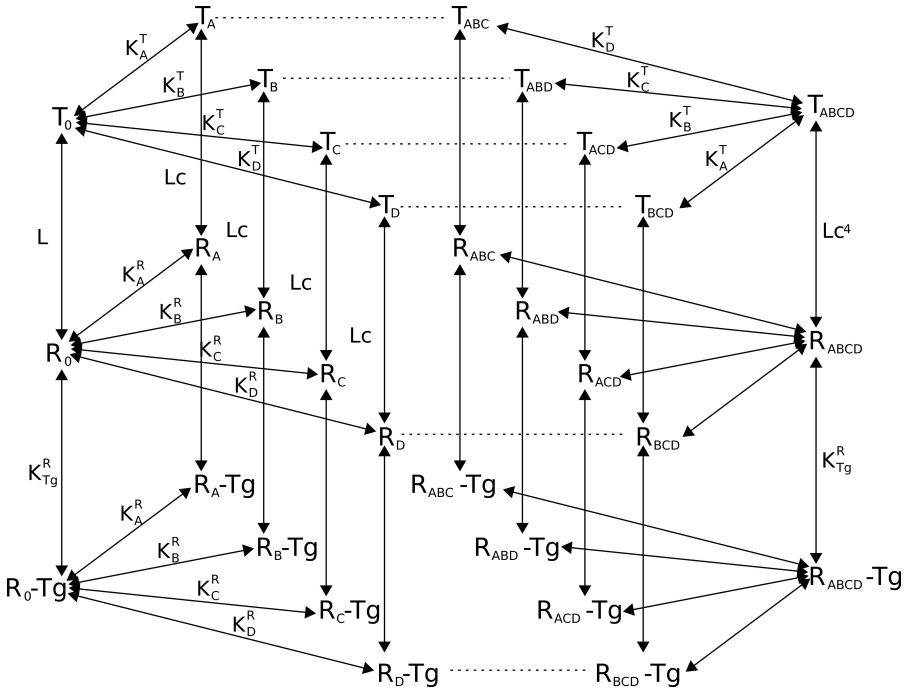

Figure 6: Scheme of reactions used in the allosteric model of calmodulin. For clarity, only the first and fourth calcium binding events are depicted in detail. *Tg* stands for target, which in this model can be either CaMKII or PP2B.

both the R state and the T state are symmetrical and that there are effectively two pairs of binding sites, with each binding site on the N-terminal lobe mirroring a similar binding site on the C-terminal lobe. Because symmetry is conserved in the transition from R to T state, a conformational change that alters one of the binding sites must alter the corresponding binding site on the other lobe to the same extent. We would therefore assume the c value for one binding site to be very similar to the c value for the corresponding binding site on the other lobe. We therefore felt it was a reasonable simplification to assume that all c values were the same, thereby greatly reducing the computational complexity of parameter determination.

Obtaining L *and* c *values*

In order to obtain an estimate of c and of the isomerisation constant L, a reduced model of calmodulin was used. In this simple model, all four calcium binding sites are equivalent and one molecule of target, acting as an allosteric activator, can bind to each molecule of calmodulin. In this case, the fractional occupancy $\bar{Y}$ of an allosteric protein in the presence of an allosteric activator can be described as (Rubin and Changeux, 1966):

$$\bar{Y} = \frac{\frac{[X]}{K^R}\left(1+\frac{[X]}{K^R}\right)^3 + L\left(\frac{1+\gamma e}{1+\gamma}\right)c\frac{[X]}{K^R}\left(1+c\frac{[X]}{K^R}\right)^3}{\left(1+\frac{[X]}{K^R}\right)^4 + L\left(\frac{1+\gamma e}{1+\gamma}\right)\left(1+c\frac{[X]}{K^R}\right)^4} \tag{4.1}$$

In this equation, $[X]$ is the concentration of ligand, $\gamma = \frac{[A]}{K^{AR}}$ and $e = \frac{K^{AR}}{K^{AT}}$; K^R denotes the dissociation constant for ligand binding to the R state, L the allosteric equilibrium constant, $[A]$ the concentration of allosteric activator, K^{AR} the dissociation constant for binding of the allosteric activator to the R state and K^{AT} the dissociation constant for binding of the allosteric activator to the T state. The factor $(\frac{1+\gamma e}{1+\gamma})$ modulates the apparent isomerisation constant as a function of activator concentration: if more target is present, the apparent value of L decreases.

Peersen *et al.* (1997) have measured calcium binding to calmodulin in the absence and presence of several target proteins, which act

as allosteric effectors of calmodulin. By taking the calcium concentration at $\bar{Y} = \frac{1}{2}$ from four different binding curves (absence of target, presence of skeletal myosin light chain kinase (skMLCK), phosphorylase kinase (PhK5) or Ca^{2+}-ATPase (CaATPase), respectively) and inserting them into the above equation, we obtain a system of four equations, which depend on L, c, and on e values for skMLCK, PhK5 and CaATPase, respectively. In order to get K^R from the reported K_d value, we need to dissect K_d into its two contributing factors: binding to the R state and binding to the T state:

$$\begin{aligned} K_d &= \frac{[CaM][Ca^{2+}]}{[CaM{-}Ca]} = \\ &= \frac{([R]+[T])[Ca^{2+}]}{[R{-}Ca]+[T{-}Ca]} = \\ &= \frac{[R][Ca^{2+}](1+L)}{[R{-}Ca](1+Lc)} = K^R \frac{1+L}{1+Lc} \end{aligned}$$

Hence, $K^R = K_d \frac{1+Lc}{1+L}$.

For each condition (presence of specific targets, or absence of target), the objective function ϵ to minimise is the difference between the measured value of $\bar{Y}$ at half-saturating calcium concentration ($\frac{1}{2}$) and the theoretical value of $\bar{Y}$ at the same calcium concentration, as computed from the equation given above (which should also equal $\frac{1}{2}$, given the right choice of parameters). This results in a system of equations (one for each conditions) to be minimised simultaneously. The equations read as follows:

NO TARGET PRESENT:

$$\epsilon_1 = \frac{1}{2} - \frac{\frac{[Ca^{2+}]_{0.5}}{K^R}\left(1+\frac{[Ca^{2+}]_{0.5}}{K^R}\right)^3 + Lc\frac{[Ca^{2+}]_{0.5}}{K^R}\left(1+c\frac{[Ca^{2+}]_{0.5}}{K^R}\right)^3}{\left(1+\frac{[Ca^{2+}]_{0.5}}{K^R}\right)^4 + L\left(1+c\frac{[Ca^{2+}]_{0.5}}{K^R}\right)^4} \tag{4.2}$$

where $[Ca^{2+}]_{0.5} = 7.5 \times 10^{-6}\, M$ and $K^R = 1.4 \times 10^{-5}\, M$.

skMLCK:

$$\epsilon_2 = \frac{1}{2} - \frac{\frac{[Ca^{2+}]_{0.5_1}}{K^R}\left(1+\frac{[Ca^{2+}]_{0.5_1}}{K^R}\right)^3 + L\left(\frac{1+\frac{A_1}{K_1^{AR}}e_1}{1+\frac{A_1}{K_1^{AR}}}\right)c\frac{[Ca^{2+}]_{0.5_1}}{K^R}\left(1+c\frac{[Ca^{2+}]_{0.5_1}}{K^R}\right)^3}{\left(1+\frac{[Ca^{2+}]_{0.5_1}}{K^R}\right)^4 + L\left(\frac{1+\frac{A_1}{K_1^{AR}}e_1}{1+\frac{A_1}{K_1^{AR}}}\right)\left(1+c\frac{[Ca^{2+}]_{0.5_1}}{K^R}\right)^4} \tag{4.3}$$

where $[Ca^{2+}]_{0.5_1} = 3.4 \times 10^{-8}\,M$, $A_1 = 1 \times 10^{-5}\,M$, $K_1^{AR} = 1 \times 10^{-9}\,M$.

PhK5:

$$\epsilon_3 = \frac{1}{2} - \frac{\frac{[Ca^{2+}]_{0.5_2}}{K^R}\left(1+\frac{[Ca^{2+}]_{0.5_2}}{K^R}\right)^3 + L\left(\frac{1+\frac{A_2}{K_2^{AR}}e_2}{1+\frac{A_2}{K_2^{AR}}}\right)c\frac{[Ca^{2+}]_{0.5_2}}{K^R}\left(1+c\frac{[Ca^{2+}]_{0.5_2}}{K^R}\right)^3}{\left(1+\frac{[Ca^{2+}]_{0.5_2}}{K^R}\right)^4 + L\left(\frac{1+\frac{A_2}{K_2^{AR}}e_2}{1+\frac{A_2}{K_2^{AR}}}\right)\left(1+c\frac{[Ca^{2+}]_{0.5_2}}{K^R}\right)^4} \tag{4.4}$$

where $[Ca^{2+}]_{0.5_2} = 6 \times 10^{-7}\,M$, $A_2 = 1 \times 10^{-5}\,M$, $K_2^{AR} = 2 \times 10^{-8}\,M$.

CaATPase:

$$\epsilon_4 = \frac{1}{2} - \frac{\frac{[Ca^{2+}]_{0.5_3}}{K^R}\left(1+\frac{[Ca^{2+}]_{0.5_3}}{K^R}\right)^3 + L\left(\frac{1+\frac{A_3}{K_3^{AR}}e_3}{1+\frac{A_3}{K_3^{AR}}}\right)c\frac{[Ca^{2+}]_{0.5_3}}{K^R}\left(1+c\frac{[Ca^{2+}]_{0.5_3}}{K^R}\right)^3}{\left(1+\frac{[Ca^{2+}]_{0.5_3}}{K^R}\right)^4 + L\left(\frac{1+\frac{A_3}{K_3^{AR}}e_3}{1+\frac{A_3}{K_3^{AR}}}\right)\left(1+c\frac{[Ca^{2+}]_{0.5_3}}{K^R}\right)^4} \tag{4.5}$$

where $[Ca^{2+}]_{0.5_3} = 1.2 \times 10^{-7}\,M$, $A_3 = 10^{-5}\,M$, $K_3^{AR} = 1 \times 10^{-9}\,M$.

We minimised $(\epsilon_1, \epsilon_2, \epsilon_3, \epsilon_4)$ by using the `leastsquare` function provided in scilab (`http://www.scilab.org`). To avoid local minima, we ran 10^5 minimisations, each one with different initial values. Initial values were drawn at random: The `grand` function provided in scilab was used to determine the exponent of each parameter, with initial

values in the following range: $10^3 \leq L < 10^5$, $10^{-4} \leq c < 0.1$ and $10^{-15} < e_i < 0.5$. Out of 10^5 runs, 13 resulted in the same minimum, which we believe to be global. It is reached at $L = 20670$, $c = 3.96 \times 10^{-3}$, $e_1 = 10^{-15}$, $e_2 = 0.5$, and $e_3 = 1.57 \times 10^{-3}$. e_1 being very small (in fact, reaching the lower boundary condition) means that skMLCK binds predominantly to the R state. We can therefore assume that, in the presence of sufficient amounts of skMLCK, calmodulin exists predominantly in the R state.

Obtaining dissociation constants

To determine the dissociation constants for all four binding sites, we used a similar approach, making use of the general formula for fractional occupancy presented above (equation 3.2 on page 20). The formula can be simplified to reflect calmodulin binding to calcium under different experimental constraints. For instance, it can be reduced to the two N-terminal binding sites to describe recombinant versions of calmodulin in which the C-terminal binding sites are ablated. Using the available experimental literature, one thus obtains a system of four equations and corresponding data: the full equation for $\bar{Y}$ (using data from Bayley *et al.* (1996)), two reduced equations for $\bar{Y}$ with N-terminal or C-terminal binding sites only, respectively (using data from experiments with recombinant calmodulin from Shifman *et al.* (2006)), and one reduced equation for $\bar{Y}$ in which only the R state is considered (using data from Peersen *et al.* (1997) in the presence of skMLCK, where it can be assumed that calmodulin exists mostly in the R state). There are thus four constraints that can be used to restrict parameter space. We used the calcium concentration at $\bar{Y} = \frac{1}{2}$ and at $\bar{Y} = \frac{1}{4}$ from the experimental literature to obtain eight equations that depend on K_i^R values. The eight equations read as follows:

WILDTYPE:

$$\eta_1 = \frac{1}{2} - 0.25 \frac{\sum_i \left(\frac{[Ca^{2+}]_{0.5}}{K_i^R} \prod_j \left(1 + \frac{[Ca^{2+}]_{0.5}}{K_j^R} \right) \right) + L \sum_i \left(c \frac{[Ca^{2+}]_{0.5}}{K_i^R} \prod_j \left((1 + c \frac{[Ca^{2+}]_{0.5}}{K_j^R} \right) \right)}{\prod_i \left(1 + \frac{[Ca^{2+}]_{0.5}}{K_i^R} \right) + L \prod_i \left(1 + c \frac{[Ca^{2+}]_{0.5}}{K_i^R} \right)} \tag{4.6}$$

$$\eta_2 = \frac{1}{4} - 0.25 \frac{\Sigma_i \left(\frac{[Ca^{2+}]_{0.25}}{K_i^R} \Pi_j \left(1 + \frac{[Ca^{2+}]_{0.25}}{K_j^R} \right) \right) + L \Sigma_i \left(c \frac{[Ca^{2+}]_{0.25}}{K_i^R} \Pi_j \left(1 + c \frac{[Ca^{2+}]_{0.25}}{K_j^R} \right) \right)}{\Pi_i \left(1 + \frac{[Ca^{2+}]_{0.25}}{K_i^R} \right) + L \Pi_i \left(1 + c \frac{[Ca^{2+}]_{0.25}}{K_i^R} \right)} \tag{4.7}$$

where $i, j \in \{A, B, C, D\}$ and $j \neq i$, $[Ca^{2+}]_{0.5} = 4.4 \times 10^{-6}\, M$ and $[Ca^{2+}]_{0.25} = 1.4 \times 10^{-6}\, M$ (Bayley *et al.*, 1996).

C-terminal mutant:

$$\eta_3 = \frac{1}{2} - 0.5 \frac{\Sigma_i \left(\frac{[Ca^{2+}]_{N_{0.5}}}{K_i^R} \Pi_j \left(1 + \frac{[Ca^{2+}]_{N_{0.5}}}{K_j^R} \right) \right) + L \Sigma_i \left(c \frac{[Ca^{2+}]_{N_{0.5}}}{K_i^R} \Pi_j \left(1 + c \frac{[Ca^{2+}]_{N_{0.5}}}{K_j^R} \right) \right)}{\Pi_i \left(1 + \frac{[Ca^{2+}]_{N_{0.5}}}{K_i^R} \right) + L \Pi_i \left(1 + c \frac{[Ca^{2+}]_{N_{0.5}}}{K_i^R} \right)} \tag{4.8}$$

$$\eta_4 = \frac{1}{4} - 0.5 \frac{\Sigma_i \left(\frac{[Ca^{2+}]_{N_{0.25}}}{K_i^R} \Pi_j \left(1 + \frac{[Ca^{2+}]_{N_{0.25}}}{K_j^R} \right) \right) + L \Sigma_i \left(c \frac{[Ca^{2+}]_{N_{0.25}}}{K_i^R} \Pi_j \left(1 + c \frac{[Ca^{2+}]_{N_{0.25}}}{K_j^R} \right) \right)}{\Pi_i \left(1 + \frac{[Ca^{2+}]_{N_{0.25}}}{K_i^R} \right) + L \Pi_i \left(1 + c \frac{[Ca^{2+}]_{N_{0.25}}}{K_i^R} \right)} \tag{4.9}$$

where $i, j \in \{A, B\}$ and $j \neq i$, $[Ca^{2+}]_{N_{0.5}} = 3.3 \times 10^{-5}\, M$ and $[Ca^{2+}]_{N_{0.25}} = 1.3 \times 10^{-5}\, M$ (Shifman *et al.*, 2006).

N-terminal mutant:

$$\eta_5 = \frac{1}{2} - 0.5 \frac{\Sigma_i \left(\frac{[Ca^{2+}]_{C_{0.5}}}{K_i^R} \Pi_j \left(1 + \frac{[Ca^{2+}]_{C_{0.5}}}{K_j^R} \right) \right) + L \Sigma_i \left(c \frac{[Ca^{2+}]_{C_{0.5}}}{K_i^R} \Pi_j \left(1 + c \frac{[Ca^{2+}]_{C_{0.5}}}{K_j^R} \right) \right)}{\Pi_i \left(1 + \frac{[Ca^{2+}]_{C_{0.5}}}{K_i^R} \right) + L \Pi_i \left(1 + c \frac{[Ca^{2+}]_{C_{0.5}}}{K_i^R} \right)} \tag{4.10}$$

$$\eta_6 = \frac{1}{4} - 0.5 \frac{\Sigma_i \left(\frac{[Ca^{2+}]_{C_{0.25}}}{K_i^R} \Pi_j \left(1 + \frac{[Ca^{2+}]_{C_{0.25}}}{K_j^R} \right) \right) + L \Sigma_i \left(c \frac{[Ca^{2+}]_{C_{0.25}}}{K_i^R} \Pi_j \left(1 + c \frac{[Ca^{2+}]_{C_{0.25}}}{K_j^R} \right) \right)}{\Pi_i \left(1 + \frac{[Ca^{2+}]_{C_{0.25}}}{K_i^R} \right) + L \Pi_i \left(1 + c \frac{[Ca^{2+}]_{C_{0.25}}}{K_i^R} \right)} \tag{4.11}$$

where $i, j \in \{C, D\}$ and $j \neq i$, $[Ca^{2+}]_{C_{0.5}} = 3.5 \times 10^{-5}\, M$ and $[Ca^{2+}]_{C_{0.25}} = 1.4 \times 10^{-5}\, M$ (Shifman *et al.*, 2006).

R STATE ONLY:

$$\eta_7 = \frac{1}{2} - 0.25 \frac{\sum_i \left(\frac{[Ca^{2+}]_{R_{0.5}}}{K_i^R} \prod_j \left(1 + \frac{[Ca^{2+}]_{R_{0.5}}}{K_j^R} \right) \right)}{\prod_i \left(1 + \frac{[Ca^{2+}]_{R_{0.5}}}{K_i^R} \right)} \tag{4.12}$$

$$\eta_8 = \frac{1}{4} - 0.25 \frac{\sum_i \left(\frac{[Ca^{2+}]_{R_{0.25}}}{K_i^R} \prod_j \left(1 + \frac{[Ca^{2+}]_{R_{0.25}}}{K_j^R} \right) \right)}{\prod_i \left(1 + \frac{[Ca^{2+}]_{R_{0.25}}}{K_i^R} \right)} \tag{4.13}$$

where $i, j \in \{A, B, C, D\}$ and $j \neq i$, $[Ca^{2+}]_{R_{0.5}} = 3.4 \times 10^{-8}\, M$ and $[Ca^{2+}]_{R_{0.25}} = 1.5 \times 10^{-8}\, M$ (Peersen *et al.*, 1997).

To avoid the problem of local minima, we first sampled all possible combinations of K_i^R values in a broad range ($10^{-9} \leq K_i^R < 10^{-4}$), using a logarithmic scan with 50 sample points per dimension. Out of these, we selected the parameter configuration that minimises $\sum_{i=1}^{8} \eta_i^2$. The result was then used as an initial vector for a refined search using a smaller interval (of two orders of magnitude) around the initial results and 66 sample points per dimension. The resulting values are $K_A^R = 8.32 \times 10^{-6}\, M$, $K_B^R = 1.66 \times 10^{-8}\, M$, $K_C^R = 1.74 \times 10^{-5}\, M$, and $K_D^R = 1.45 \times 10^{-8}\, M$.

4.2.3 *Kinetic simulations*

Although equation 3.2 on page 20 provides a general formula for calcium saturation in the case of four non-equivalent binding sites in the absence of allosteric effectors, the situation becomes less tractable in the presence of two competing allosteric activators (CaMKII and PP2B, in this case), especially at low calcium concentrations, where initial calcium concentration can differ significantly from free calcium concentration at steady-state. Moreover, our intention was to provide an accurate model of calmodulin activation, which can serve as a basis for more complex models of signalling networks within the postsynaptic density (PSD). Both these concerns can be met by formulating the model as a system of reactions for kinetic simulations.

Every reaction was split into a separate forward and backward reaction. The full model comprises 352 reactions: 32 reactions describing calcium binding to the target-free T state, 32 reactions describing the corresponding dissociation events, 64 reactions describing calcium binding to and dissociation from the target-free R state, 32 reactions describing transitions between the R and T states, 32 reactions describing the binding and dissociation of CaMKII, another 32 reactions describing the binding and dissociation of PP2B, and 128 reactions describing calcium binding to and dissociation from CaMKII-bound or PP2B-bound calmodulin.

A complete list of reactions can be found in appendix A on page 135.

The k_{on} for calcium binding was assumed to be the same for all four binding sites and both states, since it can be assumed to be controlled only by calcium and calmodulin diffusion and size (random exploration). Different affinities were represented by different k_{off} values. A complete list of parameters can be found in table 3 on the following page.

The Model was deposited in BioModels database (Le Novère *et al.*, 2006) with Model ID BIOMD0000000183 (access: `http://www.ebi.ac.uk/biomodels-main/publ-model.do?mid=BIOMD0000000183`).

Simulations were run using the parameter-scan facility of the Complex Pathway Simulator (COPASI) (Hoops *et al.*, 2006).

K_A^R	$8.32 \times 10^{-6}\,M$	this study
K_B^R	$1.66 \times 10^{-8}\,M$	this study
K_C^R	$1.74 \times 10^{-5}\,M$	this study
K_D^R	$1.45 \times 10^{-8}\,M$	this study
K_A^T	$2.10 \times 10^{-3}\,M$	K_A^R / c
K_B^T	$4.19 \times 10^{-6}\,M$	K_B^R / c
K_C^T	$4.39 \times 10^{-3}\,M$	K_C^R / c
K_D^T	$3.66 \times 10^{-6}\,M$	K_D^R / c
k_{on}	$10^6\,M^{-1}s^{-1}$	assumption
$k^R_{off_A}$	$8.32\,s^{-1}$	$K_A^R \times k_{on}$
$k^R_{off_B}$	$1.66 \times 10^{-2}\,s^{-1}$	$K_B^R \times k_{on}$
$k^R_{off_C}$	$17.4\,s^{-1}$	$K_C^R \times k_{on}$
$k^R_{off_D}$	$1.45 \times 10^{-2}\,s^{-1}$	$K_D^R \times k_{on}$
$k^T_{off_A}$	$2.10 \times 10^{3}\,s^{-1}$	$K_A^T \times k_{on}$
$k^T_{off_B}$	$4.19\,s^{-1}$	$K_B^T \times k_{on}$
$k^T_{off_C}$	$4.39 \times 10^{3}\,s^{-1}$	$K_C^T \times k_{on}$
$k^T_{off_D}$	$3.66\,s^{-1}$	$K_D^T \times k_{on}$
L	20670	this study
k_{RT}	$1 \times 10^6\,s^{-1}$	assumption
k_{TR}	$48.38\,s^{-1}$	k_{RT} / L
c	0.00396	this study
$k_{on_{CaMKII}}$	$3.2 \times 10^6\,M^{-1}s^{-1}$	(Tzortzopoulos and Török, 2004)
$k_{off_{CaMKII}}$	$0.343\,s^{-1}$	(Tzortzopoulos and Török, 2004)
$k_{on_{PP2B}}$	$4.6 \times 10^7\,M^{-1}s^{-1}$	(Quintana *et al.*, 2005)
$k_{off_{PP2B}}$	$0.0013\,s^{-1}$	(Quintana *et al.*, 2005)
$[T_0]$	$2 \times 10^{-7} - 3 \times 10^{-5}\,M$	depending on simulation run
[calcium]	$10^{-8} - 10^{-1}\,M$	multiple runs with varying concentrations
[PP2B]	$1.6 \times 10^{-6}\,M$	(cf. Goto *et al.*, 1986)
[CaMKII]	$7 \times 10^{-5}\,M$	(cf. Petersen *et al.*, 2003)
spine volume	$10^{-15}\,l$	(cf. Carlisle and Kennedy, 2005)

Table 3: List of parameters used for simulation of the calmodulin model.

4.3 Simulation results

4.3.1 *Comparison of calcium binding curve to experimental results*

To validate the model, we compared it to experimental measurements of calmodulin binding to calcium, some of which (Crouch and Klee, 1980; Porumb, 1994) had not been used to constrain parameter space.

Figure 7 on the next page compares the outcome of our simulations with results reported by Crouch and Klee (1980), Porumb (1994) and Peersen *et al.* (1997). The figure indicates good agreement between our model and experimental data.

In order to further quantify this agreement, apparent sequential association constants were obtained by converting the MWC constants to Adair-Klotz constants (Adair, 1925; Klotz, 1946) (see chapter 3 on page 19). The resulting constants are listed in table 4. All of them lie within the range of constants reported in the experimental literature (Burger *et al.*, 1984; Crouch and Klee, 1980; Haiech *et al.*, 1981; Porumb, 1994; Shifman *et al.*, 2006), thus confirming that the model agrees well with experimental data.

4.3.2 *Robustness analysis for k_{RT}*

To determine whether the choice of the R to T transition rate, k_{RT}, affects the outcome of the simulation, we performed a robustness analysis on this parameter. We looked at calcium binding to calmo-

	this paper	reported range
K_1	5.19×10^5	1.16×10^5 (Burger *et al.*) – 1.7×10^6 (Burger *et al.*)
K_2	5.16×10^5	1.4×10^5 (Burger *et al.*) – 8.9×10^5 (Porumb)
K_3	1.34×10^5	2.86×10^4 (Shifman *et al.*) – 2.9×10^6 (Burger *et al.*)
K_4	3.88×10^4	1.7×10^3 (Haiech *et al.*) – 1.12×10^5 (Shifman *et al.*)

Table 4: Apparent Adair-Klotz constants (in M) for our model, and comparison to experimental reports (Burger *et al.*, 1984; Crouch and Klee, 1980; Haiech *et al.*, 1981; Porumb, 1994; Shifman *et al.*, 2006) and data reviews (Burger *et al.*, 1984). Constants were obtained from our model by computing Adair-Klotz constants (Adair, 1925; Klotz, 1946) from MWC constants as discussed in chapter 3 on page 19.

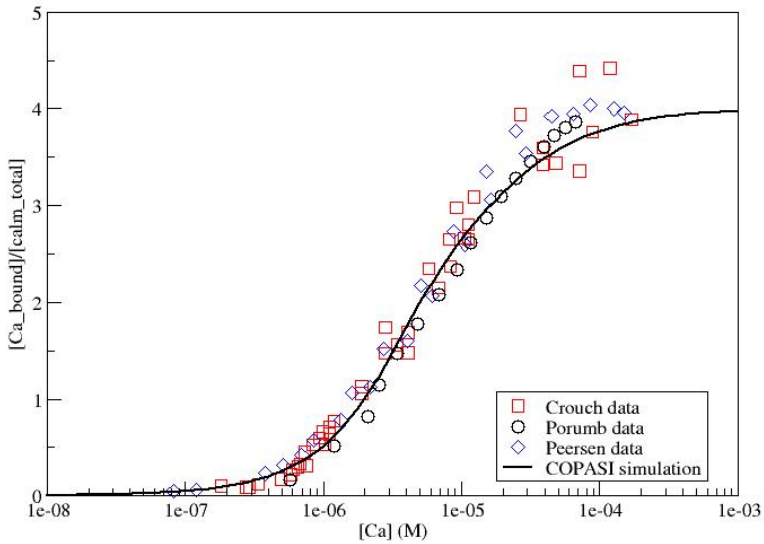

Figure 7: Comparison between simulation results and various sets of experimental results for calcium binding to calmodulin. Moles of calcium bound per mole of calmodulin are shown as a function of initial calcium concentration. Red squares: data points measured by Crouch and Klee (1980), black circles: data points measured by Porumb (1994), blue diamonds: data points measured by Peersen *et al.* (1997), solid line: steady-state results of simulations at different initial calcium concentrations. Calmodulin concentration used was $2 \times 10^{-7} M$.

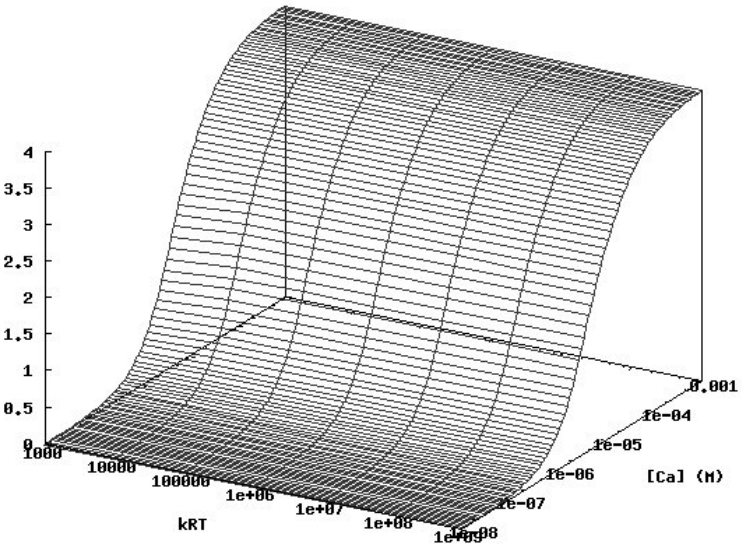

Figure 8: Robustness of the parameter k_{RT}: Moles of calcium bound per mole of calmodulin are shown as a function of calcium concentration and of the parameter value chosen for k_{RT}. Calmodulin concentration used was $2 \times 10^{-7}\,M$.

dulin as a function of calcium concentration for k_{RT} values between 10^3 and 10^9, and found no difference in output (see figure 8).

4.3.3 *Activity of various forms of non-saturated calmodulin*

By calculating the equilibrium constants for the transition between R and T states for calmodulin species that are bound to one or more calcium ions, one can see what fraction of calmodulin is active under steady-state conditions.

For instance, the relation between the R and T states for calmodulin with exactly two calcium ions bound is given by $\frac{R_2}{T_2} = \frac{1}{Lc^2} \approx 3$. Similarly, without any calcium bound, there are more than 20 000 times more calmodulin molecules in the T state than in the R state. With one calcium ion bound, there are still about 80 times more calmodulin molecules in the T state than in the R state. The equilibrium shifts towards the R state when two or more calcium ions are bound: with three calcium ions bound, there is about 800 times as much calmo-

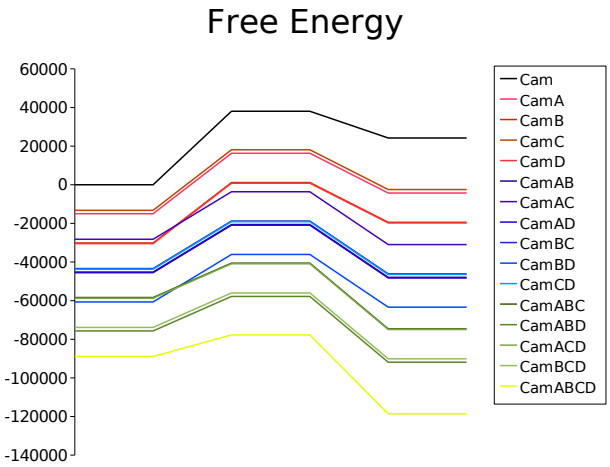

Figure 9: Free energy diagram for the different states of calmodulin showing the different binding sites. Energy levels (in J/mol) were computed as in Edelstein *et al.* (1996). Free energy differences between T state and corresponding R state relate to the allosteric isomerisation constant. Between corresponding T and R states, a hypothetical transition state is depicted based on estimates of rate constants. T state is shown on the left, R state on the right, and the transition state in the middle. Calcium-free calmodulin is shown in black, calmodulin with one calcium ion bound in shades of red, calmodulin with two calcium ions bound in shades of blue, calmodulin with three calcium ions bound in shades of green, fully saturated calmodulin in yellow. Note that some of the curves overlap.

dulin in the R state as in the T state, and when fully saturated, there are nearly 200 000 calmodulin molecules in the R state for each calmodulin molecule in the T state. The shift of equilibrium from T to R state with three or more calcium ions bound can also be seen from the site-specific free energy diagram (see figure 9).

4.3.4 *Altered affinity of calmodulin for calcium in the presence of target*

It has been reported (Burger *et al.*, 1983; Olwin *et al.*, 1984; Shifman *et al.*, 2006) that the apparent affinity of calmodulin for calcium increases if calmodulin is bound to a target. To reproduce this effect, we simulated calcium binding to $2 \times 10^{-7}\,M$ calmodulin at varying

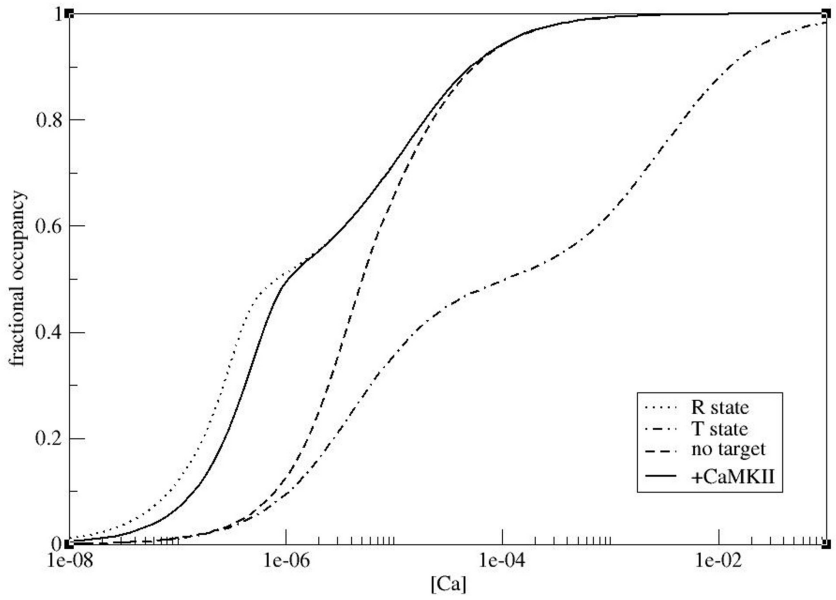

Figure 10: Increased affinity of calmodulin for calcium in the presence of a target protein. Fractional occupancy is shown as a function of initial calcium concentration for four different conditions: Upper dotted line: R state only, lower dotted/dashed line: T state only, dashed line: combined R and T states in the absence of target, solid line: combined R and T states in the presence of CaMKII. All lines are steady-state results of simulations at different initial calcium concentrations. Calmodulin concentration was 2×10^{-7} M.

initial calcium concentrations in the absence of target and in the presence of CaMKII. In addition, we constructed two reduced models of calmodulin where R to T transition was impaired, i. e. where all calmodulin molecules are locked either in the R state or in the T state. These models were also used to simulate calcium binding to calmodulin at different initial calcium concentrations in order to investigate calcium binding of the R state and the T state in isolation.

Results are shown in figure 10. The fractional occupancy curve illustrates how, with increasing initial calcium concentration, the calmodulin population shifts from mostly T state to mostly R state, with the corresponding affinities for calcium. The presence of target further stabilises the R state, resulting in the observed increase of affinity.

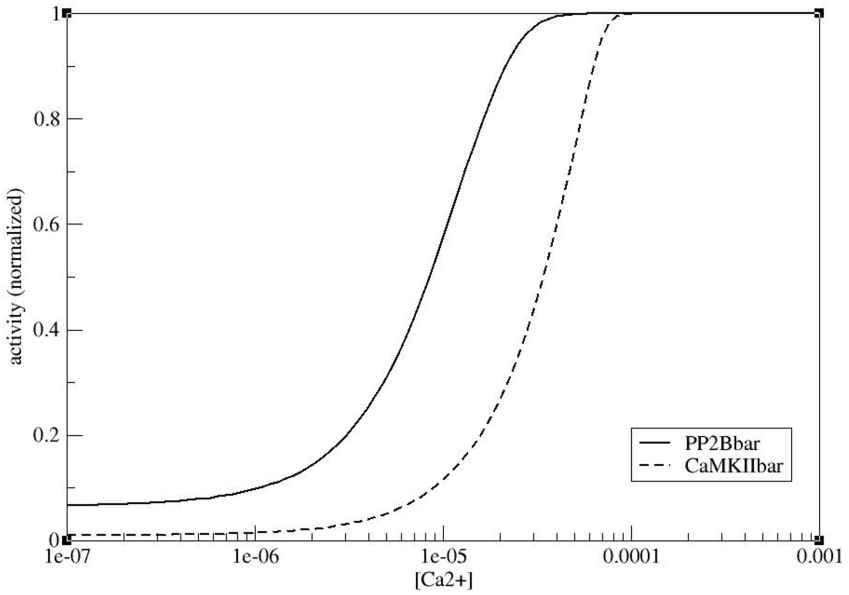

Figure 11: Differential activation of PP2B and CaMKII at different calcium concentrations. Binding of both PP2B and CaMKII to calmodulin is shown normalised to maximum binding. Steady-state results of simulations at different initial concentrations of calcium are shown. Solid line: PP2B, dashed line: CaMKII. Calmodulin concentration was 3×10^{-5} *M* (cf. Kakiuchi *et al.*, 1982).

4.3.5 *Differential activation of CaMKII and PP2B*

An intriguing feature of calmodulin is its ability to differentially activate PP2B or CaMKII, depending on calcium input. It is known that PP2B has a much higher affinity for calmodulin (Quintana *et al.*, 2005) than CaMKII (Tzortzopoulos and Török, 2004). But while PP2B has merely been detected in PSD fractions (reviewed in Collins *et al.*, 2006), CaMKII is far more abundant and, in fact, constitutes a major PSD protein (Chen *et al.*, 2005; Cheng *et al.*, 2006). Together with our allosteric model, this information can explain the differential activation of PP2B at low calcium concentrations and of CaMKII at high calcium concentrations.

As figure 11 shows, we can reproduce a differential activation of PP2B and CaMKII in our model. At sub-saturating calcium concentrations, PP2B becomes preferentially activated due to its high affinity for the R state. PP2B binding stabilises the R state and thus increases

the apparent affinity of calmodulin for its targets. At higher calcium concentrations, more calmodulin in the R state is available and can bind to CaMKII. Due to the abundance of CaMKII, there is more active CaMKII than PP2B in absolute terms.

4.4 Discussion

4.4.1 *Sequential/induced fit models vs thermal equilibrium models*

Both experimentalists (Pifl *et al.*, 1984) and theoreticians (d'Alcantara *et al.*, 2003) have directly related calmodulin activity to calcium concentration, often by using a Hill function (Hill, 1913). This allows for some calmodulin activity even at low calcium concentrations. Furthermore, together with the information that calmodulin affinity for PP2B (Quintana *et al.*, 2005) is higher than for CaMKII (Tzortzopoulos and Török, 2004) and that CaMKII concentration in the postsynaptic density (PSD) (Petersen *et al.*, 2003) is higher than PP2B concentration (Goto *et al.*, 1986), it can explain why PP2B is preferentially activated at lower calcium concentrations. Models of this type do not allow for the possibility that the different binding sites might have different affinities for calcium. Spectroscopic measurements, as well as experiments on mutant versions of calmodulin, show, however, that this is the case (Linse *et al.*, 1991; Shifman *et al.*, 2006). Finally, the use of a Hill function to compute calmodulin activity as a function of calcium concentration is purely phenomenological and does not provide an explanation for how calcium binding relates to calmodulin activity.

Many investigators measuring the binding of calcium to calmodulin (Burger *et al.*, 1984; Crouch and Klee, 1980; Mirzoeva *et al.*, 1999; Shifman *et al.*, 2006) have used an Adair-Klotz function (Adair, 1925; Klotz, 1946), or a modified version, to describe calmodulin binding to calcium. This approach allows for different microscopic affinities for the four binding events, and thus for detailed models of calcium binding to calmodulin. These models do not, however, explain the transition of calmodulin between closed ("inactive") and open ("active") structures, which have been experimentally determined (Babu *et al.*, 1985; Kuboniwa *et al.*, 1995).

Another way to model calmodulin action is by assuming a sequential mechanism, where calmodulin first binds four calcium ions, and only then becomes activated (Franks *et al.*, 2001; Naoki *et al.*, 2005). These models are useful approximations of how calmodulin activates CaMKII, but they fail to account for important aspects of calmodulin function, all of which can be explained by our model. A sequential model fails to explain why calmodulin can activate PP2B or CaMKII when bound to less than four calcium ions (Huang *et al.*, 1981; Kincaid and Vaughan, 1986; Shifman *et al.*, 2006). Some models *assume* that calmodulin can activate PP2B with two, three, or four calcium ions bound, but requires four calcium ions bound in order to activate CaMKII (Bhalla and Iyengar, 1999). While these models are decent phenomenological approximations for modelling the differential activation of CaMKII and PP2B, they do not provide a satisfactory mechanism by which calmodulin with three bound calcium ions would activate PP2B, but not CaMKII. They also fail to explain data on mutant calmodulin where two calcium binding sites are ablated, yet calmodulin still activates CaMKII to some degree (Shifman *et al.*, 2006).

By postulating an equilibrium between inactive and active states that is shifted towards the active state by calcium, our model allows for calmodulin activity even when bound to less than four calcium ions. One can see the extent of this by looking at what fraction of sub-saturated calmodulin becomes activated. As shown above, about 75 % of calmodulin molecules are active even when only two molecules of calcium are bound. This can explain experiments with mutant calmodulin showing that even when two of the calcium binding sites are ablated, calmodulin can still activate CaMKII to a certain extent (Shifman *et al.*, 2006). It is also consistent with experimental data showing that conformational transitions exist in *apo* calmodulin (Tjandra *et al.*, 1995), and that both *apo* calmodulin and calmodulin bound to only one calcium ion can exist in open and closed states (Malmendal *et al.*, 1999). Finally, calmodulin open structures have been found where only one head was populated by calcium (Schumacher *et al.*, 2001).

Since purely sequential models do not allow for sub-saturated calmodulin binding to its target, they necessarily fail to account for the observation that the affinity of calmodulin for calcium increases once calmodulin is bound to a target (Burger *et al.*, 1983; Olwin *et al.*, 1984;

Shifman *et al.*, 2006). In our model, sub-saturated calmodulin can bind to its targets. The apparent increase in affinity for calcium upon binding to targets arises from the fact that targets act as allosteric activators, drawing the equilibrium towards the high-affinity R state.

A calmodulin model that allows for target binding by sub-saturated forms of calmodulin has been proposed in a study about calmodulin binding to cyclic nucleotide phosphodiesterase (Huang *et al.*, 1981). The increased affinity of calmodulin for calcium in the presence of target was modelled by assigning higher calcium affinities to target-bound calmodulin, but without providing a mechanistic explanation.

Note that a simple model based on thermal equilibrium has been proposed before (Czerlinski, 1984), although based on sequential bindings of calcium. Furthermore, the author did not try to estimate parameters using experimental information, or to validate the model.

Experimental support for our model has recently been published by Gsponer *et al.* (2008).

4.4.2 *Structural considerations*

It is important to notice that the conformation of calmodulin which we call the T state is not necessarily exactly identical to the reported *apo* structure (Kuboniwa *et al.*, 1995) of calmodulin. Rather, the T state represents a collection of structures that may differ somewhat in the conformation of the calcium binding sites, but whose overall structure resembles that of what has been called *apo* calmodulin. The existence of an ion-bound form that resembles the *apo* conformation has recently been established (Warren *et al.*, 2007). Likewise, the R state is a collection of structures that resemble the reported open structure of active calmodulin (Babu *et al.*, 1988; Fallon and Quiocho, 2003). Asymmetric forms of calmodulin with one lobe in an open state and one lobe in a closed state have been reported in the presence of some targets (Drum *et al.*, 2002). However, the binding mechanism of these targets differs from that of CaMKII and PP2B, where both lobes are involved in target binding.

4.4.3 *Lisman hypothesis*

The model proposed here explains how different amounts of calcium can trigger the activation of either PP2B or CaMKII, and thus provides support for the Lisman hypothesis (Lisman, 1989) on a molecular level. The question of how different *frequencies* of calcium signals lead to differential activation of PP2B or CaMKII is not addressed in the model. It has been suggested, however, that, at least under some conditions, high frequencies of calcium input result in high local concentrations of calcium, while low calcium frequencies result in moderate local calcium concentrations in the spine (Bhalla, 2002; Franks *et al.*, 2001; Gamble and Koch, 1987). This seems plausible given the relative concentrations of calcium and calcium-binding proteins in a dendritic spine. After a calcium spike, the local calcium concentration rises to about $1 - 2 \times 10^{-6}\,M$ (reviewed in Hook and Means, 2001), which is much lower than that of calcium-binding proteins: The concentration of calmodulin alone is about an order of magnitude higher (Kakiuchi *et al.*, 1982). Calcium in the spine will therefore be buffered away quite quickly, which means that high frequencies of calcium influx are needed in order to achieve high amounts of free calcium. In addition, calcium frequency has a direct impact on CaMKII, because of the requirement for two adjacent subunits to be active for autophosphorylation at Thr^{286}, which confers constitutive activity (De Koninck and Schulman, 1998; Dosemeci and Albers, 1996; Dupont *et al.*, 2003). Other factors the model does not account for include variations in the subcellular localisation of PP2B (reviewed in Colbran, 2004) and CaMKII (Bayer *et al.*, 2006) and the inhibitory effect of PP2B on CaMKII (reviewed in Groth *et al.*, 2003). The latter effect, if included, would increase the window of calcium concentrations at which PP2B is preferably activated, enhancing the distinction between PP2B and CaMKII activation. We believe, however, that our model provides a valid and useful biophysical basis on which to develop further models of synaptic plasticity mechanisms.

4.4.4 *Re-using the model*

The model presented here is a mechanistic model of regulation of calmodulin activity by calcium, based on first principles and experimental biochemical and structural knowledge. Although fairly large, this model could be reused in further quantitative models of signalling pathways. For instance one could create a "module" that would only take as inputs the concentrations of calcium, of calmodulin, and a vector of triplets containing the concentration of a target, plus its affinities for calmodulin R and T states. This module could then be "plugged" into any model requiring calmodulin. Alternatively, a more abstract version can easily be created by computing the proportion of R, R1, R2, R3 and R4 as a function of calcium concentration, and writing an assignment rule that computes the total concentration of active calmodulin. In a similar fashion, an assignment rule can be created which computes $\bar{R}$ and $\bar{Y}$ as a function of calcium concentration using the equations presented in chapter 3 on page 19.

Contributions

A modified version of this chapter has been published (Stefan *et al.*, 2008). I designed the model and simulations together with Nicolas Le Novère and implemented it in COPASI. Stuart Edelstein and Nicolas Le Novère helped me develop a strategy for parameter determination. Stuart Edelstein helped me with constructing the free energy diagram and with data analysis. All three of us wrote the publication together.

5

LIGAND DEPLETION AND COOPERATIVITY

5.1 Introduction

Many biological processes are tightly regulated by cooperative protein-protein or protein-ligand interactions involving multi-site proteins that transduce signals via conformational isomerisation (Bray and Duke, 2004; Changeux and Edelstein, 2005; Goldbeter and Koshland, 1981; Monod *et al.*, 1965). Ultra-sensitivity in such processes occurs through non-independent interactions of the sites (cooperativity). The non-linear properties of an ultra-sensitive system define a dynamic range of signal intensities for which the responses vary. Cooperativity is generally evaluated by the Hill coefficient, n_H (Hill, 1910), with n_H obtained as the slope of the Hill plot, $\log \frac{\bar{Y}}{1-\bar{Y}}$ versus $\log[X]$, where $\bar{Y}$ is the fractional occupancy of the binding site and $[X]$ is the concentration of ligand (Edelstein, 1971; Monod *et al.*, 1965). The value of n_H provides an empirical index of cooperativity: its upper limit is the number of interacting sites and it is directly related to non-cooperative systems, because for a monomeric protein with a single site, $n_H = 1$. Application of the Hill coefficient has been used to characterise many cooperative biological processes. However, for conformational isomerisation of a multi-site protein, n_H is not a reliable measure of cooperativity. This is illustrated with classical studies on the allosteric enzyme aspartate transcarbamylase (ATCase).

5.1.1 *Example: ATCase*

Following the formulation of the two-state MWC model (Monod *et al.*, 1965), it was recognised that under certain conditions, the graphs for ligand binding ($\bar{Y}$) and change of conformational state ($\bar{R}$) as a function of ligand concentration would not overlap (Rubin and Changeux, 1966). In a classic study, the direct binding of succinate ($\bar{Y}$) was compared to succinate-dependent conformational change ($\bar{R}$) (Changeux

and Rubin, 1968; Gerhart and Schachman, 1968). ATCase was initially characterised as a tetramer, but later studies revealed a hexamer (Weber, 1968; Wiley and Lipscomb, 1968) and subsequent structural studies have thoroughly characterised the two hexameric conformational states, T and R, and their concerted interconversion (Fetler *et al.*, 2007; Kantrowitz and Lipscomb, 1990). Using the parameters of the MWC model established for the binding and conformational state data on the basis of four sites, the theoretical curves were recalculated with six sites, as presented in figure 12 on page 63 (solid lines). Under the experimental conditions employed, the curve for $\bar{R}$ is substantially to the left of the curve for $\bar{Y}$, which constitutes strong evidence of a conformational equilibrium pre-existing to ligand binding (Changeux and Rubin, 1968). The Hill coefficients were determined at 50 % for both the $\bar{Y}$ and $\bar{R}$ curves. While the value of $n_H = 1.24$ for $\bar{Y}$ is a reliable measure of cooperativity, the value of $n_H = 1.12$ for $\bar{R}$ dramatically underestimates its cooperativity.

5.2 Introducing a new index of cooperativity

5.2.1 *Equivalent monomer*

In order to establish the true cooperativity in systems with conformational isomerisation, the reference state should be the equivalent monomer, characterised by the same intrinsic affinities for ligand of the R and T states as the protein. The equivalent monomer is defined as follows: Its affinity for the ligand in each state is the geometric mean of the affinities of all binding sites in that respective state:

$$K_{em}^{R} = \sqrt[n]{K_1^R K_2^R \dots K_n^R} \tag{5.1}$$

$$K_{em}^{T} = \sqrt[n]{K_1^T K_2^T \dots K_n^T} \tag{5.2}$$

where n is the number of ligand binding sites of the protein. As a consequence, c_{em} is the geometric mean of all individual c values for each binding site:

$$c_{em} = \sqrt[n]{c_1 c_2 \dots c_n} \tag{5.3}$$

The allosteric isomerisation constant for the equivalent monomer, λ, is related to that of the full protein by

$$\lambda = \sqrt[n]{L} \tag{5.4}$$

This reflects the fact that the energy of isomerisation is divided by the number of subunits.

Hence, ligand binding ($\bar{Y}^*$) and conformational transition ($\bar{R}^*$) for the equivalent monomer can be expressed, respectively, as follows:

$$\bar{Y}^* = \frac{\frac{[X]}{K_{em}^R} + \lambda c_{em} \frac{[X]}{K_{em}^R}}{\left(1 + \frac{[X]}{K_{em}^R}\right) + \lambda \left(1 + c_{em} \frac{[X]}{K_{em}^R}\right)} \tag{5.5}$$

$$\bar{R}^* = \frac{1}{1 + \lambda \Omega_{em}} \tag{5.6}$$

with $\Omega_{em} = \frac{1 + c_{em} \frac{[X]}{K_{em}^R}}{1 + \frac{[X]}{K_{em}^R}}$, $[X]$ the concentration of ligand, and all other variables as defined above.

Case of identical binding sites

If all binding sites are identical, this means that the ligand affinity of the equivalent monomer is the same as for each individual binding site on the original protein. The same holds for c_{em} and, of course, K_{em}^R. Hence, $\Omega_{em} = \Omega$. We can now examine the intersection between the curves for conformational transition of the protein ($\bar{R}$) and its equivalent monomer ($\bar{R}^*$), i. e. the point where $\bar{R} = \bar{R}^*$.

$$\begin{aligned}
\bar{R} &= \bar{R}^* \\
\tfrac{1}{1+L\Omega^n} &= \tfrac{1}{1+\lambda\Omega} \\
\tfrac{1}{1+(\lambda\Omega)^n} &= \tfrac{1}{1+\lambda\Omega} \\
1+\lambda\Omega &= 1+(\lambda\Omega)^n \\
\lambda\Omega &= 1 \\
\lambda &= \tfrac{1}{\Omega}
\end{aligned}$$

This provides an alternative definition of λ for proteins with identical binding sites: It equals the value of $\frac{1}{\Omega}$ where the protein and its equivalent monomer cross. At this point then,

$$\begin{aligned}
\bar{R}^* &= \tfrac{1}{1+\lambda\Omega} = \\
&= \tfrac{1}{2} = \bar{R}
\end{aligned} \tag{5.7}$$

Hence, $\bar{R}$ and $\bar{R}^*$ cross exactly at half-saturation. Note that this only holds for proteins in which all binding sites are identical. For reasons of simplicity, the analytical calculations in the next sections are only performed for proteins with identical binding sites. The case of non-identical binding sites will, however, be kept in mind and an example will be presented later (see section 5.2.5 on page 64).

5.2.2 *Hill coefficients for the equivalent monomer*

In order for the Hill coefficient to be a reliable measure of cooperativity, we would expect it to be equal to 1 for the equivalent monomer. If we look at ligand binding, this is indeed the case:

$$\begin{aligned}
\tfrac{\bar{Y}^*}{1-\bar{Y}^*} &= \frac{\frac{\frac{[X]}{K^{\bar{R}}}+\lambda c\frac{[X]}{K^{\bar{R}}}}{1+\frac{[X]}{K^{\bar{R}}}+\lambda(1+c\frac{[X]}{K^{\bar{R}}})}}{\frac{1+\frac{[X]}{K^{\bar{R}}}+\lambda(1+c\frac{[X]}{K^{\bar{R}}})-\frac{[X]}{K^{\bar{R}}}-\lambda c\frac{[X]}{K^{\bar{R}}}}{1+\frac{[X]}{K^{\bar{R}}}+\lambda(1+c\frac{[X]}{K^{\bar{R}}})}} = \\
&= \frac{\frac{[X]}{K^{\bar{R}}}+\lambda c\frac{[X]}{K^{\bar{R}}}}{1+\frac{[X]}{K^{\bar{R}}}+\lambda+\lambda c\frac{[X]}{K^{\bar{R}}}-\frac{[X]}{K^{\bar{R}}}-\lambda c\frac{[X]}{K^{\bar{R}}}} = \frac{\frac{[X]}{K^{\bar{R}}}+\lambda c\frac{[X]}{K^{\bar{R}}}}{1+\lambda}
\end{aligned}$$

$$\begin{aligned}
\frac{d\log\left(\frac{\bar{Y}^*}{1-\bar{Y}^*}\right)}{d\log[X]} &= \frac{d}{d\log[X]}\log\left(\frac{\frac{[X]}{K^R}+\lambda c\frac{[X]}{K^R}}{1+\lambda}\right) = \\
&= \frac{d}{d\log[X]}\log\left([X]\frac{1+\lambda c}{K^R(1+\lambda)}\right) = \\
&= \frac{d}{d\log[X]}\left(\log[X]+\log\frac{1+\lambda c}{K^R(1+\lambda)}\right) = \\
&= \frac{d}{d\log[X]}\log[X] = 1
\end{aligned}$$

However, computing the Hill coefficient for $\bar{R}^*$ gives a different result:

$$\frac{\bar{R}^*}{1-\bar{R}^*} = \frac{\frac{1}{1+\lambda\Omega}}{\frac{1+\lambda\Omega-1}{1+\lambda\Omega}} = \frac{1}{\lambda\Omega}$$

$$\begin{aligned}
\frac{d}{d\log[X]}\log\frac{\bar{R}^*}{1-\bar{R}^*} &= \frac{d}{d\log[X]}\log\left(\frac{1}{\lambda\Omega}\right) = \\
&= \frac{d}{d\log[X]}\log 1 - \frac{d}{d\log[X]}\log\lambda - \frac{d}{d\log[X]}\log\Omega = \\
&= \frac{d}{d\log[X]}\log\frac{1}{\Omega} = \\
&= \Omega\frac{d}{d\log[X]}\left(\frac{1}{\Omega}\right) = \\
&= \Omega\frac{d}{d\log[X]}\left(\frac{1+\frac{[X]}{K^R}}{1+c\frac{[X]}{K^R}}\right)
\end{aligned}$$

Defining $\log[X] := a$, we get

$$\begin{aligned}
\frac{d}{da}\log\frac{\bar{R}^*}{1-\bar{R}^*} &= \Omega\frac{d}{da}\frac{1+\frac{e^a}{K^R}}{1+c\frac{e^a}{K^R}} = \\
&= \Omega\frac{\frac{1}{K^R}e^a\left(1+c\frac{e^a}{K^R}\right)-\left(1+\frac{e^a}{K^R}\right)c\frac{e^a}{K^R}}{\left(1+c\frac{e^a}{K^R}\right)^2} = \\
&= \frac{1+c\frac{[X]}{K^R}}{1+\frac{[X]}{K^R}}\frac{\frac{[X]}{K^R}+c\frac{[X]^2}{(K^R)^2}-c\frac{[X]}{K^R}-c\frac{[X]^2}{(K^R)^2}}{\left(1+c\frac{[X]}{K^R}\right)^2} = \frac{\frac{[X]}{K^R}-c\frac{[X]}{K^R}}{\left(1+\frac{[X]}{K^R}\right)\left(1+c\frac{[X]}{K^R}\right)}
\end{aligned}$$

This expression is positive since $c < 1$.
A higher limit for this expression can be estimated as follows:

$$\begin{array}{ccccc} \frac{\frac{[X]}{K^R}-c\frac{[X]}{K^R}}{(1+\frac{[X]}{K^R})(1+c\frac{[X]}{K^R})} & < & \frac{\frac{[X]}{K^R}}{(1+\frac{[X]}{K^R})(1+c\frac{[X]}{K^R})} & < & \\ & < & \frac{\frac{[X]}{K^R}}{1+\frac{[X]}{K^R}} & < & 1 \end{array}$$

Thus, the Hill coefficient for the equivalent monomer is always smaller than one, meaning that it systematically underestimates the cooperativity of conformational change. Moreover, the Hill coefficient does not vary with the intrinsic parameter of the conformational isomerisation, L (Karlin, 1967). This indicates that the Hill coefficient is not suitable as a measure of cooperativity for conformational isomerisation of an allosteric protein. We have therefore replaced the Hill analysis for conformational isomerisation by a new cooperativity index, ν, based on the ratio of the derivatives of functions for $\bar{R}$ and $\bar{R}^*$.

5.2.3 *Deriving ν*

The derivative of $\bar{R}$ can be computed as follows:

$$\begin{array}{rcrcl} \frac{d\bar{R}}{d[X]} & = & \frac{d}{d[X]}\frac{1}{1+L\Omega^n} & = & \\ & = & -\frac{1}{(1+L\Omega^n)^2}\frac{d}{d[X]}\left(1+L\Omega^n\right) & = & \\ & = & -\frac{1}{(1+L\Omega^n)^2}nL\Omega^{n-1}\frac{d}{d[X]}\Omega & = & \\ & = & -\frac{nL\Omega^{n-1}}{(1+L\Omega^n)^2}\frac{d}{d[X]}\frac{1+c\frac{[X]}{K^R}}{1+\frac{[X]}{K^R}} & = & \\ & = & -\frac{nL\Omega^{n-1}}{(1+L\Omega^n)^2}\frac{c-1}{(1+\frac{[X]}{K^R})^2K^R} & = & \frac{nL\Omega^{n-1}(1-c)}{(1+L\Omega^n)^2(1+\frac{[X]}{K^R})^2K^R} \end{array}$$

In a similar manner, the derivative of $\bar{R}^*$ can be computed as follows:

$$\begin{array}{rcrcl} \frac{d\bar{R}^*}{d[X]} & = & \frac{d}{d[X]}\frac{1}{1+\lambda\Omega} & = & \\ & = & -\frac{1}{(1+\lambda\Omega)^2}\frac{d}{d[X]}(1+\lambda\Omega) & = & \\ & = & -\frac{\lambda}{(1+\lambda\Omega)^2}\frac{c-1}{(1+\frac{[X]}{K^R})^2K^R} & = & \frac{\lambda(1-c)}{(1+\lambda\Omega)^2(1+\frac{[X]}{K^R})^2K^R} \end{array}$$

The true cooperativity or amplification of the signal reflected by the properties of $\bar{R}$ can then be obtained by a new parameter, represented by the coefficient ν and calculated from the ratio of the two derivatives above:

$$\nu = \frac{\frac{d\bar{R}}{d[X]}}{\frac{d\bar{R}^*}{d[X]}} \tag{5.8}$$

This simplifies to:

$$\nu = \frac{n(1+\lambda\Omega)^2(\lambda\Omega)^{n-1}}{(1+(\lambda\Omega)^n)^2} \tag{5.9}$$

For a monomer ($n = 1$), it is easy to see that $\nu = 1$. The coefficient ν thus gives the cooperativity of conformational change of the oligomer in a manner analogous to n_H (the Hill coefficient) for the binding function ($\bar{Y}$), which describes cooperativity with respect to a monomer that in every case displays a value of $n_H = 1$.

In order to estimate the range of ν, we first look at the cases where $\lambda\Omega < 1$ or $\lambda\Omega > 1$ (note that $\lambda\Omega$ is always positive). If two constants a and b are *both* greater than one or *both* smaller than one, then the following inequality holds:

$$1 + ab > a + b$$

In our case, for any exponent $n > 1$, if $\lambda\Omega > 1$, so are $(\lambda\Omega)^{n+1}$ and $(\lambda\Omega)^{n-1}$. And likewise, if $0 < \lambda\Omega < 1$, then this also holds for $(\lambda\Omega)^{n+1}$ and $(\lambda\Omega)^{n-1}$. Therefore, we can apply the above inequality and obtain:

$$
\begin{aligned}
(\lambda\Omega)^{n-1} + (\lambda\Omega)^{n+1} &< 1 + (\lambda\Omega)^{n-1}(\lambda\Omega)^{n+1} \\
(\lambda\Omega)^{n-1} + (\lambda\Omega)^{n+1} &< 1 + (\lambda\Omega)^{2n} \\
(\lambda\Omega)^{n-1} + 2(\lambda\Omega)^{n} + (\lambda\Omega)^{n+1} &< 1 + 2(\lambda\Omega)^{n} + (\lambda\Omega)^{2n} \\
(1 + 2\lambda\Omega + (\lambda\Omega)^2)(\lambda\Omega)^{n-1} &< (1 + (\lambda\Omega)^n)^2 \\
(1 + \lambda\Omega)^2(\lambda\Omega)^{n-1} &< (1 + (\lambda\Omega)^n)^2 \\
\frac{(1+\lambda\Omega)^2(\lambda\Omega)^{n-1}}{(1+(\lambda\Omega)^n)^2} &< 1 \\
\nu &< n
\end{aligned}
$$

Therefore, ν is always smaller than n when $\lambda\Omega \neq 1$. If $\lambda\Omega = 1$, then $\nu = n$, as can be seen from equation 5.9 on the previous page. As seen before, $\lambda\Omega = 1$ where both $\bar{R}$ and $\bar{R}^*$ reach half-maximal activation. In other words, for a multi-site protein that undergoes a concerted conformational transition, as defined by the MWC model (Monod *et al.*, 1965), the maximal cooperativity is always equivalent to the number of ligand-binding sites present and may be grossly underestimated on the basis of the Hill coefficient. This property reflects the absolute linkage, or infinite junctional energy, between binding sites in the MWC framework (Duke *et al.*, 2001).

Again, the property that the maximal cooperativity is always equal to the number of binding sites only holds for proteins with identical binding sites. If binding sites are different, this is not necessarily the case, as will be seen in the example of calmodulin below.

5.2.4 *Application to the ATCase example*

Considering again the case of ATCase as an example, it can be observed that with respect to ligand binding, the curves for $\bar{Y}$ and $\bar{Y}^*$ are similar and characterised by Hill coefficients of $n_H = 1.241$ and $n_H = 1.000$, respectively. In contrast, the $\bar{R}^*$ curve, with a Hill coefficient of $n_H = 0.19$ is much less cooperative, as shown in figure 12 on the facing page.

Applying our new method to ATCase by calculating the derivative functions for $\bar{R} = \bar{R}^* = 0.5$, the values of the derivatives are 0.710 and 0.118, respectively, with a ratio of 6.0. Therefore, the revised analysis

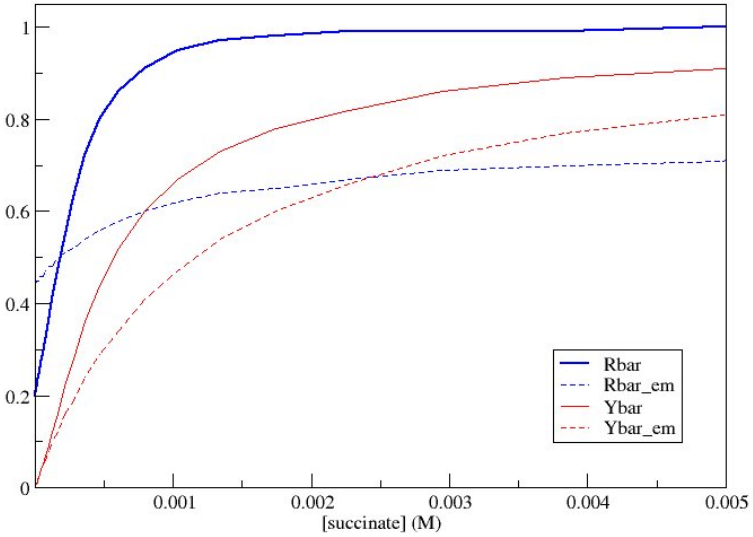

Figure 12: Ligand binding and conformational change in ATCase. Curves for $\bar{R}$ and $\bar{R^*}$ (in blue) and $\bar{Y}$ and $\bar{Y^*}$ (in red) as a function of succinate concentration (in M); the curves for $\bar{R^*}$ and $\bar{Y^*}$ are dashed. While curves for $\bar{R}$ and $\bar{R^*}$ cross at $[\text{succinate}]_{50}$ (defined by $[\text{succinate}]_{50} = K^R \frac{\lambda-1}{1-\lambda c}$) with a value of 0.5 at this point (see equation 5.7 on page 58), the curves for $\bar{Y}$ and $\bar{Y^*}$ cross at the same succinate concentration, but their value is $\bar{Y} = \bar{Y^*} = \frac{\lambda+\lambda c(\lambda-1)-1}{2\lambda(1-c)}$, which only equals 0.5 for $\lambda = \sqrt{\frac{1}{c}}$. For the conditions of this figure, $\bar{Y} = \bar{Y^*} = 0.19$ at the cross point. The original analysis based on the MWC model with four subunits used the values of $K_R = 4.75 \times 10^{-4}\, M$, $L = 4$ and $c = 0.001$ (Changeux and Rubin, 1968). The model was re-analysed by generating theoretical curves with the original parameters for a tetramer and performing a least-squares fit to obtain the best parameters for the hexamer, resulting in a change of the value of c to 0.26, when K_R and L were unchanged.

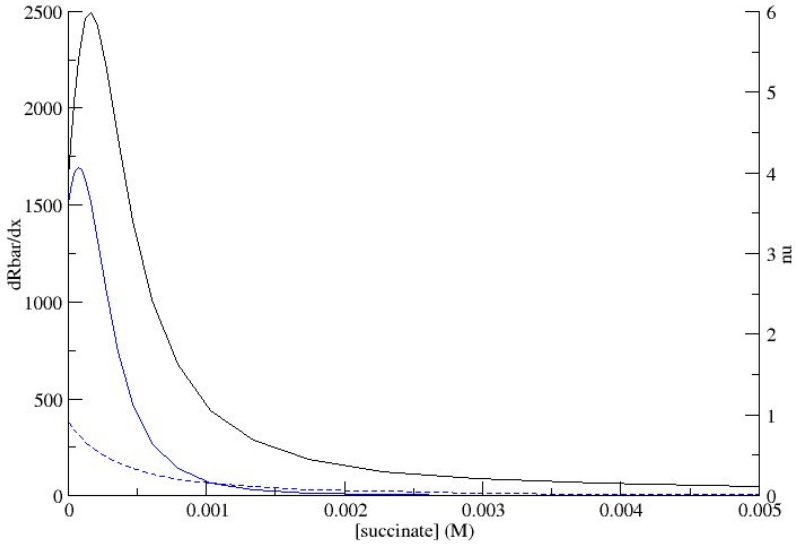

Figure 13: New measure of cooperativity for ATCase based on equivalent monomer. Values of ν in black corresponding to the right ordinate and values of the derivatives $\frac{d\bar{R}}{d[X]}$ and $\frac{d\bar{R}^*}{d[X]}$ in blue corresponding to the left ordinate, with the latter as a dashed curve.

of ATCase illustrates that the true cooperativity at $\bar{R} = 0.5$ for a protein with identical binding sites is maximal and equal to the number of binding sites, n.

5.2.5 *Example with non-identical binding sites: calmodulin*

An example of a protein with non-identical ligand binding sites is calmodulin. Calmodulin exists as a relatively small monomer, but with four calcium binding sites. An analysis based on the MWC model has recently been presented (Stefan *et al.*, 2008) (see chapter 4 on page 31). For this study, an equivalent monomer for calmodulin was constructed as described above; the full list of parameters is given in table 5 on page 66. Analysis was carried out using python (`http://www.python.org/`); a flowchart of operations is seen in figure 14 on the next page. Results were plotted using grace (`http://plasma-gate.weizmann.ac.il/Grace/`).

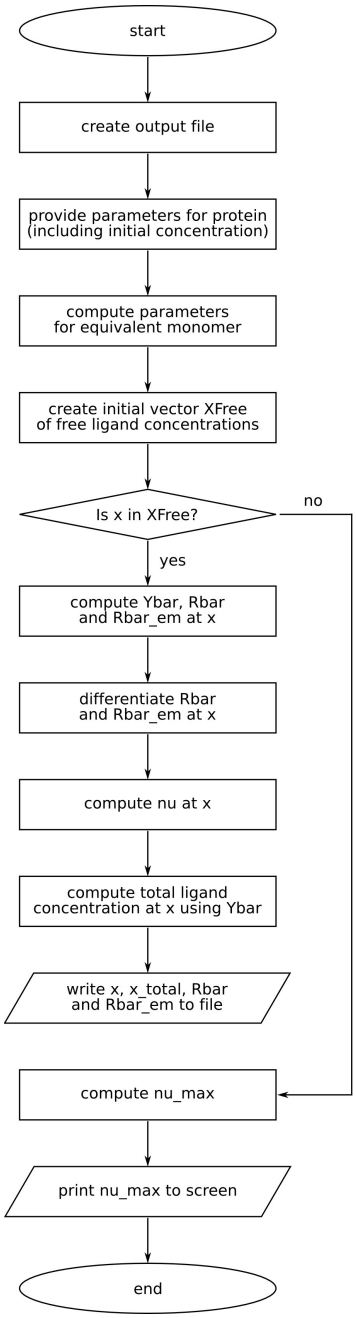

Figure 14: Flowchart for simple cooperativity calculations, used for the calmodulin model. The programme calculates $\bar{R}$, $\bar{R}^*$, their respective derivatives, and ν at each calcium concentration in a given range, and writes the results to an output file.

full calmodulin	
K_A^R	$8.32 \times 10^{-6}\,\mathrm{M}$
K_B^R	$1.66 \times 10^{-8}\,\mathrm{M}$
K_C^R	$1.74 \times 10^{-5}\,\mathrm{M}$
K_D^R	$1.45 \times 10^{-8}\,\mathrm{M}$
L	20670
equivalent monomer	
K_{em}^R	$4.32 \times 10^{-7}\,\mathrm{M}$
λ	12

Table 5: Parameters used for calmodulin and its equivalent monomer. K_i^R and L for calmodulin as described in Chapter 4 on page 31, K_{em}^R and λ obtained as described above.

Figure 15 on the facing page shows $\bar{R}$ both for full calmodulin and for its equivalent monomer. Note that in this case, the two curves do not cross at $\bar{R} = \frac{1}{2}$. In addition, the maximal cooperativity ν_{max} is not equal to the number of binding sites. In the case of calmodulin, the maximal cooperativity ν_{max} is 2.04. This is consistent with previous studies indicating that the organisation of calmodulin into two globular domains might affect its cooperativity (Linse *et al.*, 1991).

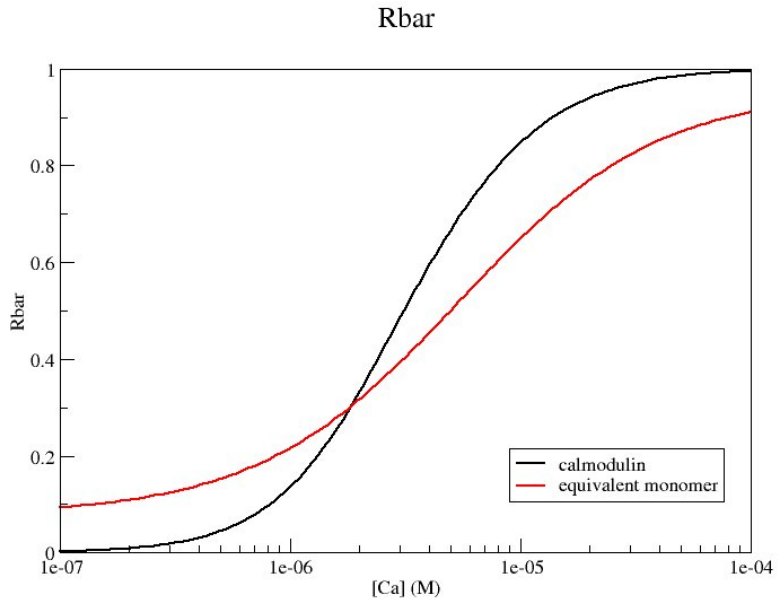

Figure 15: $\bar{R}$ for calmodulin and its equivalent monomer as a function of calcium concentration. Calmodulin is shown in black, the equivalent monomer in red. Note that the two curves do not cross at $\bar{R} = \frac{1}{2}$. Calmodulin concentration used was 10^{-7} M.

5.3 Ligand depletion

For various signal transduction systems, cooperativity can be modulated by ligand depletion effects. Ligand depletion is significant for concentrations of a receptor that are close to the dissociation constant for its ligand, resulting in the free concentration of the ligand being significantly below the total concentration that is the actual input signal. This effect can be particularly important under *in vivo* conditions, where most proteins and dissociation constants are within the nano- to micro-molar range. Using the new cooperativity index ν, we will introduce a new measure for the effect of ligand depletion and illustrate the consequences of ligand depletion using calmodulin as an example.

The new measure of the effect of ligand depletion, $\nu_{apparent}$ normalises ν_{max} using the ratio of two maximal slopes: The maximal slope of $\bar{R}$ with respect to total ligand and the maximal slope of $\bar{R}$ with respect to free ligand.

$$\nu_{apparent} = \nu_{max} \frac{\left(\frac{d\bar{R}}{d[X]_{total}}\right)_{max}}{\left(\frac{d\bar{R}}{d[X]_{free}}\right)_{max}} \tag{5.10}$$

Under undepleted conditions, $\nu_{apparent} = \nu_{max}$; with increasing ligand depletion, $\nu_{apparent}$ will approach zero. $\nu_{apparent}$ therefore provides a measure of the extent to which ligand depletion affects cooperativity.

5.3.1 *Ligand depletion for calmodulin*

Calmodulin concentrations used for the model presented earlier (Stefan *et al.*, 2008) (Chapter 4 on page 31) were in the range of $10^{-7}\,M$, a concentration in which the effect of ligand depletion can presumably be ignored. The *in vivo* concentration of calmodulin, however, is about $5 \times 10^{-5}\,M$ in dendritic spines (Gamble and Koch, 1987). An easy illustration of ligand depletion is to plot $\bar{R}$ twice on the same graph: Once as a function of total ligand concentration and once as a function of free ligand concentration. If ligand depletion is negli-

gible, both curves should coincide. The stronger the effect of ligand depletion, the bigger the difference between the two curves.

The total ligand concentration was computed from the free ligand concentration and calmodulin concentration using the formula

$$[X]_{total} = X_{free} + 4[CaM]\bar{Y}$$

As above, analyses were carried out using python (`http://www.python.org/`) – a flowchart describing the script is shown in figure 16 on the following page – and results were plotted with grace (`http://plasma-gate.weizmann.ac.il/Grace/`).

Figure 18 on page 72 and figure 17 on page 71 show the difference between depleted and undepleted conditions. Note that, while ligand depletion results in a decrease in cooperativity, it increases the dynamic range of signal response (illustrated here by showing the range of signal concentrations that elicit between 10 % and 90 % of the maximal response).

Figure 19 on page 73 shows the effect of ligand depletion on $\nu_{apparent}$: With increasing calmodulin concentration, $\nu_{apparent}$ decreases, i. e. the effect of ligand depletion on cooperativity is more pronounced.

Therefore, even for signalling systems with low cooperativity, ligand depletion effects can be important and ignoring such effects can lead to biased interpretations.

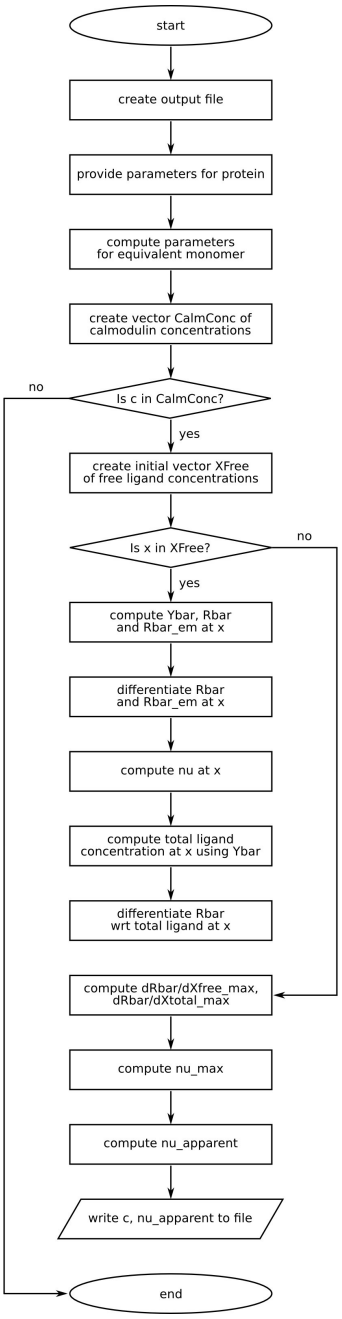

Figure 16: Flowchart for determining $\nu_{apparent}$, used for the calmodulin model. The programme loops over calcium concentrations in a given range to calculate $\nu_{apparent}$ at different calmodulin concentrations.

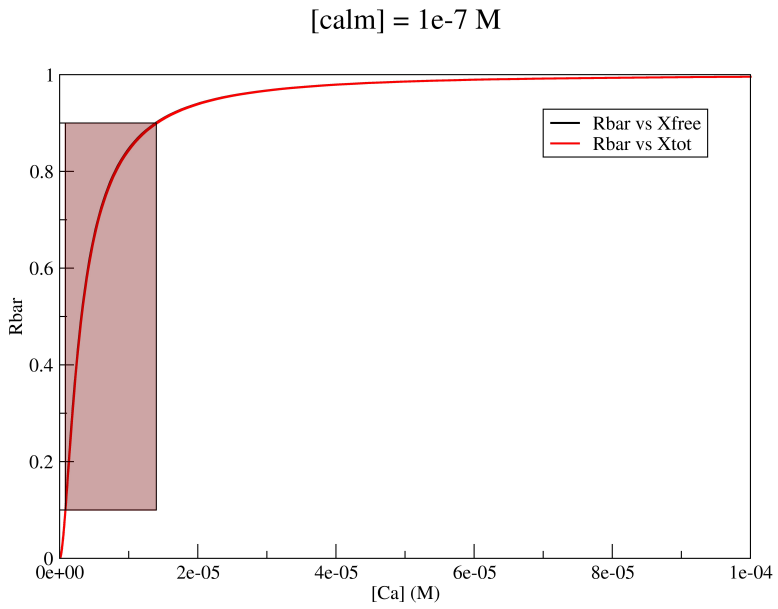

Figure 17: $\bar{R}$ without ligand depletion. This figure shows $\bar{R}$ as a function of free ligand concentration (black curve) and as a function of total ligand concentration (red curve) at a low calmodulin concentration ($10^{-7}\,M$). Total and free ligand concentration are nearly the same, so both curves for $\bar{R}$ coincide. The box shows the dynamic range, defined here as the range of signal concentrations that yield between 10 % and 90 % of the maximal response.

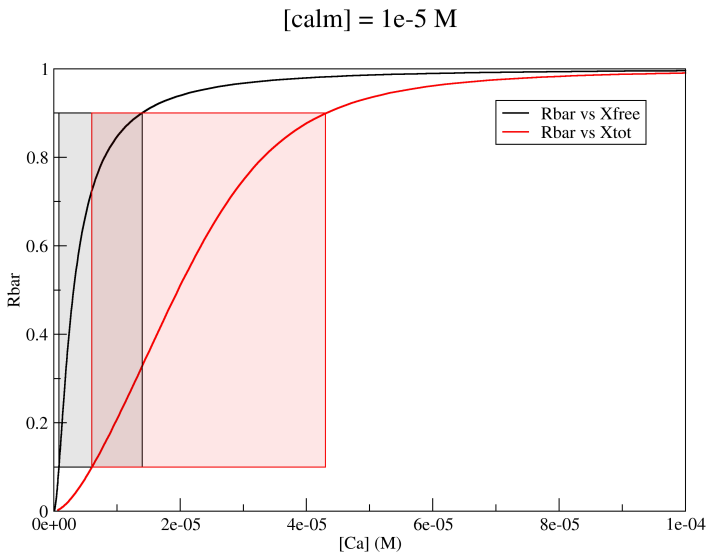

Figure 18: $\bar{R}$ under conditions of ligand depletion. This figure shows $\bar{R}$ as a function of free ligand concentration (black curve) and as a function of total ligand concentration (red curve) at a high calmodulin concentration ($1 \times 10^{-5}\,M$). Total and free ligand concentration are substantially different, so there is a shift between $\bar{R}$ as a function of free ligand concentration and $\bar{R}$ as a function of total ligand concentration. Boxes show the dynamic range of signal response, as defined above, as a function of free (gray box) or total (red box) ligand concentration.

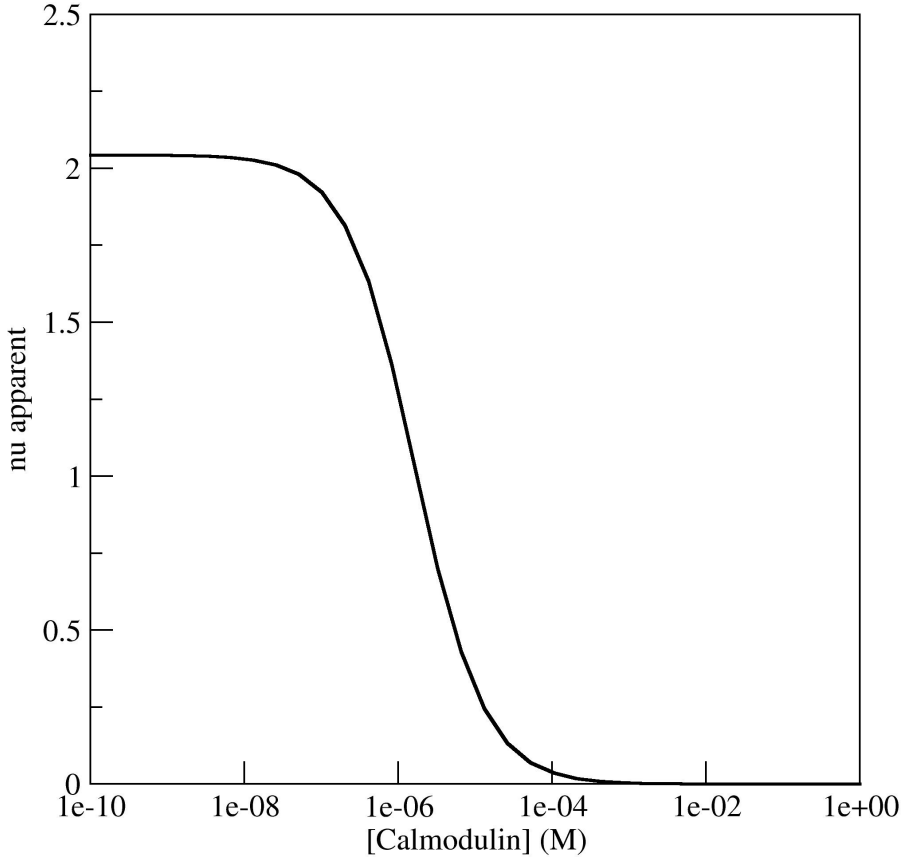

Figure 19: Effect of ligand depletion on calmodulin cooperativity. Each data point represents $\nu_{apparent}$ for a given calmodulin concentration. Note that $\nu_{apparent} = \nu_{max}$ at small concentrations of calmodulin, but $\nu_{apparent} \to 0$ as calmodulin concentrations increase.

5.4 Conclusions and discussion

The Hill coefficient may be an adequate measure for the cooperativity of ligand binding, but it underestimates the cooperativity of conformational change. We therefore propose an alternative index for cooperativity, ν, based on the notion of a non-cooperative "equivalent monomer".

For proteins with identical subunits, this index is maximal and equal to the number of subunits where the conformational transition reaches half-saturation. Note that in other concentration regimes, ν is smaller than ν_{max}. In terms of biology, this means that the available ligand concentration determines the cooperativity of ligand binding. The same protein can thus show different cooperativity patterns in different biological contexts, e. g. different tissues or different stages of a biological process.

For proteins with non-identical binding sites, ν_{max} is, in general, smaller than the number of binding sites. Thus, for these proteins ν_{max} provides a measure for maximal cooperativity which is not obvious from the number of binding sites.

Using the new index of cooperativity, ν, we have investigated the effect of ligand depletion on the apparent cooperativity of a system and show that while the apparent maximum cooperativity decreases, the dynamic range of signal response widens under conditions of ligand depletion. This is exemplified by calmodulin, where ligand depletion is common under physiological conditions (Gamble and Koch, 1987).

The concentration of most signalling proteins is not very different from their dissociation constants, in the nano- to micro-molar range. It is known that the available pools can be quickly modified by segregation, inhibition or change in expression. We propose that the use of ligand depletion could be a widespread mechanism for the cell to quickly adapt non-linear properties and sensitivity ranges to evolving environmental conditions.

Contributions

A modified version of this chapter has been submitted for publication. Stuart Edelstein and Nicolas Le Novère developed the definition of the equivalent monomer and of ν. I performed all the algebraic derivations. Stuart Edelstein performed the analysis of ATCase. All three of us worked on the problem of finding a measure for ligand depletion. I wrote the python scripts in order to perform analysis on the calmodulin model; Stuart Edelstein independently analysed the calmodulin model to allow for cross-validation. All three of us discussed and analysed results and contributed to the manuscript.

6

CONCLUSIONS: EXTENDING AND APPLYING ALLOSTERIC THEORY

6.1 Generalised MWC framework

The classic version of the MWC framework (Monod *et al.*, 1965) was developed for proteins composed of identical subunits containing one ligand binding site each. It is conceivable, however, that an MWC-type mode of action is not confined to this very specific group of proteins. First, one can imagine a protein made up of identical subunits that contain more than one binding site each for a given ligand and where two binding sites on the same subunit do not necessarily have the same affinity. The binding sites can therefore be grouped into sets of binding sites with the same affinity. Taking the abstraction a step further, one could imagine that even a monomeric protein containing several non-equivalent (or not necessarily equivalent) ligand binding sites could be regulated in an MWC-type manner. Indeed, the mode of regulation of calmodulin seems to be consistent with MWC-type activation, as shown in chapter 4 on page 31.

Therefore, there is a need to extend and generalise the MWC framework to cater for non-equivalent binding sites. The general MWC framework presented in chapter 3 does just that. If the case of a protein with k different groups of m equivalent binding sites each is regarded as the most general case, then two special cases can immediately be derived from this: If $m = 1$, all binding sites are different, as is the case with calmodulin. If $k = 1$, all binding sites are equivalent, as in the classical MWC model.

It is interesting to note that in the case of calmodulin, the classical MWC assumption that an allosteric protein is composed of identical protomers no longer holds. However, calmodulin still fulfils the requirement of symmetry. (Interestingly, symmetry between binding sites, with one low-affinity and one high-affinity site on each lobe was not an assumption of the calmodulin model, but an emergent

property.) What structural conditions a protein must fulfil in order for the generalised allosteric model to be applicable to it is an issue that could be further investigated in the future. It is sure, however, that the generalisation presented here increases the set of proteins that can be investigated under the MWC framework, potentially elucidating mechanisms that have so far been poorly understood.

We have only but started to explore the consequences of a generalised allosteric model and to formulate equations and rules pertaining to it, and there is more exploration to be done in this field.

6.2 Conversion between frameworks

The advent of Systems Biology has revived interest in quantitative descriptions in biology (reviewed in Kitano, 2002). Computer systems are well equipped to handle quantitative mathematical models of ever increasing complexity. At the same time, new measurement techniques in the wetlab now allow for quantitative descriptions (e. g. counting the number of molecules of one species in one type of cell (Cheng *et al.*, 2006)) where only coarse-grained "yes/no"-type answers could be obtained in the past (reviewed in Kitano, 2002). Quantitative descriptions allow for a different level of analysis, for the detection of subtle changes, for the development and testing of hypotheses, for validation and for fine-grained distinction between alternative models.

Often, several alternative quantitative descriptions can be applied to the same biological phenomenon, and the framework chosen for a specific study will depend on the experimental or theoretical paradigm used. For instance, experimentalists measuring ligand binding to a protein often use the Adair-Klotz framework (Adair, 1925; Klotz, 1946), while modellers concerned with the allosteric regulation of the same protein might apply an MWC-type framework. With the increasing interdisciplinarity found in modern biology, this multiplicity of frameworks is likely to increase. It is, however, crucial that results are shared between scientists working on the same system, to allow for cross-validation and hypothesis testing. Therefore, there is a need for methods of translating between frameworks, e. g. of converting characteristic parameters of one framework into parameters of another.

We have suggested one such conversion, from the characteristic parameters of a generalised MWC model into the apparent association constants of an Adair-Klotz model in chapter 3 on page 19. This allows allosteric theoreticians to compare the outcomes of their models to experimental data. The calmodulin model presented in chapter 4 on page 31 gives an example of cross-validation using these conversion equations. It is, in principle, also possible to use these conversion equations for parameter determination.

The conversion equations are necessarily one-directional, because they use $(n+2)$ parameters of a generalised MWC model (intrinsic affinities for n binding sites, the allosteric isomerisation constant L and the ratio of affinities between R and T state, c) to compute n parameters of an Adair-Klotz equation (n apparent dissociation constants). In the other direction, the system is, in general, underdetermined, i. e. it is not possible to compute all parameters of an allosteric model from the characteristic parameters of an Adair-Klotz model. They can, however, be used to constrain parameter space, especially in conjunction with additional information about the allosteric properties of a protein.

6.3 An allosteric model of calmodulin

The allosteric model of calmodulin presented in chapter 4 on page 31 uses the generalised MWC framework presented in chapter 3 on page 19. It is the first model that reconciles various experimental observations that have been made with respect to calmodulin function, notably the activity of sub-saturated forms of calmodulin (Huang *et al.*, 1981; Kincaid and Vaughan, 1986; Shifman *et al.*, 2006), the increase in calcium-affinity in the presence of targets (Burger *et al.*, 1983; Olwin *et al.*, 1984; Shifman *et al.*, 2006), and the different affinities of different calcium binding sites (Crouch and Klee, 1980). Importantly, it also reproduces the preferential activation of PP2B at low calcium levels and of CaMKII at high calcium levels, thereby providing a possible molecular explanation for the Lisman hypothesis. The model also provides testable predictions which are amenable to experimental investigations.

6.3.1 *Conceptual simplicity*

With its wealth of reaction equations, the calmodulin model might seem overly – and maybe unnecessarily – complicated at first sight and the question might arise whether the characteristics of calmodulin could not be explained by means of a simpler model. I will argue, however, that the model presented here *is* indeed quite simple. This becomes obvious if the model is thought of as a set of rules, rather than a system of reaction equations. The set of rules can be written as follows:

- For any binding site, if it is not occupied, then calcium can bind to it with forward binding rate k_{on}.
- If binding site i is occupied, calcium can dissociate from it. The rate of calcium dissociation from binding site i in the R state is $k^R_{off_i}$ (for $i \in \{A, B, C, D\}$).
- Dissociation rates for the T state equal dissociation rates for the R state multiplied by c.
- If no calcium is bound, transitions from the R to the T state proceed with a rate of k_{RT}, and transitions from the T to the R state with a rate of k_{TR}; the ratio of these rates equals L.
- If i calcium ions are bound, transitions from the R to the T state proceed with a rate of $k_{RT} \times \sqrt{c^i}$, and transitions from the T to the R state with a rate of $\frac{k_{TR}}{\sqrt{c^i}}$, with $1 \leq i \leq n$.
- CaMKII binds to the R state with an association rate of $k^R_{on_{CaMKII}}$ and dissociates with a rate of $k^R_{off_{CaMKII}}$.
- PP2B binds to the R state with an association rate of $k^R_{on_{PP2B}}$ and dissociates with a rate of $k^R_{off_{PP2B}}$.
- If calmodulin is bound to either CaMKII or PP2B, there is no transition to the T state, but calcium binding and dissociation are not affected.

Seeing these rules, it is clear that the calmodulin model is conceptually quite simple. The large number of reaction equations arises from the need to enumerate every single possible combination of these

rules – a problem called "combinatorial explosion", which will be addressed in Part 2 of this thesis (see chapter 7 on page 87). In fact, the model can be thought of as a simple allosteric model for a two-state protein with four different binding sites, as described in chapter 3. The simplicity is reflected in the small number of parameters required for the model and in the fact that very few *ad hoc* assumptions have to be made. For instance, the intrinsic affinity of calcium for binding site A in the R state is always the same, no matter whether or not the other binding sites are occupied. The observed cooperativity of calcium binding to calmodulin is an emergent property arising from the presence of two states; there is no need to modify the intrinsic association constants. In this sense, this model *is* very simple and it is, indeed, hard to imagine a simpler one that could account for all the properties of calmodulin mentioned above. Although simplicity in itself is, obviously, not a criterion by which to assess the value of a model, it is widely believed that out of two models with the same explanatory power, the one that makes the smallest number of *ad hoc* assumptions is the better one. This principle – known as "Ockham's razor" – has received support from Bayesian statistics (Jefferys and Berger, 1991).

6.3.2 *Re-using the model*

An Systems Biology Markup Language (SBML) file for the calmodulin model has been deposited in BioModels Database (Le Novère *et al.*, 2006) with Model ID BIOMDoooooooo183 (`http://www.ebi.ac.uk/biomodels-main/publ-model.do?mid=BIOMD0000000183`). This can, in principle, be re-used and plugged into bigger models of postsynaptic signalling. However, for modellers only interested in the values of $\bar{Y}$ and $\bar{R}$ at a given calcium concentration, the full list of reactions is probably not necessary. Both $\bar{R}$ and $\bar{Y}$ at a given calcium concentration can be computed directly using the model parameters listed in chapter 4 and the generalised MWC equations presented in chapter 3 on page 19. Indeed, this is exactly the approach that was taken in chapter 5 on page 55 to assess the effects of ligand depletion on calmodulin activation.

6.4 Cooperativity revisited

While being an adequate measure for the cooperativity of ligand binding, the Hill coefficient is not suitable for estimating the cooperativity of conformational change in an allosteric protein, because it systematically underestimates it. Since conformational change is associated with changes in activity (e. g. in affinities for a given substrate), the Hill coefficient underestimates the cooperativity of activation itself. This is why a new measure for cooperativity is required.

We introduce a new measure of cooperativity based on the notion of an "equivalent monomer", which is defined by its affinity (the geometric mean of the affinities for each binding site of the protein) and allosteric isomerisation constant (the n^{th} root of L of the protein, where n is the number of ligand binding sites). If all binding sites are identical, this definition is equivalent to fractional conformational change for the protein ($\bar{R}$) and its equivalent monomer ($\bar{R}^*$) reaching half their maxima at the same ligand concentration. Importantly, however, this is not the case for proteins with non-identical binding sites.

The new measure for cooperativity we present, ν, uses the concept of the "equivalent monomer". For proteins with n identical binding sites, ν is maximal and exactly equal to the number of binding sites where the conformational change reaches half saturation. This is a direct consequence of how ν is defined, assuming absolute linkage between binding sites. However, at ligand concentrations other than the ones required for half-maximal saturation, ν is smaller than the number of binding sites, so calculating ν yields novel information about cooperativity at a given ligand concentration.

For proteins with non-equivalent ligand binding sites, ν_{max} is smaller than the number of binding sites, and computing both ν at a given concentration and ν_{max} yields important insights into cooperative mechanisms within the protein. This is a first theoretical result about proteins within a generalised allosteric model, as presented in chapter 3 on page 19. In terms of biology, this new measure for cooperativity has allowed us to further explore the activation of calmodulin and consequences of the model presented in chapter 4 on page 31.

6.5 Ligand depletion as a way to modulate sensitivity

Very often, a system needs to respond to a precise intensity of input. In effect the cell implements a thresholding function, transforming a linear increase of signal into a "sigmoidal" curve. This is mostly done through various forms and mechanisms of ultrasensitivity (Goldbeter and Koshland, 1984; Koshland *et al.*, 1982). One way to achieve ultrasensitivity in signalling systems is to use allosteric proteins. They effectively feature a "built-in" cooperative system based on multiple binding sites for regulators. Using the new measure for cooperativity presented in chapter 5 on page 55, we have investigated the effects of ligand depletion on the sensitivity of signal response. We show that ligand depletion reduces the cooperativity, but increases the dynamic range of signal response. This suggests that the modulation of protein concentration might be an effective measure to modulate sensitivity in biological systems.

Part II

STOCHASTIC AND AGENT-BASED MODELS OF CAMKII

7

COMBINATORIAL EXPLOSION AND STOCHASTIC MODELLING

7.1 CaMKII: a multi-state protein

CaMKII is a protein that can adopt multiple possible states. As explained earlier (see Chapter 1 on page 1), each subunit of a CaMKII holoenzyme can adopt two structural conformations: Open (active) and closed (inactive). Each subunit can bind to calmodulin, which stabilises the open state (Hanley *et al.*, 1988), we can thus distinguish between CaMKII subunits in a "calmodulin-free" and a "calmodulin-bound" state. Each subunit can be phosphorylated on various residues, of which Thr^{286} and Thr^{306} have been shown to be functionally relevant, with phosphorylation at Thr^{286} conferring autonomous activity (Hanson *et al.*, 1994) and an increase in calmodulin affinity (Meyer *et al.*, 1992), while phosphorylation at Thr^{306} provides a possible desensitisation mechanism by preventing calmodulin binding (Patton *et al.*, 1990; Colbran, 1993). Depending on what aspects of CaMKII function one is investigating, other possible states of a subunit (for instance, NMDA receptor-bound or NMDA receptor-free) or of the whole holoenzyme (e. g. within the PSD or outside the PSD) become relevant.

7.2 Combinatorial explosion

Complex multistate proteins such as CaMKII confront modellers with the problem of combinatorial explosion (reviewed in Hlavacek *et al.*, 2003), if each of the possible states is to be modelled explicitly. Imagine a very simple model of a single CaMKII subunit that can only open or close and be phosphorylated at Thr^{306}. Such a model would have to include four species of CaMKII: open and phosphorylated, open and not phosphorylated, closed and phosphorylated, closed and not phosphorylated. Each additional state flag multiplies the

number of possible species by two. For a monomer with n binary state flags, there are 2^n possible combinations. As seen in the last paragraph, even a fairly simple model of CaMKII function would include at least four or five state flags per subunit, i. e. 24 or 30 state flags per hexameric ring. A modelling regime where each possible state configuration of a molecule needs to be explicitly enumerated would thus have to list at least 2^{24} species, that is more than 16 million, and all the reactions involving one of these species. This is why modelling approaches in which all possible pools of entities – even if empty – have to be created and defined cannot be applied to complex multistate molecules. New modelling approaches therefore focus on reducing combinatorial complexity using different methods. Rule-based modelling systems (reviewed in Hlavacek *et al.*, 2006) take reaction rules rather than reactions as input and generate reactions at runtime. (A rule-based description of the calmodulin model has been briefly discussed in chapter 6 on page 77.) In contrast, agent-based modelling systems define reactions that apply to sets of entities, contingent on some state flags, but not necessarily all of them. In the CaMKII case, an example of such a reaction would be: "A CaMKII subunit can undergo phosphorylation at Thr^{306} if it is not bound to calmodulin." This effectively bundles all species of CaMKII that can undergo phosphorylation at Thr^{306} (i. e. all species that are not bound to calmodulin, regardless of the respective states of the other flags) into one group and defines a reaction applicable to each member of this group. In this work, I have used the agent-based stochastic simulator StochSim (Le Novère and Shimizu, 2001), which will be described in the following section.

7.3 Stochastic modelling

Models based on differential equations rely on two fundamental assumptions about the system in question: That it is continuous and that it is deterministic, or at least, that it can be approximated as a continuous and deterministic system. For chemical reactions in small biological compartments neither of these assumption is automatically fulfilled: The very small numbers of molecules mean that every observed change is necessarily stepwise and thus discrete. Molecules

move around and interact in a stochastic manner, which is not averaged out if the entity pools involved are small (reviewed in Tolle and Le Novère, 2006). In these cases, stochastic modelling frameworks are a useful alternative. The most widely known stochastic algorithm for chemical reactions is the Gillespie algorithm (Gillespie, 1977), which changes the composition of entity pools through a progression of random reaction events, the probability of which is computed from reaction rates and molecule numbers. The drawback of the Gillespie algorithm is that it operates on entity pools which need to be explicitly defined – even if empty – and is thus incapable of avoiding combinatorial explosion for multi-state molecules (reviewed in Tolle and Le Novère, 2006).

StochSim (Le Novère and Shimizu, 2001) avoids the problem of combinatorial complexity by operating on individual entities, rather than pools of entities. Each molecule is represented as a separate software object, which means that empty species pools do not have to be represented at all. In StochSim, a number of binary state flags can be assigned to a given species. Specific configurations of state flags can alter the probability of reactions (including preventing a reaction altogether or triggering it with a probability of 1), and the outcome of a reaction can include changing one or more flags (the reaction "Calmodulin binds to CaMKII", for instance, would set the flag "calmodulin-bound" to 1). Moreover, entities can be arranged in geometric arrays (for instance, CaMKII subunits can be arranged in a ring of six), and reactions can be "neighbour-sensitive", i. e. the probability of a reaction for a given entity is affected by the value of a state flag on a neighbouring entity. These properties make StochSim the ideal software tool to model CaMKII.

In order to model dodecamers of CaMKII (see chapter 9 on page 109), I had to slightly modify the StochSim code in order to allow for two-dimensional arrays that are toroidal in one dimension (to represent hexameric rings), but not toroidal in the other dimension (to represent dimeric interactions between adjacent rings). The modified version of StochSim was also used in the model of calmodulin trapping by CaMKII (chapter 8 on page 91) and can be downloaded from `http://sourceforge.net/projects/stochsim/`.

7.4 Contents of the following chapters

Chapter 8 on the next page investigates the phenomenon of calmodulin trapping by CaMKII (Meyer *et al.*, 1992). Structural modelling and stochastic simulations are combined to investigate alternative hypotheses about the underlying mechanism. I show that the standard model of CaMKII activation, in which there is one binding site for calmodulin on each subunit and calmodulin binding is sufficient for CaMKII activation, cannot reproduce trapping. Building on recent experimental results by Tse *et al.* (2007), I propose an alternative model with two calmodulin binding sites per subunit, where calmodulin binding to one site is sufficient to stabilise the active state, but binding to the other site does not affect CaMKII activity. This model can indeed reproduce calmodulin trapping and can be used to explore the biological functions of trapping.

While chapter 8 on the facing page has investigated hexameric rings of CaMKII, chapter 9 on page 109 goes a step further by investigating the whole CaMKII dodecamer. While interactions within a hexameric ring have been well characterised in the past (Hanson *et al.*, 1994; Mukherji and Soderling, 1994), little is known about potential interactions between adjacent subunits on different rings. In particular, while it is clear how autophosphorylation at Thr^{286} can spread between subunits on the same ring, it is not fully understood how – or whether – phosphorylation at Thr^{286} can spread between rings on a holoenzyme. I construct a stochastic model of CaMKII that includes the formation of a coiled-coil between two adjacent subunits on different rings (based on the structural model of CaMKII published by Rosenberg *et al.* (2005)) and show that such a mechanism would allow CaMKII activation to exhibit cooperativity, not just within one ring but between two rings.

8

CALMODULIN TRAPPING BY CAMKII

8.1 Introduction

Upon phosphorylation at Thr^{286}, CaMKII displays an increased apparent affinity for calmodulin, a phenomenon referred to as "calmodulin trapping" (Meyer *et al.*, 1992). Since calmodulin trapping increases the lifetime of the CaMKII-calmodulin complex, it might be a means of transforming a short, transient calcium signal into a longer-lasting effect. This could serve as a basis for calcium frequency detection: At low frequencies, trapped calmodulin would dissociate between two spikes, at higher frequencies, it would remain bound to CaMKII and hence enhance its activity (Meyer *et al.*, 1992). This might be an important mechanism in frequency-dependent LTP. More importantly, calmodulin binding to CaMKII precludes autophosphorylation of CaMKII at Thr^{306}, and *vice versa* (Patton *et al.*, 1990; Colbran, 1993). Thus, calmodulin trapping might be a way of preventing CaMKII desensitisation.

Experimental evidence suggests that the change in apparent affinity seen in trapping consists of a reduction in (apparent) dissociation rate, while the rate of binding between CaMKII and calmodulin remains unchanged (Meyer *et al.*, 1992). A recent paper (Tse *et al.*, 2007) suggests that each CaMKII subunit has two binding sites for calmodulin that have different affinities, and that calmodulin trapping might be a result of this.

We used docking and molecular dynamics approaches as well as stochastic modelling to investigate binding of calmodulin to different conformations of CaMKII. We show that the structures of CaMKII and calmodulin are consistent with the existence of two binding sites, as proposed by Tse *et al.* (2007). We further show that a two-binding-site model where calmodulin binding to one of the sites is compatible with CaMKII inactivation is sufficient to explain trapping. A corre-

sponding model with only one binding site, however, fails to reproduce calmodulin trapping.

8.2 Structural model of calmodulin trapping

8.2.1 *Modelling approach*

Structural modelling was performed using Modeller (Šali and Blundell, 1993) and Amber (Case *et al.*, 2002). We used the structure of autoinhibited CaMKII reported by Rosenberg *et al.* (2005) (PDB: 2BDW) and the structure of calmodulin bound to the inhibitory helix of CaMKII reported by Wall *et al.* (1997) (PDB:1CM1). In order to model calmodulin binding to non-inhibited CaMKII, the structure of CaMKII was modified by omitting structural information regarding the loop between main kinase structure and inhibitory helix, allowing movement of the helix away from the catalytic domain. The resulting structure was then used as a template to which calmodulin was fitted. Using this structure, we modelled calmodulin binding to the two binding domains on the autoinhibitory helix proposed by Tse *et al.* (2007): the low affinity binding domain within residues 298–312 and the high affinity binding domain within residues 291–312.

8.2.2 *Results*

Modes of calmodulin binding to high- and low-affinity sites

Structural modelling revealed that, in principle, binding of calmodulin to the supposed high-affinity binding site is possible, but only if there is at least some opening of the CaMKII subunit (see figure 20b on the facing page). In contrast, binding to the low-affinity site seems to be sterically compatible with closure of the inhibitory helix (20a on the next page) (as well as with the open state required for calmodulin binding to the high-affinity site). This suggests that binding of calmodulin to the low-affinity site is independent of the opening status of a CaMKII subunit, while binding to the high-affinity site requires the subunit to be open.

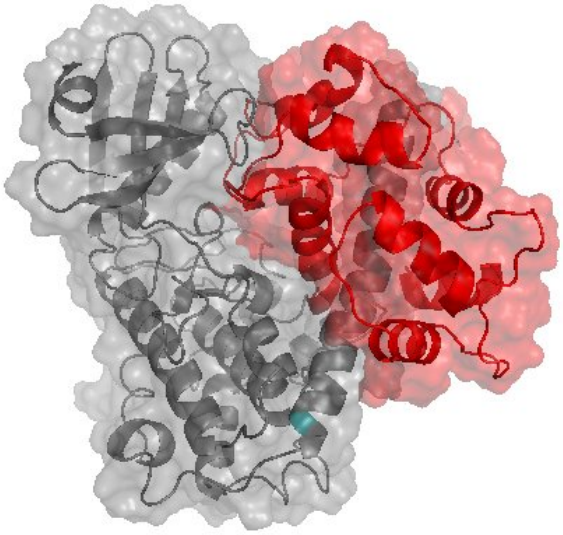

(a) low-affinity binding.

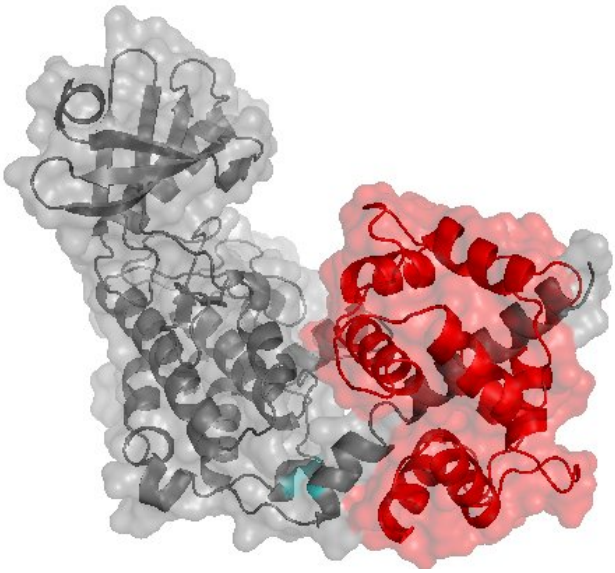

(b) high-affinity binding.

Figure 20: Structural model of calmodulin binding to CaMKII. Top: calmodulin binding to the low-affinity site. Bottom: calmodulin binding to the high-affinity site. Calmodulin is shown in red, CaMKII in grey, and the autophosphorylation site at Thr^{286} in teal.

Modelling calmodulin binding to the high-affinity domain included the interaction between phenylalanine residue 293 (Phe^{293}) on CaMKII and glutamate residue 120 (Glu^{120}) and methionine residue 124 (Met^{124}) on calmodulin, previously shown to be crucial for calmodulin trapping (Singla *et al.*, 2001).

The structural model also indicates that, although there are two binding sites for calmodulin on each CaMKII subunit, no more than one calmodulin molecule can be bound at the time. All of these observations were used in the construction of the stochastic model of CaMKII, which is described below.

8.3 Stochastic model of calmodulin trapping

8.3.1 *Model setup*

A diagram of the reaction scheme used in the stochastic model can be found in figure 21 on the facing page. Stochastic simulations were performed using StochSim (Le Novère and Shimizu, 2001).

CaMKII is modelled as a hexamer. Each subunit of the hexamer can open and close, become phosphorylated at Thr^{306} and Thr^{286}, and bind to calmodulin in two modes: one low-affinity mode and one high-affinity mode. A list of flags for each subunit is given in table 6. The open form is assumed to be active. Since phosphorylation at Thr^{306} is an intra-subunit autophosphorylation, it can only happen if CaMKII is open. The phosphorylation at this residue, however, does not preclude CaMKII from closing again. For structural reasons, Thr^{306} phosphorylation and calmodulin binding to either

flag name	description
open	open (active)
P286	phosphorylated at Thr^{286}
P306	phosphorylated at Thr^{306}
calm	bound to calmodulin (at either binding site)
ha	bound to calmodulin at the high-affinity binding site

Table 6: List of state flags for the model of calmodulin trapping by CaMKII. All flags affect CaMKII and can be either 1 or 0.

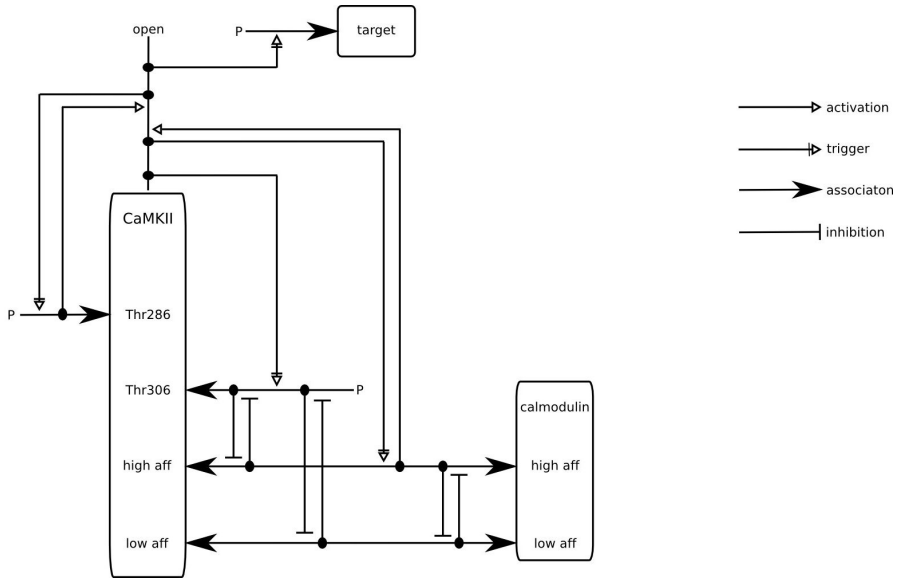

Figure 21: Model of calmodulin trapping. For clarity, only one monomeric subunit is shown. In the actual model, six such subunits form an array, and autophosphorylation at Thr^{286} of one subunit is dependent on the neighbouring subunit being open.

state are mutually exclusive, because both binding domains include residue Thr^{306}. Since Thr^{286} is located at the "hinge" between the main kinase structure and the autoinhibitory domain, Thr^{286} phosphorylation is only possible in the open state, and the kinase remains open once phosphorylated at Thr^{286}. Autophosphorylation at Thr^{286} is neighbour-sensitive: A subunit can only be phosphorylated at this residue if its neighbouring subunit is open. Phosphorylation can be reversed by phosphatase action, in this case by PP1. In line with results of the structural model presented above, binding of calmodulin to the high-affinity binding sites precludes closing of a CaMKII subunit. Binding of calmodulin to the low-affinity site, in contrast, is compatible with closing. Calmodulin can bind directly to the low-affinity or to the high-affinity site or slide along the helix from the low-affinity to the high-affinity binding site or back. The reaction here called "sliding" is actually a placeholder for an unknown mechanism (or a set of unknown mechanisms) by which binding of a calmodulin molecule to the high-affinity site is in some way facilitated if that same calmodulin molecule is already bound to the low-affinity binding site on the same helix. A possible candidate for such a mechanism is confor-

mational change of calmodulin bound to the low-affinity site, which would allow it to move along the helix and bind to the high-affinity site, as suggested by Tse *et al.* (2007). Another possibility is that if a calmodulin molecule dissociates from the low-affinity site, the local effective calmodulin concentration in the immediate neighbourhood increases, which makes binding to the high-affinity binding site on the same helix more likely. It is impossible to distinguish between those two (and possible other) mechanisms; the sliding reaction is therefore a purely phenomenological one, taking CaMKII with calmodulin bound to the low-affinity site as a substrate and CaMKII with calmodulin bound to the high-affinity site as a product. A full list of reactions is given in appendix 11 on page 147.

8.3.2 *Parameter determination*

For most parameters, values can be found in the literature. Other parameters were estimated or computed as described below. A full list of parameters is given in table 7 on page 98.

Binding of calmodulin to the high-affinity site

In order to estimate parameters for binding of calmodulin to the high-affinity site, I constructed a minimal model of interactions between a CaMKII peptide and calmodulin with COPASI (Hoops *et al.*, 2006). The model was constructed so as to reproduce experiments on calmodulin binding to CaMKII fragments of different length performed by Tse *et al.* (2007). It contains only six reactions, namely direct binding of calmodulin to the low-affinity binding site, direct binding of calmodulin to the high-affinity binding site and sliding of calmodulin between high- and low-affinity sites (and the respective backwards reactions). The affinity of calmodulin for the low-affinity binding site was $5.9 \times 10^{-6}\,M$, corresponding to the low-affinity peptide used by Tse *et al.* (2007). A forward rate of $4.2 \times 10^{6}\,M^{-1}s^{-1}$ was chosen for calmodulin binding (Meyer *et al.*, 1992). The calmodulin concentration used in this model was $10^{-5}\,M$ and the concentration of CaMKII peptide was $10^{-4}\,M$, corresponding to the experimental concentrations used by Tse *et al.* (2007). Since "sliding" is actually a combination of possible mechanisms, parameters for this reaction are difficult to

obtain. I have assumed that sliding is an intrinsically symmetrical process, i. e. that once dissociated from one binding site, the probability of binding to the other binding site should be the same in either direction. Therefore, the equilitbrium constant for the sliding reaction (and hence, the probability of sliding from one site to the other) should be determined by the dissociation rates (and hence, the dissociation constants) for both sites:

$$K_{sliding} = \frac{K_{d_{ha}}}{K_{d_{la}}} \tag{8.1}$$

The forward rate (low-affinity to high-affinity) for sliding was assumed to be $10^8\, s^{-1}$, reflecting the idea that sliding should be a fairly fast process.

The only independent parameter left to determine, then, was the dissociation constant for the high-affinity site. This was done using the `Optimization` function in COPASI. As an objective function, I used the apparent K_d for calmodulin binding to the "intermediate" CaMKII peptide ($1.7 \times 10^{-10}\, M$), as described by Tse *et al.* (2007). This is, in fact, a combination of calmodulin binding to both the low-affinity and high-affinity binding sites:

$$K_{d_{ha,app}} = \frac{[CaMKII][CaM]}{[CaMKII - CaM]_{ha} + [CaMKII - CaM]_{la}}$$

The `Genetic Algorithm` function was used for optimisation with lower bound $10^{-14}\, M$ and upper bound $5.9 \times 10^{-6}\, M$ (corresponding to the dissociation constant for the low-affinity site). Ten optimisation runs were performed with different, randomly picked initial values, all of which resulted in the same optimum K_d for the high-affinity binding site of $1.7 \times 10^{-10}\, M$. (Note that this also means that the high-affinity site dominates calmodulin binding to the "intermediate" peptide, such that the contribution of binding to the low-affinity site to the overall K_d for the high-affinity peptide can be neglected.) Inserting the high-affinity K_d into equation 8.1, this results in a K_d for sliding of 2.9×10^{-5}, which corresponds to a probability of 0.99997 for sliding of calmodulin from the low-affinity to the high-affinity site.

Subunit opening

The minimal COPASI model was then extended in order to obtain an estimate of the opening probability of a single CaMKII subunit. In addition to the reactions described above, this model also contained opening and closing of a CaMKII subunit. This was used for another optimisation run in order to estimate the probability of CaMKII opening. The objective function used this time was the apparent combined K_d for a single subunit:

$$K_{d_{combined}} = \frac{([open] + [closed])[CaM]}{[open - CaM]_{la} + [open - CaM]_{ha}}$$

This value has been reported by Tzortzopoulos and Török (2004) to be $4 \times 10^{-8}\,M$ for calmodulin binding to CaMKII with a threonine residue 286 to alanine (T286A) mutation. This was chosen in order to be able to include the effects of calmodulin binding and opening/closing only, without having to account for autophosphorylation. Again, the inbuilt `Genetic Alogrithm` optimisation function in COPASI was run ten times, with ten randomly chosen initial values. The resulting value for the opening probability was 0.004.

Volume of the post-synaptic density

The volume of the post-synaptic density was estimated based on reports of a PSD thickness of $30\,nm$ (Chen *et al.*, 2005) and a PSD diameter of $180 - 750\,nm$ (Chen *et al.*, 2005; Petersen *et al.*, 2003).

Table 7: Parameters used in the model of calmodulin trapping by CaMKII.

Parameter	value	reference
k_f for CaMKII phosphorylation at residue 286	$30\,s^{-1}$	(Lučić *et al.*, 2008)
k_f for dephosphorylation of CaMKII at residue 286 by PP1	$1.6 \times 10^{-7}\,s^{-1}$	computed from (Strack *et al.*, 1997a)
k_f for CaMKII phosphorylation at residue 306	$0.55\,s^{-1}$	(Lučić *et al.*, 2008)

Table 7: continued

k_f for dephosphorylation of CaMKII at residue 306 by PP1	$1.6 \times 10^{-7}\, s^{-1}$	computed from (Strack *et al.*, 1997a)
K_d for calmodulin binding to the low-affinity site	$5.9 \times 10^{-6}\, M$	(Tse *et al.*, 2007)
k_f for calmodulin binding to the low-affinity site	$4.2 \times 10^{6}\, M^{-1}s^{-1}$	(Meyer *et al.*, 1992)
k_b for calmodulin binding to the low-affinity site	$24.8\, s^{-1}$	$K_d \times k_f$
K_d for calmodulin binding to the high-affinity site	$1.7 \times 10^{-10}\, M$	*this study*
k_f for calmodulin binding to the high-affinity site	$4.2 \times 10^{6}\, M^{-1}s^{-1}$	(Meyer *et al.*, 1992)
k_b for calmodulin binding to the high-affinity site	$7.1 \times 10^{-4}\, s^{-1}$	$K_d \times k_f$
probability of spontaneous CaMKII opening	0.004	*this study*
probability of calmodulin sliding to the high-affinity site	0.99997	*this study*
number of CaMKII hexamers in the PSD	60	(Petersen *et al.*, 2003)
number of calmodulin molecules in the PSD	20	computed from (Kakiuchi *et al.*, 1982)
number of PP1 molecules in the PSD	1	computed from (Kötter, 1994)
PSD volume	$10^{-18}\, l$	*this study*

Table 7: Parameters used in the model of calmodulin trapping by CaMKII.

8.3.3 *Results*

The two-binding site model can reproduce trapping

To assess whether our model can reproduce the trapping of calmodulin observed *in vitro*, we ran simulations on both wildtype CaMKII and an *in silico* mutant version that cannot be phosphorylated at Thr^{286}. Following the experimental procedure in Meyer *et al.* (1992), the system was allowed to saturate for thirty seconds, and calmodulin then inactivated, corresponding to the withdrawal of calcium in the experimental setup. The ratio between calmodulin and CaMKII concentration used for this simulation was the same as used by Meyer *et al.* (1992) (60 hexamers of CaMKII for 450 molecules of calmodulin), and no phosphatase was present. The simulation (see figure 22) shows that although both versions of CaMKII were equally saturated with calmodulin after thirty seconds, calmodulin dissociation proceeded slower from the wildtype than from the mutant, showing a trapping effect that is, indeed, due to different apparent *off* rates.

To ensure that the observed result is not just a stochastic effect, the same simulation was repeated ten times on wildtype and mutant CaMKII. Figure 23 on page 102 shows that the difference between wildtype and mutant is indeed consistent, regardless of stochastic fluctuations in single simulation runs.

Calmodulin trapping in vivo

Protein concentrations *in vivo* differ from concentrations in test tubes, and it is therefore a valid question whether the phenomenon of calmodulin trapping is likely to play a role *in vivo*. To investigate this, I have run simulations on both wildtype and T286A mutant CaMKII under conditions typically found in the PSD (see table 7 on page 98). The results of ten simulation runs (shown in figure 24 on page 103) confirm that there is indeed a marked effect of Thr^{286} autophosphorylation *in vivo*.

Exploring an alternative model

The model presented here makes two important assumptions: First, that there are two binding sites for calmodulin on CaMKII and sec-

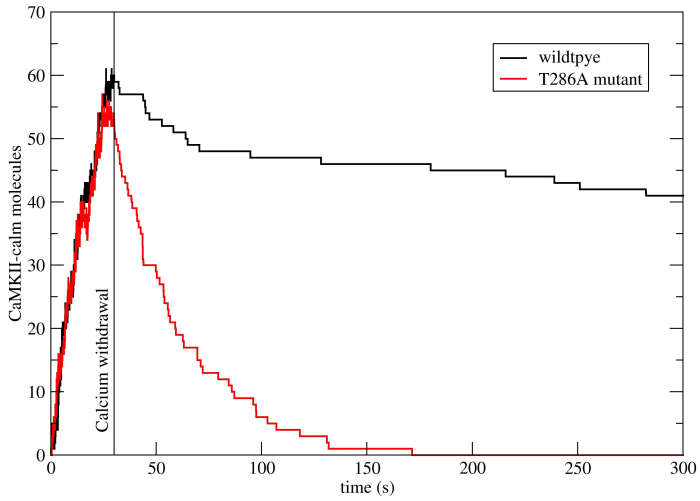

Figure 22: Single trapping simulation on wildtype and mutant CaMKII: Calmodulin is inactivated, mimicking calcium withdrawal after 30 s. The ratio of calmodulin to CaMKII concentration used in the simulation was the same as used in the experimental setup by Meyer *et al.* (1992). The number of monomeric CaMKII subunits bound to calmodulin is plotted against time. Wildtype is shown in black, T286A mutant in red. One single simulation run is shown for each.

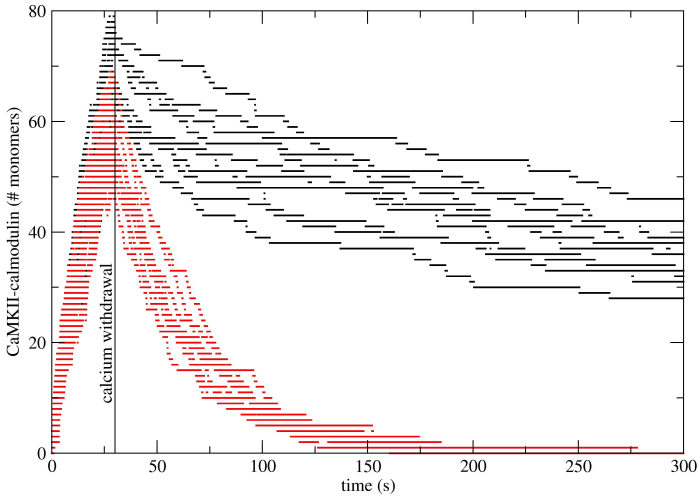

Figure 23: Several trapping simulations on wildtype and mutant CaMKII: Calmodulin is inactivated, mimicking calcium withdrawal after 30 *s*. The ratio of calmodulin to CaMKII concentration used in the simulation was the same as used in the experimental setup by Meyer *et al.* (1992). The number of calmodulin-bound monomeric CaMKII subunits is plotted against time for each simulation run. Wildtype is shown in black, T286A mutant in red. Ten simulation runs are shown for each.

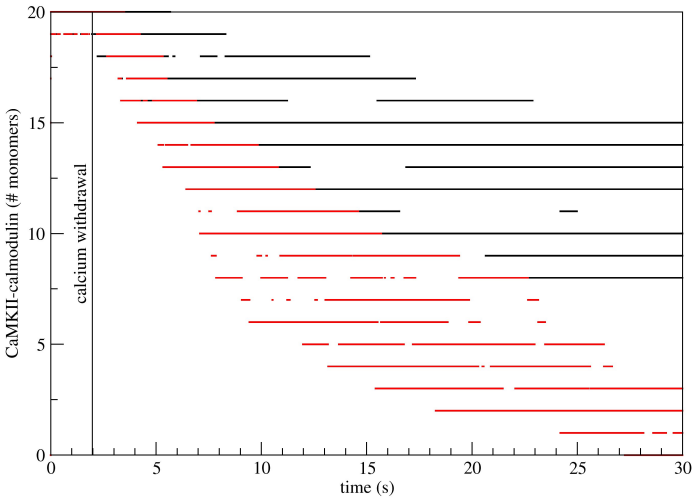

Figure 24: Trapping *in vivo*: Simulation of calmodulin trapping by CaMKII under *in vivo* conditions. CaMKII is allowed to fully saturate with calmodulin for 2 *s*; after that, calmodulin is removed to mimic withdrawal of calcium. The number of calmodulin-bound monomeric CaMKII subunits is plotted against time for ten simulation runs both for wildtype (black dots) and T286A mutant (red dots), respectively.

ond, that binding to one of these sites is compatible with closing of CaMKII, i. e. that calmodulin is not sufficient for CaMKII activation. By measuring calmodulin binding to CaMKII peptides of different lengths, Tse *et al.* (2007) have made a plausible case for the first assumption, though whether both binding sites are actually used for calmodulin binding to full-length CaMKII has not been experimentally confirmed yet. (Note, however, that experimental work by Chin and Means (2002) on full-length CaMKII seems to be consistent with the existence of two calmodulin binding sites, although the authors themselves do not draw the same conclusion). The second assumption is somewhat more controversial; in fact, most of the literature on CaMKII implicitly or explicitly assumes that calmodulin binding is sufficient for CaMKII activation (reviewed in Yamauchi, 2005). The question therefore arises whether both these assumptions are needed in order to reproduce trapping of calmodulin by CaMKII.

In order to address this question, a model of CaMKII has been constructed with only one (high-affinity) calmodulin binding site. In this model, calmodulin binding and closing of a CaMKII subunit are mutually exclusive, meaning that calmodulin binding is sufficient for CaMKII activation. All other reactions and parameters are the same as in the model presented above. Figure 25 on the facing page shows the result of a single simulation on wildtype calmodulin and on T286A mutant calmodulin with this alternative model. As in the trapping simulation presented above, CaMKII was first saturated with calmodulin (here: at the beginning of the simulation) and all free calmodulin then withdrawn, such that dissociation of calmodulin from CaMKII can be monitored. The results show that this alternative model cannot reproduce the change in apparent k_{off} that characterises calmodulin trapping.

Figure 26 on page 106 shows the pooled results of ten simulation runs on wildtype and T286A mutant CaMKII, confirming that there is no difference in apparent k_{off}.

The failure of the alternative model to reproduce calmodulin trapping is perhaps not surprising: The higher number of open subunits due to Thr^{286} autophosphorylation will increase the apparent k_{on} for calmodulin binding in the wildtype (since more binding sites will be available), but has no influence on the apparent k_{off}, because once cal-

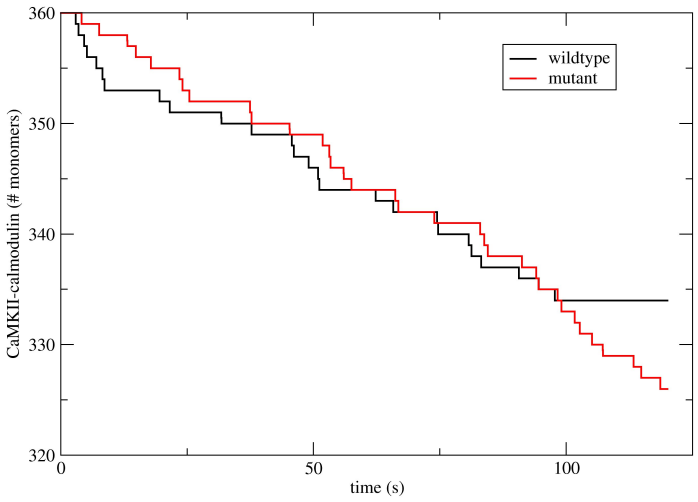

Figure 25: Trapping simulation on CaMKII with just one binding site for calmodulin: All CaMKII molecules are open and fully saturated with calmodulin to begin with, and calmodulin is withdrawn, mimicking calcium withdrawal, at the start of the simulation. The ratio of calmodulin to CaMKII concentrations was the same as used in the experimental setup by Meyer *et al.* (1992). The number of calmodulin-bound monomeric CaMKII subunits is plotted against time. Wildtype is shown in black, T286A mutant in red. One single simulation run is shown for each.

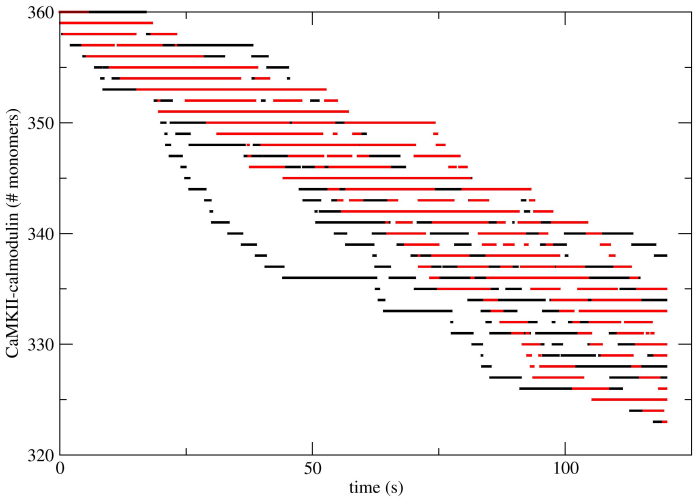

Figure 26: Several trapping simulations on CaMKII with just one binding site for calmodulin. Conditions are the same as in figure 25 on the previous page, but ten simulations were run on wildtype CaMKII (black dots) and on T286A mutant CaMKII (red dots), respectively. There is no difference in slope between mutant and wildtype.

modulin has dissociated from the only binding site, it is immediately inactivated and is therefore no longer available. This is independent of the autophosphorylation state of the subunit from which calmodulin has dissociated. In order to reproduce trapping, a one-binding-site model would need to include an *ad hoc* increase in calmodulin affinity for autophosphorylated CaMKII, which will reproduce the effect, but without providing an explanation of the mechanism. The full trapping model presented here overcomes the need for an *ad hoc* increase in affinity by postulating the existence of an additional binding site. In this case, not all of the calmodulin dissociating from the high-affinity site is immediately inactivated, but some of it merely "slides" to the low-affinity binding site and thus remains on the same subunit. In this case, autophosphorylation matters: Phosphorylated subunits remain open, calmodulin can therefore "slide back" to the high-affinity binding site. In contrast, unphosphorylated subunits are likely to close, which makes re-binding to the high-affinity site impossible. The existence of a second binding site is thus important in order to "retain" calmodulin close by for a while after it has dissociated, rather than releasing it completely. By the same argument, binding to one of the binding sites has to be compatible with closing. Otherwise, a CaMKII subunit would only be able to close once calmodulin has completely dissociated from either binding site, which means that the additional stabilisation of the open state by autophosphorylation at Thr^{286} has no effect on the apparent k_{off} (note that, again, it would have an effect on apparent k_{on}, however). Thus, a two-binding site model where binding of calmodulin to one of the sites is compatible with subunit closing seems to be necessary for calmodulin trapping, unless some other yet unknown mechanism is involved. Interestingly, this also means that binding of calmodulin to CaMKII as such is not sufficient for CaMKII activation, although binding of calmodulin to the high-affinity site seems to be.

8.4 Potential experimental validation

While the structure of calmodulin bound to the low-affinity binding site of CaMKII is known, the structure of calmodulin bound to the high-affinity binding site is a prediction from our model. The experi-

mental determination of this structure could be used to validate this model.

This model predicts that calmodulin binding is not *per se* sufficient for CaMKII activation. A way to test this experimentally would be to measure both calmodulin binding and CaMKII activity for monomeric T286A mutant CaMKII. With no autophosphorylation mechanism in place to confer calmodulin-independent activity, it can be assumed that calmodulin binding would be the only mechanism that could stabilise the active state in such an experiment. If the proportion of calmodulin-bound CaMKII molecules in the mixture is significantly higher than that of active molecules, this would confirm the hypothesis that calmodulin binding is not sufficient for CaMKII activation.

Contributions

David Marshall carried out structural modelling and molecular dynamics simulations. I designed the stochastic model, implemented it in STOCHSIM, and analysed the results. Nicolas Le Novère supervised the study.

9

MODEL OF A CAMKII DODECAMER

9.1 Introduction

According to the structure of the CaMKII holoenzyme proposed by Rosenberg *et al.* (2005), CaMKII is a dodecamer formed of two hexameric rings stacked on each other. The holoenzyme is supposed to have a "hub-and-spoke" structure with association domains in the centre and active domains on the periphery (see figure 27 on the following page). The focus of this study is on interactions and behaviour of active domains, which contain both the catalytic site and the inhibitory helix. Therefore, the term "subunit" in this chapter is used as a shorthand for "active domain of a subunit".

Within the CaMKII dodecamer, there is interaction both between adjacent subunits on the same ring and between adjacent subunits on different rings. Such a "double-pair" of subunits is represented in figure 28 on page 111.

Intra-holoenzyme autophosphorylation on Thr^{286} (Payne *et al.*, 1988) is an example for interaction between adjacent subunits on the same ring, while the formation of a coiled-coil between two inhibitory helices is an interaction between subunits on different rings. While the trans-autophosphorylation reaction at Thr^{286} provides a mechanism of spreading activity within one hexameric ring, it is unclear how the activation status is communicated from one ring to the next. The coiled-coil interaction between subunits on two different rings might provide a mechanism to achieve this.

According to the model presented by Rosenberg *et al.* (2005), there are two pairs of conditions that would have to be fulfilled for a phosphorylation event at Thr^{286} to take place. Two adjacent subunit on the same hexameric ring (the "kinase" subunit and the "substrate" subunit in the phosphorylation reaction) would both need to be open and neither of them could be involved in coiled-coil interactions with their respective partner subunit on the other ring. Opening and coiled-coil

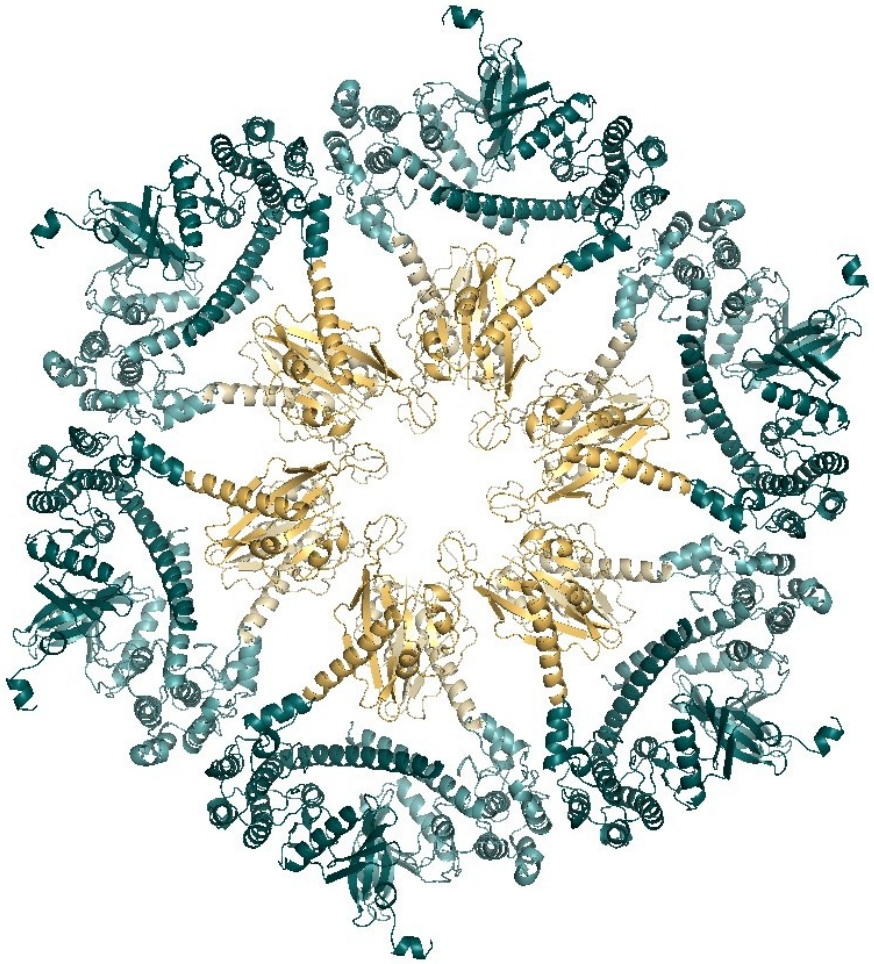

Figure 27: Structure of a dodecamer of CaMKII, as proposed by Rosenberg *et al.* (2005). Association domains in the centre are shown in yellow, active domains in teal.

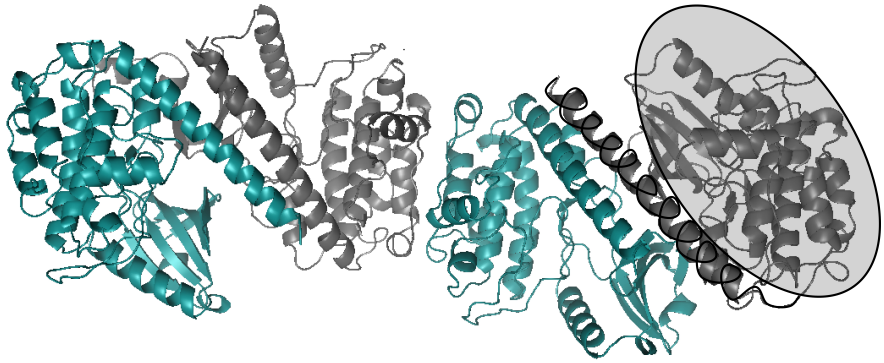

Figure 28: Two adjacent pairs of CaMKII subunits. Subunits on the "upper" ring are shown in teal, subunits on the lower ring in gray. A subunit on one ring interacts with its neighbour on the other ring by forming a coiled-coil. Only active domains are shown. The figure is based on the structure proposed by Rosenberg *et al.* (2005), and represents a fragment of figure 27 on the facing page, rotated to show the coiled-coil interaction. Also shown is a schematic drawing of one subunit; the same schema will be used in figure 29 on the next page.

disruption would be independent of each other. This is represented in figure 29 on the following page. Opening/closing of one subunit does not affect the adjacent subunit on the other ring (figure 29b on the next page). Disruption of the coiled coil affects both adjacent subunits on different rings (figure 29c on the following page). Trans-autophosphorylation can only happen if two adjacent coiled-coils are disrupted and two subunits on the same ring are both open (figure 29d on the next page).

It is worthwhile considering for a moment why all four conditions for autophosphorylation stated by Rosenberg *et al.* (2005) (both "kinase" and "substrate" subunit open and both of them released from their respective coiled-coil) need to be fulfilled at the same time. That both subunits need to be open can be explained by the fact that both the active site on the "kinase" subunit and Thr^{286} on the "substrate" subunit need to be accessible. In principle, opening of the subunit is enough for accessibility of both Thr^{286} and the active site, regardless of whether or not the subunit participates in a coiled-coil interaction. However, if one or both of the subunits are within a coiled-coil in-

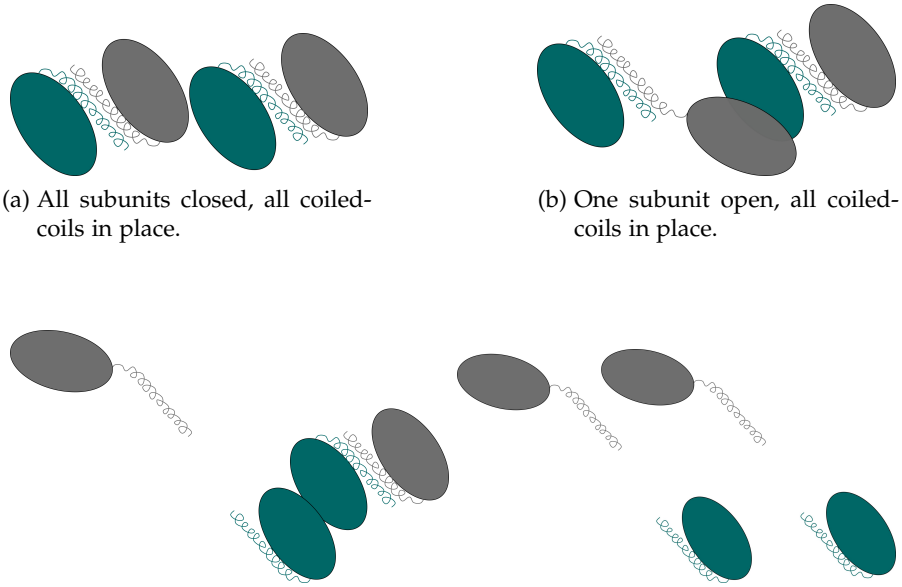

(a) All subunits closed, all coiled-coils in place.

(b) One subunit open, all coiled-coils in place.

(c) One subunit open, one coiled-coil disrupted.

(d) Two subunits open, two coiled-coils disrupted.

Figure 29: Opening and coiled-coil formation on two adjacent pairs of subunits. Subunits of the same colour are adjacent to each other on the same ring. Subunits interacting through the coiled-coil are adjacent to each other on different rings.

teraction with their respective adjacent subunits on the other ring, the distance between the active site of one subunit and Thr^{286} on the other subunit is probably too large for the phosphorylation reaction to take place. Thus, an open subunit within a coiled-coil might be active with respect to some substrates, but not active with respect to its neighbouring subunit.

I here present a stochastic model of CaMKII that investigates the effects of different kinds of interaction within a CaMKII dodecamer.

9.2 Model of a CaMKII dodecamer

9.2.1 *Model description*

The dodecamer is modelled as a ring consisting of six dimers. A list of state flags affecting each subunit is given in table 8. Most of the flags are the same as in the model of calmodulin trapping (see chapter 8 on page 91); there is one additional flag denoting the presence of a coiled-coil between two adjacent subunits on different rings.

A scheme of the reactions within each dimer is shown in figure 30 on the following page. The figure shows the reactions within each monomer and the neighbour-sensitive formation of a coiled-coil between two adjacent subunits on different rings. In the actual model, six such dimers are combined to form the double-ring structure and phosphorylation at Thr^{286} is defined as a neighbour-sensitive reaction between adjacent subunits on the same ring.

flag name	description
open	open (active)
P286	phosphorylated at Thr^{286}
P306	phosphorylated at Thr^{306}
calm	bound to calmodulin (either binding site)
ha	bound to calmodulin (high-affinity site)
coil	inhibitory helix forms coiled-coil with adjacent subunit

Table 8: List of state flags for the model of a CaMKII dodecamer. All flags affect a single subunit, except for the "coil" flag, which affects two subunits at a time. Each flag can be either 1 or 0.

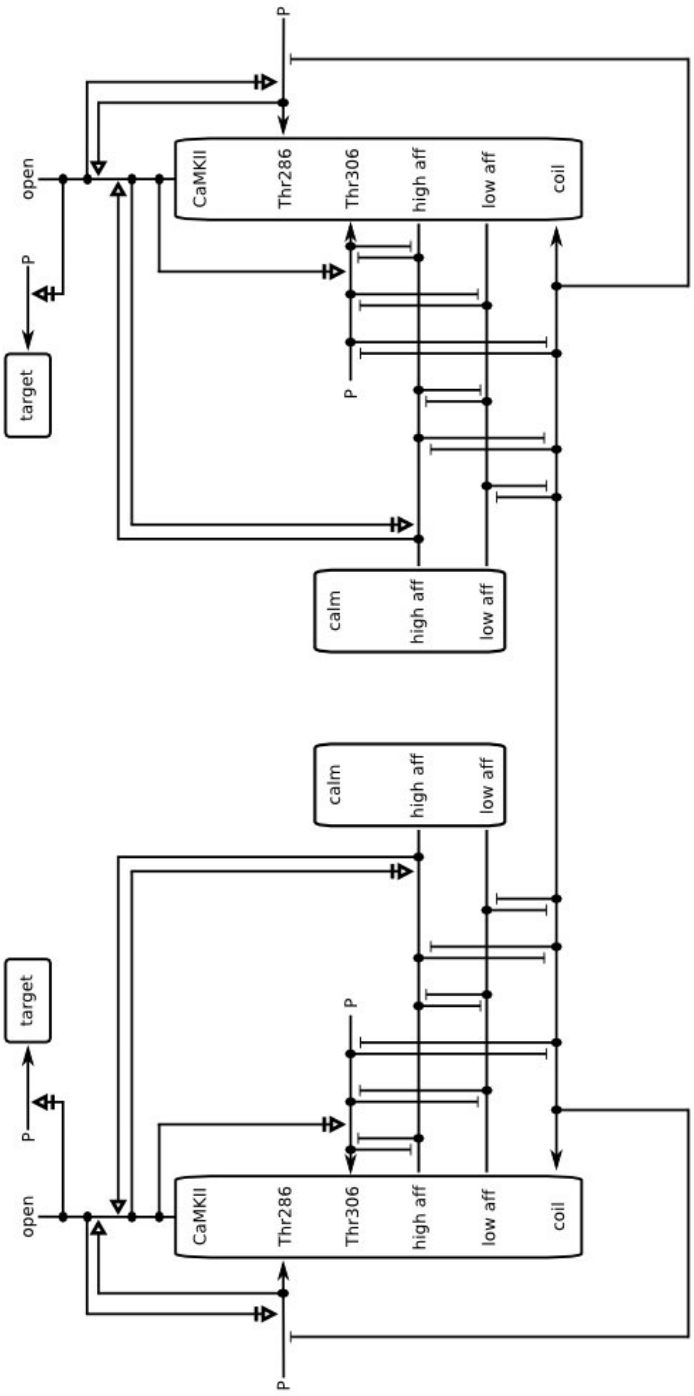

Figure 30: Reaction scheme for a CaMKII dimer. The dodecamer is a toroidal array of six such dimers, with phosphorylation at Thr^{286} as a neighbour-sensitive reaction between adjacent subunits on the same ring.

A complete list of reaction rules is given in appendix 12 on page 151.

9.2.2 *Parameter choice*

Most parameters have been retrieved from the literature or computed as described in chapter 8 on page 91. The only parameters left to be determined were those governing the formation of a coiled-coil between adjacent subunits on the same ring.

Parameters governing coiled-coil interaction

Rosenberg *et al.* (2005) suggest that coiled-coil formation between adjacent subunits is weaker than calmodulin binding (Rosenberg *et al.*, 2005). This provides us with an lower limit for the K_d for coiled-coil formation, corresponding to the K_d for calmodulin binding for the low-affinity binding site: $5.9 \times 10^{-6}\,M < K_{d_{coil}}$.

Furthermore, Rosenberg *et al.* (2005) report that the formation of coiled-coils between subunits is stronger in the holoenzyme than with monomeric CaMKII and has, indeed, not been observed at all at monomer concentrations of under $100\,\mu M$. This can help determine an upper limit for $K_{d_{coil}}$. If no coiled-coil interaction is detectable at monomer concentrations of under $100\,\mu M$, this means that a very low proportion of monomers (say, 1 in 1000 or less) undergo a coiled-coil formation. In a mixture with $10^{-4}\,M$ CaMKII monomers, then, one would find at most 10^{-7} dimers. In that case, the K_d would be $\frac{[\text{monomer}]^2}{[\text{dimer}]} = 10^{-1}$. Now, in a dodecamer, the effective concentration of subunits is about $3 \times 10^{-3}\,M$ (Rosenberg *et al.*, 2005), which is 30 times higher than in the mixture of monomers. This means that the K_d computed for monomeric CaMKII will have to be divided by ≈ 1000 in order to account for the increased local concentration in a dodecamer, resulting in an upper limit for $K_{d_{coil}}$ of $10^{-4}\,M$.

This means that $K_{d_{coil}}$ probably lies in the region between 10^{-6} and $10^{-4}\,M$. I have used $10^{-4}\,M$ for the model presented here.

For the forward reaction rate, I assume that it is about an order of magnitude faster than the forward rate of calmodulin binding, due to the spatial proximity of interacting subunits, resulting in a k_f for coiled-coil formation of 1×10^7 and hence, a k_b of 1000.

Full list of parameters

A full list of parameters used for the model of a CaMKII dodecamer is given in table 9.

Table 9: List of parameters for the model of a CaMKII dodecamer.

Parameter	value	reference
k_f for CaMKII phosphorylation at residue 286	$30\,s^{-1}$	(Lučić *et al.*, 2008)
k_f for dephosphorylation of CaMKII at residue 286 by PP1	$1.6 \times 10^{-7}\,s^{-1}$	computed from (Strack *et al.*, 1997a)
k_f for CaMKII phosphorylation at residue 306	$0.55\,s^{-1}$	(Lučić *et al.*, 2008)
k_f for dephosphorylation of CaMKII at residue 306 by PP1	$1.6 \times 10^{-7}\,s^{-1}$	computed from (Strack *et al.*, 1997a)
K_d for calmodulin binding to the low-affinity site of CaMKII	$5.9 \times 10^{-6}\,M$	(Tse *et al.*, 2007)
k_f for calmodulin binding to the low-affinity site of CaMKII	$4.2 \times 10^{6}\,M^{-1}s^{-1}$	(Meyer *et al.*, 1992)
k_b for calmodulin binding to the low-affinity site of CaMKII	$24.8\,s^{-1}$	$K_d \times k_f$
K_d for calmodulin binding to the high-affinity site of CaMKII	$1.7 \times 10^{-10}\,M$	see chapter 8 on page 91
k_f for calmodulin binding to the high-affinity site of CaMKII	$4.2 \times 10^{6}\,M^{-1}s^{-1}$	(Meyer *et al.*, 1992)
k_b for calmodulin binding to the high-affinity site of CaMKII	$7.1 \times 10^{-4}\,s^{-1}$	$K_d \times k_f$
K_d for coiled-coil interaction between two adjacent dimers	$10^{-4}\,M$	*this chapter*
k_f for coiled-coil interaction between two adjacent dimers	$10^{7}\,M^{-1}s^{-1}$	*this chapter*
k_b for coiled-coil interaction between two adjacent dimers	$1000\,s^{-1}$	*this chapter*

Table 9: continued

probability of spontaneous CaMKII opening	0.007	see chapter 8 on page 91
probability of calmodulin sliding to the high-affinity site	0.999	see chapter 8 on page 91
total number of CaMKII molecules in the PSD	30	(Petersen *et al.*, 2003)
total number of calmodulin molecules used for simulation	450	see chapter 8 on page 91
number of PP1 molecules in the PSD	1	computed from (Kötter, 1994)
volume of a PSD	$10^{-18}\,l$	see chapter 8 on page 91

Table 9: List of parameters for the model of a CaMKII dodecamer.

9.2.3 *Stochastic simulations*

Stochastic simulations were performed using StochSim (Le Novère and Shimizu, 2001).

9.3 Results and discussion

9.3.1 *Single molecule results*

Figure 31 on the next page shows the behaviour of a single CaMKII dodecamer over time; the three subfigures represent the state of different flags (open, coiled-coil, Thr^{286} phosphorylated) for the same dodecamer. As expected, the disruption of the coiled-coil is intrinsically symmetrical, opening and closing is determined by a rapid equilibrium, and both opening and coiled-coil disruption of two adjacent subunits on the same ring are necessary for one of these subunits to become phosphorylated at Thr^{286}.

Figure 31: Opening, coiled-coil formation and autophosphorylation of a single CaMKII dodecamer. Evolution of the same dodecamer is shown over time, with different flags visualised: Opening (red), coiled-coil formation (turquoise) and Thr^{286} phosphorylation (black). For each of these, the first six rows represent the "top" hexamer, while the second six rows represent the "bottom" hexamer, meaning that the subunit in row 1 is immediately adjacent to the subunit in row 7, etc. Columns represent time, with each column corresponding to the state of the enzyme after a 0.01 *s* interval. The simulation starts off with all subunits closed, within their coiled-coil and unphosphorylated. Total simulation time is 3 *s*.

But tracking of a single molecule also reveals other properties: For instance, while there is no strict one-to-one correlation, coiled-coil disruption still seems to facilitate subunit opening. This is surprising at first sight, since the open state is not directly stabilised by coiled-coil disruption. However, a subunit within a coiled-coil interaction cannot bind to calmodulin or be phosphorylated at Thr^{286}, which means the open state can only be stabilised if the coiled-coil is disrupted. Since disruption of the coiled-coil simultaneously releases two subunits on different rings, the likelihood of the open state being stabilised increases simultaneously for both these subunits. This, in turn, increases the likelihood for both subunit of being phosphorylated at Thr^{286}. Therefore, although both opening and Thr^{286} phosphorylation of a subunit on one ring do not necessarily entail opening or Thr^{286} phosphorylation of its neighbour on the other ring, there is still a strong correlation, because coiled-coil disruption, which is intrinsically symmetrical, facilitates both processes. This provides a way of spreading autonomous activity not only within a hexamer, but between two hexameric rings.

9.3.2 *Population results*

On the whole-population level, the results confirm that both coiled-coil disruption and opening are necessary for Thr^{286} phosphorylation: Figure 32 on the following page illustrates how the number of Thr^{286} phosphorylated subunits increases with increasing numbers of open subunits and with decreasing numbers of coiled-coils.

9.3.3 *Population response to calcium pulses*

The population response to calcium pulses (see figure 34 on page 122) shows that there is indeed a stepwise increase in CaMKII phosphorylation if calcium frequencies are sufficiently high. This is the first confirmation of the model proposed by Hudmon and Schulman (2002) and discussed in chapter 1 on page 1, whereby high enough calcium frequencies will lead to an increase in CaMKII activation, because the probability of two neighbouring subunits being open at the same

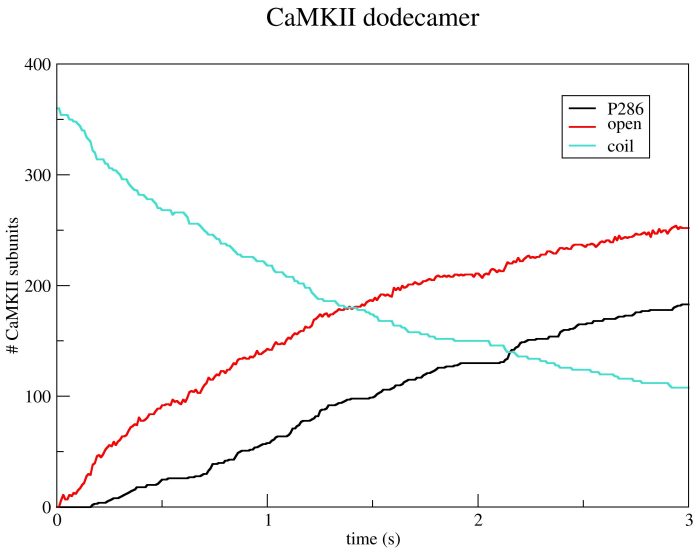

Figure 32: Simulation on a population of CaMKII dodecamers. Numbers of subunits are shown that are open (red), Thr^{286} phosphorylated (black) or within a coiled-coil (turquoise). The simulation starts off with all subunits closed, within their coiled-coil and unphosphorylated. Data points were taken after each 0.01 seconds of simulation.

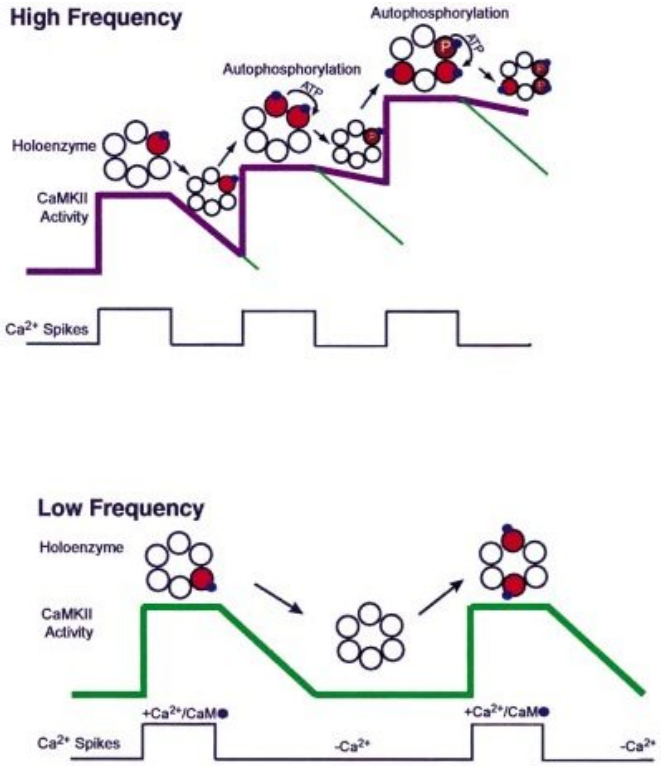

Figure 33: Model of CaMKII activation at different calcium frequencies. Figure taken from Hudmon and Schulman (2002). At high calcium frequencies, a specific subunit is likely to stay active until the next calcium pulse. The activity of the overall population of CaMKII molecules will therefore show a stepwise increase. At lower calcium frequencies, activity is likely to go back down to the baseline between pulses.

time increases with increasing calcium frequencies (see figure 33 on page 121).

9.3.4 *Two modes of cooperativity*

The analysis of the model of the CaMKII dodecamer shows that there are two directions in which subunits in a CaMKII dodecamer cooperate: "Horizontal" with neighbouring subunits on the same hexameric ring and "vertical" with the neighbouring subunit on the other ring. Since the disruption of the "vertical" coiled-coil interaction is necessary for phosphorylation at Thr^{286}, the likelihood of phosphorylation for two adjacent subunits on different rings increases simultaneously,

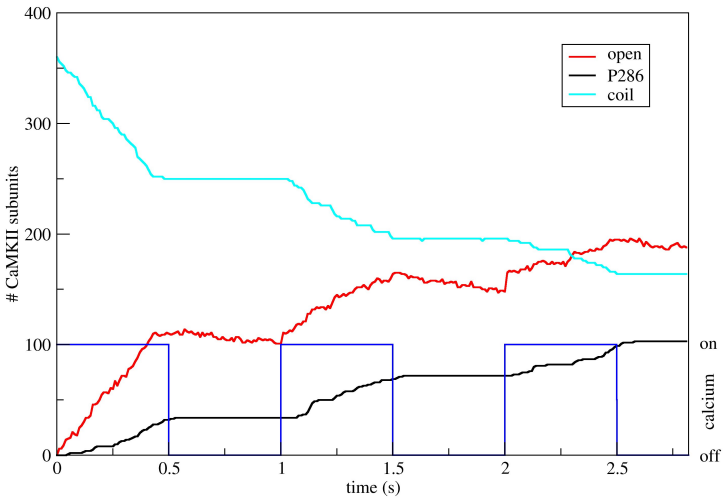

Figure 34: Simulation of a CaMKII dodecamer at high calcium frequency. Conditions were as in figure 32 on page 120, only with calmodulin activity turned on and off every 0.5 *s*, in order to mimic a calcium pulse. Numbers of subunits which are open (red), Thr^{286} phosphorylated (black) or within a coiled-coil (turquoise) are shown, corresponding to the left ordinate. Calcium pulses are shown in blue, corresponding to the right ordinate. It is assumed that a given calcium pulse is strong enough to saturate all available calmodulin.

thus providing a way of spreading activity (or at least the potential to be activated) not only within one hexameric ring, but between two rings. This cooperativity between the two rings means that earlier models that have described CaMKII as a bistable switch (Lisman and Zhabotinsky, 2001; Zhabotinsky, 2000) are still plausible, although they have only considered the propagation of activity within one ring.

It is worth noting that cooperativity between the two rings is thus, strictly speaking, not mediated by the coiled-coil interaction between subunits on different rings, but precisely by the disruption of this interaction. Thus, the "inhibitory helix" is not only inhibitory with respect to occluding the active site on its own subunit, but also with respect to locking an adjacent subunit in a state where it cannot be autonomously activated.

9.3.5 *Possible experimental validation*

A way to experimentally dissect the contributions of subunit opening and coiled-coil disruption would be to ablate the high-affinity calmodulin binding site and then study the activity of this mutated version of CaMKII both in the presence and absence of calmodulin. The model predicts increased (albeit still low) activity in the presence of calmodulin, because calmodulin binding to the low-affinity site would favour coiled-coil disruption, whilst not affecting subunit opening. Indeed the activity of such a low-affinity-only dodecamer in the presence of calmodulin would probably be similar to that of a monomer in the absence of calmodulin: While there is, in both cases, no stabilisation of the open state by calmodulin binding, there is also no (or not much) coiled-coil formation that interferes with activity.

10

CONCLUSIONS AND OUTLOOK: MODES OF CAMKII REGULATION

A picture emerges in which a variety of regulatory mechanisms are at work to fine-tune CaMKII activity over different time-scales. Some of these mechanisms involve external interaction partners, others are internal to CaMKII and yet others are indirect effects that emerge as by-products of other processes. Some of these mechanisms have been included in the models described in chapters 8 on page 91 and 9 on page 109, while others will have to be modelled and investigated in more detail in the future.

10.1 Ligand binding

By binding to the autoinhibitory helix, calmodulin stabilises the active state of CaMKII (Hanley *et al.*, 1988). It has long been known that calmodulin binding is not necessary for CaMKII activity (for instance, the active state can be maintained independently of calmodulin when CaMKII is autophosphorylated at Thr^{286} (Payne *et al.*, 1988)). The model presented in chapter 8 on page 91 shows that calmodulin binding to CaMKII is not even sufficient for CaMKII activation (although calmodulin binding specifically to the presumed high-affinity binding site is). This is a hypothesis which has not been brought forward so far. A possible experimental way of testing this hypothesis is to measure both calmodulin binding and CaMKII activity on T286A mutant CaMKII, as described in chapter 8 on page 91. Note that according to the model presented in chapter 8 on page 91, calmodulin binding to the high-affinity site of CaMKII *is* sufficient for CaMKII activation, which means that there is still a strong positive correlation between calmodulin activity and CaMKII activity, especially in wild-type CaMKII. This is probably the reason why CaMKII has always been described as a calmodulin-dependent protein.

Calmodulin binding has the additional effect of preventing Thr^{306} autophosphorylation and hence, desensitisation of CaMKII. Phosphorylation at Thr^{286} increases the lifetime of calmodulin-bound CaMKII and could thus be a way of avoiding desensitisation (see chapter 8 on page 91).

Another ligand that stabilises the open state of CaMKII is subunit 2B of the NMDA receptor (NR2B) (Bayer *et al.*, 2001; Petersen *et al.*, 2003; Bayer *et al.*, 2006). In addition, binding to NR2B increases the dwell-time of CaMKII in the PSD, which potentially has indirect effects on CaMKII activity.

10.2 Intra-molecular interactions and cooperativity

Trans-autophosphorylation at Thr^{286} confers calmodulin-independent activity (Hanson *et al.*, 1994). Since one subunit phosphorylates its neighbouring subunit in the same hexameric ring, this autophosphorylation reaction is a way of spreading activity within one half of the holoenzyme.

The formation of a coiled-coil between adjacent subunits on different hexamers might be a way of communicating activation status between the two hexamers. Although opening and coiled-coil interaction are not directly dependent on each other, the coiled-coil prevents both calmodulin binding and autophosphorylation at Thr^{286} and will therefore decrease the likelihood of the subunit being open. Since the disruption of the coiled-coil simultaneously releases two subunits on adjacent rings, it increases the opening probability for both of them, hence providing a way of spreading activation (or, at least, a high probability of activation) between two rings, as described in chapter 9 on page 109.

Autophosphorylation at Thr^{306} is incompatible with calmodulin binding and is therefore likely to provide a desensitisation mechanism in the longer term. It is important to note that this autophosphorylation reaction occurs within one subunit, i. e. there is no mechanism for spreading the desensitisation status between adjacent subunit on the same hexamer. Since the phosphorylation site is located on the autoinhibitory helix, though, the formation of a coiled-coil probably prevents autophosphorylation at Thr^{306}. Thus, the *ability* of

a subunit to be desensitised can spread between two hexamers (and, given that autophosphorylation at Thr^{286} probably prevents desensitisation, also within a hexamer). The incompatibility of Thr^{306} phosphorylation and coiled-coil formation also means that open subunits within a coiled coil effectively constitute active subunits which cannot be desensitised. Since the coiled-coil interaction also prevents calmodulin binding and Thr^{286} autophosphorylation, this activity is, however, merely transient. Thus, the same conditions that are necessary for persistent activity are also necessary for desensitisation.

10.3 Subcellular localisation

The location of CaMKII within the dendritic spine is dynamic, with CaMKII cycling in and out of the PSD (Shen and Meyer, 1999; Shen *et al.*, 2000). CaMKII activity and location mutually affect each other in several ways. In unstimulated cells, CaMKII is distributed in the cytoplasm (Shen and Meyer, 1999), and translocation of CaMKII to the PSD depends on calcium entry through NMDA receptors (Thalhammer *et al.*, 2006). This is consistent with observations that the dwell-time of CaMKII in the PSD increases if CaMKII is bound to calmodulin (Shen and Meyer, 1999) or phosphorylated at Thr^{286} (Shen *et al.*, 2000; Strack *et al.*, 1997b). In contrast, phosphorylation at Thr^{306} seems to destabilise CaMKII association with the PSD (Shen *et al.*, 2000). One mechanism of prolonging the dwell-time of CaMKII in the PSD is the interaction between CaMKII and NR2B. This interaction is contingent on CaMKII being either phosphorylated at Thr^{286} (Bayer *et al.*, 2001) (reviewed in Soderling *et al.*, 2001) or bound to calmodulin (Bayer *et al.*, 2001).

The increased dwell-time in the PSD mediated by NR2B binding might have indirect effects on CaMKII activity: It would allow CaMKII to act on substrates that are concentrated in the PSD (Shen and Meyer, 1999) and improve access to calcium entering through NMDA receptors. It could also alter the accessibility of CaMKII to agents that modulate its function. A recent paper by Mullasseril *et al.* (2007) found that CaMKII is not dephosphorylated by PP1 in the PSD, probably because of the relative positions of both molecules within the postsynaptic protein scaffold. Cycling of CaMKII out of the PSD might

therefore be a necessary mechanism in order to reverse the effect of autophosphorylation and to bring CaMKII back to its native state.

I have started to implement a stochastic model of CaMKII cycling, which includes NMDA receptor binding and differential phosphatase access in different compartments. Work on this project is still in an early stage and will be continued in the future.

10.4 Future directions

A full understanding of CaMKII function and regulation will not only require a synthesis of the mechanisms described here, but possibly also the inclusion of additional mechanisms. Additional phosphorylation sites might play a role in regulating CaMKII activity. Phosphorylation at threonine residue 253 (Thr^{253}) has recently been reported to increase CaMKII binding to the PSD, without directly modulating its activity (Migues *et al.*, 2006). Other studies have suggested that CaMKII can self-associate to form inactive clusters, which might provide a quick way of depleting active CaMKII pools (Grant *et al.*, 2008; Hudmon *et al.*, 1996). Similar to NMDA receptors, other proteins might bind to CaMKII and thus help regulate its subcellular localisation (see, for instance, Colbran and Brown, 2004; Walikonis *et al.*, 2001). On a longer time scale, the amount of available CaMKII in the dendritic spine will depend on the synthesis and transport of CaMKII messenger RNA (mRNA) (reviewed in Colbran and Brown, 2004). In addition, the subunit composition of CaMKII, i. e. the content of α and β isoforms, changes both with neuronal activity and in the course of development (reviewed in Colbran and Brown, 2004; Gaertner *et al.*, 2004). As seen with calmodulin (chapter 4 on page 31), the interaction partners of CaMKII are themselves tightly regulated, and analysis of the complete signalling pathway will therefore be necessary to put CaMKII function into context.

11

CONCLUSIONS

11.1 Summary

In this work, I have provided mechanistic explanations for the regulation of two crucial signalling proteins in synaptic plasticity: calmodulin and CaMKII. The behaviour of calmodulin is consistent with MWC-type allosteric regulation. This makes calmodulin the first example of a "generalised" MWC protein, which has non-identical binding sites. I have presented the corresponding generalised MWC model and a way of relating parameters of this model to the Adair-Klotz framework in order to facilitate communication between allosteric theoreticians and experimentalists. I have provided a way of describing the cooperativity of conformational change and used this description to show that ligand depletion might be an important factor in regulating the cooperativity of signal response *in vivo*. For CaMKII, I have presented a mechanistic explanation of calmodulin trapping, a consequence of which is that calmodulin binding is not in all cases sufficient for CaMKII activation. Investigating interactions between subunits, I have for the first time provided a plausible model of how CaMKII activity spreads not just within a hexameric ring, but between the two rings that constitute the dodecamer.

11.2 Towards a molecular understanding of memory

Both calmodulin and CaMKII play a vital role in NMDA receptor-dependent bidirectional synaptic plasticity. Understanding their function and activation patterns might help elucidate the molecular mechanisms that underlie learning and memory.

The calmodulin model explains how calmodulin can act as a switch, mediating CaMKII activation, and hence, LTP at high intracellular calcium concentrations, and PP2B activation and, in consequence, LTD at low calcium concentrations. This provides a molecular explana-

tion for the Lisman hypothesis (Lisman, 1989), which states that an increase in postsynaptic calcium levels will result in an increase in synaptic strength, while moderate calcium levels will result in a decrease of synaptic strength. Since calcium levels in the PSD are dependent on coordinated pre- and postsynaptic activity, calmodulin performs the function of a molecular decision-maker between Hebb and Anti-Hebb processes. This highlights once again the suitability of the postsynaptic signalling pathway as a Hebbian learning device and of LTP and LTD as plausible physiological correlates of learning and memory.

CaMKII has long been known to be important both for LTP and learning. Its role as a potential memory device, the activity of which exceeds the time-scale of a transient calcium signal, is thought to rely on two mechanisms: calmodulin trapping and autonomous activity upon autophosphorylation at Thr^{286}. I have proposed a mechanistic explanation of calmodulin trapping, which suggests that trapping might serve the additional purpose of preventing CaMKII desensitisation.

It has been noted before (Lisman and Zhabotinsky, 2001; Zhabotinsky, 2000) how intra-holoenzyme autophosphorylation at Thr^{286} can help maintain autonomous CaMKII activity over long periods of time and thus make CaMKII suitable as a molecular memory device. Hudmon and Schulman (2002) have noted how the trans-subunit nature of Thr^{286} autophosphorylation might render this device frequency-dependent. Both these models were based on the idea of a CaMKII holoenzyme being a single oligomeric ring, with Thr^{286} phosphorylation taking place between two adjacent subunits on the ring. The structure of CaMKII published by Rosenberg *et al.* (2005) revealed that a CaMKII holoenzyme is, in fact, composed of two stacked hexameric rings. Autophosphorylation proceeds within a ring, but not between subunits on different rings. The detailed structure-based model presented in chapter 9 on page 109 shows how a CaMKII dodecamer can still function as a frequency-dependent memory device and provides the first confirmation of Hudmon's hypothesis.

11.3 Variations on a theme: cooperativity

A theme that has come up again and again throughout this work is that of cooperativity and of the different ways in which it can be achieved.

MWC-type allosteric regulation entails cooperativity as an emergent property. I have made the case that this type of regulation is not limited to molecules composed of identical protomers and introduced tools to analyse proteins according to a more general MWC scheme. Thus, allosteric regulation might emerge as a powerful – and quite frequent – mechanism of cooperativity in the future.

Autoregulation within a holoenzyme – including autoinhibition, autophosphorylation and autodesensitisation – can modulate activity in a cooperative manner, as shown for the case of CaMKII. Interestingly, various forms of autoregulation can co-exist within the same molecule to fine-tune cooperative signal response.

The *protein-to-ligand ratio* modulates not only the amplitude of signal response, but also its cooperativity, at least in situations of ligand depletion. Different levels of a specific protein (e. g. in different cells or at different stages of development) will create different cooperativity regimes, even in response to the same kind and amount of signal.

Indirect effects create added layers of regulation. Although such effects are not necessarily cooperative by themselves, they might interact cooperatively with other effects. For instance, binding of CaMKII to the NMDA receptor not only stabilises the active state of the kinase, but also increases its dwell-time in the PSD, thus improving its access to calcium and to PSD-bound targets and protecting it from deactivation by phosphatases.

11.4 From micro to macro scale

In biology, the same question can be addressed on different scales, from structural biology on the microscopic scale, to pathways and networks, to the behaviour of even larger systems. The models presented here look at protein-protein interactions and regulation patterns of a few molecular species, and are thus situated "in between" a structural approach and larger, pathway-based descriptions of a sys-

tem. This might be rather unusual, but it has the merits of being able to use structural information in order to explain dynamic properties of molecules on a macroscopic scale.

11.5 A case for Systems Biology

This work, I think, also makes a case for Systems Biology. For the last decades, molecular biology has focused on analysis, isolating and describing parts of biological systems. For instance, a wealth of publications on specific aspects of calmodulin and CaMKII – protein distribution, biochemical properties, structure, protein-protein interactions, mutational analyses – is now available. The models presented in this work hardly make any additional assumptions and are, in fact, completely assembled from observations and hypotheses found in the experimental literature. However, all of them turned out to be more than a mere collection or census of observations already known, but have yielded new, non-trivial and often surprising insights. Moreover, they have led to the formulation of testable predictions, potentially feeding back to the experimental community and opening up new avenues of research. Thus, the synthesis of information has generated new insights, and therein lies the power – and the beauty – of Systems Biology.

Part III

APPENDIX

A

CALMODULIN MODEL: LIST OF REACTIONS

Table 10: List of reactions included in the model of calmodulin and their respective reaction rates.

T + ca → T_ca1_A	k_{on}
T + ca → T_ca1_B	k_{on}
T + ca → T_ca1_C	k_{on}
T + ca → T_ca1_D	k_{on}
T_ca1_A + ca → T_ca2_AB	k_{on}
T_ca1_A + ca → T_ca2_AC	k_{on}
T_ca1_A + ca → T_ca2_AD	k_{on}
T_ca1_B + ca → T_ca2_AB	k_{on}
T_ca1_B + ca → T_ca2_BC	k_{on}
T_ca1_B + ca → T_ca2_BD	k_{on}
T_ca1_C + ca → T_ca2_AC	k_{on}
T_ca1_C + ca → T_ca2_BC	k_{on}
T_ca1_C + ca → T_ca2_CD	k_{on}
T_ca1_D + ca → T_ca2_AD	k_{on}
T_ca1_D + ca → T_ca2_BD	k_{on}
T_ca1_D + ca → T_ca2_CD	k_{on}
T_ca2_AB + ca → T_ca3_ABC	k_{on}
T_ca2_AB + ca → T_ca3_ABD	k_{on}
T_ca2_AC + ca → T_ca3_ABC	k_{on}
T_ca2_AC + ca → T_ca3_ACD	k_{on}
T_ca2_AD + ca → T_ca3_ABD	k_{on}
T_ca2_AD + ca → T_ca3_ACD	k_{on}
T_ca2_BC + ca → T_ca3_ABC	k_{on}
T_ca2_BC + ca → T_ca3_BCD	k_{on}
T_ca2_BD + ca → T_ca3_ABD	k_{on}
T_ca2_BD + ca → T_ca3_BCD	k_{on}

Table 10: continued

T_ca2_CD + ca → T_ca3_ACD	k_{on}
T_ca2_CD + ca → T_ca3_BCD	k_{on}
T_ca3_ABC + ca → T_ca4_ABCD	k_{on}
T_ca3_ABD + ca → T_ca4_ABCD	k_{on}
T_ca3_ACD + ca → T_ca4_ABCD	k_{on}
T_ca3_BCD + ca → T_ca4_ABCD	k_{on}
T_ca1_A → T + ca	$k^T_{off_A}$
T_ca1_B → T + ca	$k^T_{off_B}$
T_ca1_C → T + ca	$k^T_{off_C}$
T_ca1_D → T + ca	$k^T_{off_D}$
T_ca2_AB → T_ca1_A + ca	$k^T_{off_B}$
T_ca2_AB → T_ca1_B + ca	$k^T_{off_A}$
T_ca2_AC → T_ca1_A + ca	$k^T_{off_C}$
T_ca2_AC → T_ca1_C + ca	$k^T_{off_A}$
T_ca2_AD → T_ca1_A + ca	$k^T_{off_D}$
T_ca2_AD → T_ca1_D + ca	$k^T_{off_A}$
T_ca2_BC → T_ca1_B + ca	$k^T_{off_C}$
T_ca2_BC → T_ca1_C + ca	$k^T_{off_B}$
T_ca2_BD → T_ca1_B + ca	$k^T_{off_D}$
T_ca2_BD → T_ca1_D + ca	$k^T_{off_B}$
T_ca2_CD → T_ca1_C + ca	$k^T_{off_D}$
T_ca2_CD → T_ca1_D + ca	$k^T_{off_C}$
T_ca3_ABC → T_ca2_AB + ca	$k^T_{off_C}$
T_ca3_ABC → T_ca2_AC + ca	$k^T_{off_B}$
T_ca3_ABC → T_ca2_BC + ca	$k^T_{off_A}$
T_ca3_ABD → T_ca2_AB + ca	$k^T_{off_D}$
T_ca3_ABD → T_ca2_AD + ca	$k^T_{off_B}$
T_ca3_ABD → T_ca2_BD + ca	$k^T_{off_A}$
T_ca3_ACD → T_ca2_AC + ca	$k^T_{off_D}$
T_ca3_ACD → T_ca2_AD + ca	$k^T_{off_C}$
T_ca3_ACD → T_ca2_CD + ca	$k^T_{off_A}$

Table 10: continued

T_ca3_BCD → T_ca2_BC + ca	$k^T_{off_D}$
T_ca3_BCD → T_ca2_BD + ca	$k^T_{off_C}$
T_ca3_BCD → T_ca2_CD + ca	$k^T_{off_B}$
T_ca4_ABCD → T_ca3_ABC + ca	$k^T_{off_D}$
T_ca4_ABCD → T_ca3_ABD + ca	$k^T_{off_C}$
T_ca4_ABCD → T_ca3_ACD + ca	$k^T_{off_B}$
T_ca4_ABCD → T_ca3_BCD + ca	$k^T_{off_A}$
R + ca → R_ca1_A	k_{on}
R + ca → R_ca1_B	k_{on}
R + ca → R_ca1_C	k_{on}
R + ca → R_ca1_D	k_{on}
R_ca1_A + ca → R_ca2_AB	k_{on}
R_ca1_A + ca → R_ca2_AC	k_{on}
R_ca1_A + ca → R_ca2_AD	k_{on}
R_ca1_B + ca → R_ca2_AB	k_{on}
R_ca1_B + ca → R_ca2_BC	k_{on}
R_ca1_B + ca → R_ca2_BD	k_{on}
R_ca1_C + ca → R_ca2_AC	k_{on}
R_ca1_C + ca → R_ca2_BC	k_{on}
R_ca1_C + ca → R_ca2_CD	k_{on}
R_ca1_D + ca → R_ca2_AD	k_{on}
R_ca1_D + ca → R_ca2_BD	k_{on}
R_ca1_D + ca → R_ca2_CD	k_{on}
R_ca2_AB + ca → R_ca3_ABC	k_{on}
R_ca2_AB + ca → R_ca3_ABD	k_{on}
R_ca2_AC + ca → R_ca3_ABC	k_{on}
R_ca2_AC + ca → R_ca3_ACD	k_{on}
R_ca2_AD + ca → R_ca3_ABD	k_{on}
R_ca2_AD + ca → R_ca3_ACD	k_{on}
R_ca2_BC + ca → R_ca3_ABC	k_{on}
R_ca2_BC + ca → R_ca3_BCD	k_{on}
R_ca2_BD + ca → R_ca3_ABD	k_{on}
R_ca2_BD + ca → R_ca3_BCD	k_{on}

Table 10: continued

R_ca2_CD + ca → R_ca3_ACD	k_{on}
R_ca2_CD + ca → R_ca3_BCD	k_{on}
R_ca3_ABC + ca → R_ca4_ABCD	k_{on}
R_ca3_ABD + ca → R_ca4_ABCD	k_{on}
R_ca3_ACD + ca → R_ca4_ABCD	k_{on}
R_ca3_BCD + ca → R_ca4_ABCD	k_{on}
R_ca1_A → R + ca	$k^R_{off_A}$
R_ca1_B → R + ca	$k^R_{off_B}$
R_ca1_C → R + ca	$k^R_{off_C}$
R_ca1_D → R + ca	$k^R_{off_D}$
R_ca2_AB → R_ca1_A + ca	$k^R_{off_B}$
R_ca2_AB → R_ca1_B + ca	$k^R_{off_A}$
R_ca2_AC → R_ca1_A + ca	$k^R_{off_C}$
R_ca2_AC → R_ca1_C + ca	$k^R_{off_A}$
R_ca2_AD → R_ca1_A + ca	$k^R_{off_D}$
R_ca2_AD → R_ca1_D + ca	$k^R_{off_A}$
R_ca2_BC → R_ca1_B + ca	$k^R_{off_C}$
R_ca2_BC → R_ca1_C + ca	$k^R_{off_B}$
R_ca2_BD → R_ca1_B + ca	$k^R_{off_D}$
R_ca2_BD → R_ca1_D + ca	$k^R_{off_B}$
R_ca2_CD → R_ca1_C + ca	$k^R_{off_D}$
R_ca2_CD → R_ca1_D + ca	$k^R_{off_C}$
R_ca3_ABC → R_ca2_AB + ca	$k^R_{off_C}$
R_ca3_ABC → R_ca2_AC + ca	$k^R_{off_B}$
R_ca3_ABC → R_ca2_BC + ca	$k^R_{off_A}$
R_ca3_ABD → R_ca2_AB + ca	$k^R_{off_D}$
R_ca3_ABD → R_ca2_AD + ca	$k^R_{off_B}$
R_ca3_ABD → R_ca2_BD + ca	$k^R_{off_A}$
R_ca3_ACD → R_ca2_AC + ca	$k^R_{off_D}$
R_ca3_ACD → R_ca2_AD + ca	$k^R_{off_C}$
R_ca3_ACD → R_ca2_CD + ca	$k^R_{off_A}$

Table 10: continued

R_ca3_BCD → R_ca2_BC + ca	$k^R_{off_D}$
R_ca3_BCD → R_ca2_BD + ca	$k^R_{off_C}$
R_ca3_BCD → R_ca2_CD + ca	$k^R_{off_B}$
R_ca4_ABCD → R_ca3_ABC + ca	$k^R_{off_D}$
R_ca4_ABCD → R_ca3_ABD + ca	$k^R_{off_C}$
R_ca4_ABCD → R_ca3_ACD + ca	$k^R_{off_B}$
R_ca4_ABCD → R_ca3_BCD + ca	$k^R_{off_A}$
R → T	k_{RT}
R_ca1_A → T_ca1_A	$k_{RT} \times \sqrt{c}$
R_ca1_B → T_ca1_B	$k_{RT} \times \sqrt{c}$
R_ca1_C → T_ca1_C	$k_{RT} \times \sqrt{c}$
R_ca1_D → T_ca1_D	$k_{RT} \times \sqrt{c}$
R_ca2_AB → T_ca2_AB	$k_{RT} \times c$
R_ca2_AC → T_ca2_AC	$k_{RT} \times c$
R_ca2_AD → T_ca2_AD	$k_{RT} \times c$
R_ca2_BC → T_ca2_BC	$k_{RT} \times c$
R_ca2_BD → T_ca2_BD	$k_{RT} \times c$
R_ca2_CD → T_ca2_CD	$k_{RT} \times c$
R_ca3_ABC → T_ca3_ABC	$k_{RT} \times \sqrt{c^3}$
R_ca3_ABD → T_ca3_ABD	$k_{RT} \times \sqrt{c^3}$
R_ca3_ACD → T_ca3_ACD	$k_{RT} \times \sqrt{c^3}$
R_ca3_BCD → T_ca3_BCD	$k_{RT} \times \sqrt{c^3}$
R_ca4_ABCD → T_ca4_ABD	$k_{RT} \times c^2$
T → R	k_{TR}
T_ca1_A → R_ca1_A	$k_{TR} / \sqrt{c}$
T_ca1_B → R_ca1_B	$k_{TR} / \sqrt{c}$
T_ca1_C → R_ca1_C	$k_{TR} / \sqrt{c}$
T_ca1_D → R_ca1_D	$k_{TR} / \sqrt{c}$
T_ca2_AB → R_ca2_AB	k_{TR} / c
T_ca2_AC → R_ca2_AC	k_{TR} / c
T_ca2_AD → R_ca2_AD	k_{TR} / c
T_ca2_BC → R_ca2_BC	k_{TR} / c
T_ca2_BD → R_ca2_BD	k_{TR} / c

Table 10: continued

T_ca2_CD → R_ca2_CD	k_{TR}/c
T_ca3_ABC → R_ca3_ABC	$k_{TR}/\sqrt{c^3}$
T_ca3_ABD → R_ca3_ABD	$k_{TR}/\sqrt{c^3}$
T_ca3_ACD → R_ca3_ACD	$k_{TR}/\sqrt{c^3}$
T_ca3_BCD → R_ca3_BCD	$k_{TR}/\sqrt{c^3}$
T_ca4_ABCD → R_ca4_ABD	k_{TR}/c^2
R + CaMKII → R_CaMKII	$k^R_{on_{CaMKII}}$
R_ca1_A + CaMKII → R_ca1_A_CaMKII	$k^R_{on_{CaMKII}}$
R_ca1_B + CaMKII → R_ca1_B_CaMKII	$k^R_{on_{CaMKII}}$
R_ca1_C + CaMKII → R_ca1_C_CaMKII	$k^R_{on_{CaMKII}}$
R_ca1_D + CaMKII → R_ca1_D_CaMKII	$k^R_{on_{CaMKII}}$
R_ca2_AB + CaMKII → R_ca2_AB_CaMKII	$k^R_{on_{CaMKII}}$
R_ca2_AC + CaMKII → R_ca2_AC_CaMKII	$k^R_{on_{CaMKII}}$
R_ca2_AD + CaMKII → R_ca2_AD_CaMKII	$k^R_{on_{CaMKII}}$
R_ca2_BC + CaMKII → R_ca2_BC_CaMKII	$k^R_{on_{CaMKII}}$
R_ca2_BD + CaMKII → R_ca2_BD_CaMKII	$k^R_{on_{CaMKII}}$
R_ca2_CD + CaMKII → R_ca2_CD_CaMKII	$k^R_{on_{CaMKII}}$
R_ca3_ABC + CaMKII → R_ca3_ABC_CaMKII	$k^R_{on_{CaMKII}}$
R_ca3_ABD + CaMKII → R_ca3_ABD_CaMKII	$k^R_{on_{CaMKII}}$
R_ca3_ACD + CaMKII → R_ca3_ACD_CaMKII	$k^R_{on_{CaMKII}}$
R_ca3_BCD + CaMKII → R_ca3_BCD_CaMKII	$k^R_{on_{CaMKII}}$
R_ca4_ABCD + CaMKII → R_ca4_ABCD_CaMKII	$k^R_{on_{CaMKII}}$
R_CaMKII → R + CaMKII	$k^R_{off_{CaMKII}}$
R_ca1_A_CaMKII → R_ca1_A + CaMKII	$k^R_{off_{CaMKII}}$
R_ca1_B_CaMKII → R_ca1_B + CaMKII	$k^R_{off_{CaMKII}}$
R_ca1_C_CaMKII → R_ca1_C + CaMKII	$k^R_{off_{CaMKII}}$
R_ca1_D_CaMKII → R_ca1_D + CaMKII	$k^R_{off_{CaMKII}}$
R_ca2_AB_CaMKII → R_ca2_AB + CaMKII	$k^R_{off_{CaMKII}}$
R_ca2_AC_CaMKII → R_ca2_AC + CaMKII	$k^R_{off_{CaMKII}}$
R_ca2_AD_CaMKII → R_ca2_AD + CaMKII	$k^R_{off_{CaMKII}}$
R_ca2_BC_CaMKII → R_ca2_BC + CaMKII	$k^R_{off_{CaMKII}}$
R_ca2_BD_CaMKII → R_ca2_BD + CaMKII	$k^R_{off_{CaMKII}}$

Table 10: continued

R_ca2_CD_CaMKII → R_ca2_CD + CaMKII	$k^R_{off_{CaMKII}}$
R_ca3_ABC_CaMKII → R_ca3_ABC + CaMKII	$k^R_{off_{CaMKII}}$
R_ca3_ABD_CaMKII → R_ca3_ABD + CaMKII	$k^R_{off_{CaMKII}}$
R_ca3_ACD_CaMKII → R_ca3_ACD + CaMKII	$k^R_{off_{CaMKII}}$
R_ca3_BCD_CaMKII → R_ca3_BCD + CaMKII	$k^R_{off_{CaMKII}}$
R_ca4_ABCD_CaMKII → R_ca4_ABCD + CaMKII	$k^R_{off_{CaMKII}}$
R + PP2B → R_PP2B	$k^R_{on_{PP2B}}$
R_ca1_A + PP2B → R_ca1_A_PP2B	$k^R_{on_{PP2B}}$
R_ca1_B + PP2B → R_ca1_B_PP2B	$k^R_{on_{PP2B}}$
R_ca1_C + PP2B → R_ca1_C_PP2B	$k^R_{on_{PP2B}}$
R_ca1_D + PP2B → R_ca1_D_PP2B	$k^R_{on_{PP2B}}$
R_ca2_AB + PP2B → R_ca2_AB_PP2B	$k^R_{on_{PP2B}}$
R_ca2_AC + PP2B → R_ca2_AC_PP2B	$k^R_{on_{PP2B}}$
R_ca2_AD + PP2B → R_ca2_AD_PP2B	$k^R_{on_{PP2B}}$
R_ca2_BC + PP2B → R_ca2_BC_PP2B	$k^R_{on_{PP2B}}$
R_ca2_BD + PP2B → R_ca2_BD_PP2B	$k^R_{on_{PP2B}}$
R_ca2_CD + PP2B → R_ca2_CD_PP2B	$k^R_{on_{PP2B}}$
R_ca3_ABC + PP2B → R_ca3_ABC_PP2B	$k^R_{on_{PP2B}}$
R_ca3_ABD + PP2B → R_ca3_ABD_PP2B	$k^R_{on_{PP2B}}$
R_ca3_ACD + PP2B → R_ca3_ACD_PP2B	$k^R_{on_{PP2B}}$
R_ca3_BCD + PP2B → R_ca3_BCD_PP2B	$k^R_{on_{PP2B}}$
R_ca4_ABCD + PP2B → R_ca4_ABCD_PP2B	$k^R_{on_{PP2B}}$
R_PP2B → R + PP2B	$k^R_{off_{PP2B}}$
R_ca1_A_PP2B → R_ca1_A + PP2B	$k^R_{off_{PP2B}}$
R_ca1_B_PP2B → R_ca1_B + PP2B	$k^R_{off_{PP2B}}$
R_ca1_C_PP2B → R_ca1_C + PP2B	$k^R_{off_{PP2B}}$
R_ca1_D_PP2B → R_ca1_D + PP2B	$k^R_{off_{PP2B}}$
R_ca2_AB_PP2B → R_ca2_AB + PP2B	$k^R_{off_{PP2B}}$
R_ca2_AC_PP2B → R_ca2_AC + PP2B	$k^R_{off_{PP2B}}$
R_ca2_AD_PP2B → R_ca2_AD + PP2B	$k^R_{off_{PP2B}}$
R_ca2_BC_PP2B → R_ca2_BC + PP2B	$k^R_{off_{PP2B}}$
R_ca2_BD_PP2B → R_ca2_BD + PP2B	$k^R_{off_{PP2B}}$

Table 10: continued

R_ca2_CD_PP2B → R_ca2_CD + PP2B	$k^R_{off\,PP2B}$
R_ca3_ABC_PP2B → R_ca3_ABC + PP2B	$k^R_{off\,PP2B}$
R_ca3_ABD_PP2B → R_ca3_ABD + PP2B	$k^R_{off\,PP2B}$
R_ca3_ACD_PP2B → R_ca3_ACD + PP2B	$k^R_{off\,PP2B}$
R_ca3_BCD_PP2B → R_ca3_BCD + PP2B	$k^R_{off\,PP2B}$
R_ca4_ABCD_PP2B → R_ca4_ABCD + PP2B	$k^R_{off\,PP2B}$
R_CaMKII + ca → R_ca1_A_CaMKII	k^R_{on}
R_CaMKII + ca → R_ca1_B_CaMKII	k^R_{on}
R_CaMKII + ca → R_ca1_C_CaMKII	k^R_{on}
R_CaMKII + ca → R_ca1_D_CaMKII	k^R_{on}
R_ca1_A_CaMKII + ca → R_ca2_AB_CaMKII	k^R_{on}
R_ca1_A_CaMKII + ca → R_ca2_AC_CaMKII	k^R_{on}
R_ca1_A_CaMKII + ca → R_ca2_AD_CaMKII	k^R_{on}
R_ca1_B_CaMKII + ca → R_ca2_AB_CaMKII	k^R_{on}
R_ca1_B_CaMKII + ca → R_ca2_BC_CaMKII	k^R_{on}
R_ca1_B_CaMKII + ca → R_ca2_BD_CaMKII	k^R_{on}
R_ca1_C_CaMKII + ca → R_ca2_AC_CaMKII	k^R_{on}
R_ca1_C_CaMKII + ca → R_ca2_BC_CaMKII	k^R_{on}
R_ca1_C_CaMKII + ca → R_ca2_CD_CaMKII	k^R_{on}
R_ca1_D_CaMKII + ca → R_ca2_AD_CaMKII	k^R_{on}
R_ca1_D_CaMKII + ca → R_ca2_BD_CaMKII	k^R_{on}
R_ca1_D_CaMKII + ca → R_ca2_CD_CaMKII	k^R_{on}
R_ca2_AB_CaMKII + ca → R_ca3_ABC_CaMKII	k^R_{on}
R_ca2_AB_CaMKII + ca → R_ca3_ABD_CaMKII	k^R_{on}
R_ca2_AC_CaMKII + ca → R_ca3_ABC_CaMKII	k^R_{on}
R_ca2_AC_CaMKII + ca → R_ca3_ACD_CaMKII	k^R_{on}
R_ca2_AD_CaMKII + ca → R_ca3_ABD_CaMKII	k^R_{on}
R_ca2_AD_CaMKII + ca → R_ca3_ACD_CaMKII	k^R_{on}
R_ca2_BC_CaMKII + ca → R_ca3_ABC_CaMKII	k^R_{on}
R_ca2_BC_CaMKII + ca → R_ca3_BCD_CaMKII	k^R_{on}
R_ca2_BD_CaMKII + ca → R_ca3_ABD_CaMKII	k^R_{on}
R_ca2_BD_CaMKII + ca → R_ca3_BCD_CaMKII	k^R_{on}
R_ca2_CD_CaMKII + ca → R_ca3_ACD_CaMKII	k^R_{on}

Table 10: continued

R_ca2_CD_CaMKII + ca → R_ca3_BCD_CaMKII	k_{on}^{R}
R_ca3_ABC_CaMKII + ca → R_ca4_ABCD_CaMKII	k_{on}^{R}
R_ca3_ABD_CaMKII + ca → R_ca4_ABCD_CaMKII	k_{on}^{R}
R_ca3_ACD_CaMKII + ca → R_ca4_ABCD_CaMKII	k_{on}^{R}
R_ca3_BCD_CaMKII + ca → R_ca4_ABCD_CaMKII	k_{on}^{R}
R_ca1_A_CaMKII → R_CaMKII + ca	$k_{off_A}^{R}$
R_ca1_B_CaMKII → R_CaMKII + ca	$k_{off_B}^{R}$
R_ca1_C_CaMKII → R_CaMKII + ca	$k_{off_C}^{R}$
R_ca1_D_CaMKII → R_CaMKII + ca	$k_{off_D}^{R}$
R_ca2_AB_CaMKII → R_ca1_A_CaMKII + ca	$k_{off_B}^{R}$
R_ca2_AB_CaMKII → R_ca1_B_CaMKII + ca	$k_{off_A}^{R}$
R_ca2_AC_CaMKII → R_ca1_A_CaMKII + ca	$k_{off_C}^{R}$
R_ca2_AC_CaMKII → R_ca1_C_CaMKII + ca	$k_{off_A}^{R}$
R_ca2_AD_CaMKII → R_ca1_A_CaMKII + ca	$k_{off_D}^{R}$
R_ca2_AD_CaMKII → R_ca1_D_CaMKII + ca	$k_{off_A}^{R}$
R_ca2_BC_CaMKII → R_ca1_B_CaMKII + ca	$k_{off_C}^{R}$
R_ca2_BC_CaMKII → R_ca1_C_CaMKII + ca	$k_{off_B}^{R}$
R_ca2_BD_CaMKII → R_ca1_B_CaMKII + ca	$k_{off_D}^{R}$
R_ca2_BD_CaMKII → R_ca1_D_CaMKII + ca	$k_{off_B}^{R}$
R_ca2_CD_CaMKII → R_ca1_C_CaMKII + ca	$k_{off_D}^{R}$
R_ca2_CD_CaMKII → R_ca1_D_CaMKII + ca	$k_{off_C}^{R}$
R_ca3_ABC_CaMKII → R_ca2_AB_CaMKII + ca	$k_{off_C}^{R}$
R_ca3_ABC_CaMKII → R_ca2_AC_CaMKII + ca	$k_{off_B}^{R}$
R_ca3_ABC_CaMKII → R_ca2_BC_CaMKII + ca	$k_{off_A}^{R}$
R_ca3_ABD_CaMKII → R_ca2_AB_CaMKII + ca	$k_{off_D}^{R}$
R_ca3_ABD_CaMKII → R_ca2_AD_CaMKII + ca	$k_{off_B}^{R}$
R_ca3_ABD_CaMKII → R_ca2_BD_CaMKII + ca	$k_{off_A}^{R}$
R_ca3_ACD_CaMKII → R_ca2_AC_CaMKII + ca	$k_{off_D}^{R}$
R_ca3_ACD_CaMKII → R_ca2_AD_CaMKII + ca	$k_{off_C}^{R}$
R_ca3_ACD_CaMKII → R_ca2_CD_CaMKII + ca	$k_{off_A}^{R}$
R_ca3_BCD_CaMKII → R_ca2_BC_CaMKII + ca	$k_{off_D}^{R}$

Table 10: continued

R_ca3_BCD_CaMKII → R_ca2_BD_CaMKII + ca	$k^R_{off_C}$
R_ca3_BCD_CaMKII → R_ca2_CD_CaMKII + ca	$k^R_{off_B}$
R_ca4_ABCD_CaMKII → R_ca3_ABC_CaMKII + ca	$k^R_{off_D}$
R_ca4_ABCD_CaMKII → R_ca3_ABD_CaMKII + ca	$k^R_{off_C}$
R_ca4_ABCD_CaMKII → R_ca3_ACD_CaMKII + ca	$k^R_{off_B}$
R_ca4_ABCD_CaMKII → R_ca3_BCD_CaMKII + ca	$k^R_{off_A}$
R_PP2B + ca → R_ca1_A_PP2B	k^R_{on}
R_PP2B + ca → R_ca1_B_PP2B	k^R_{on}
R_PP2B + ca → R_ca1_C_PP2B	k^R_{on}
R_PP2B + ca → R_ca1_D_PP2B	k^R_{on}
R_ca1_A_PP2B + ca → R_ca2_AB_PP2B	k^R_{on}
R_ca1_A_PP2B + ca → R_ca2_AC_PP2B	k^R_{on}
R_ca1_A_PP2B + ca → R_ca2_AD_PP2B	k^R_{on}
R_ca1_B_PP2B + ca → R_ca2_AB_PP2B	k^R_{on}
R_ca1_B_PP2B + ca → R_ca2_BC_PP2B	k^R_{on}
R_ca1_B_PP2B + ca → R_ca2_BD_PP2B	k^R_{on}
R_ca1_C_PP2B + ca → R_ca2_AC_PP2B	k^R_{on}
R_ca1_C_PP2B + ca → R_ca2_BC_PP2B	k^R_{on}
R_ca1_C_PP2B + ca → R_ca2_CD_PP2B	k^R_{on}
R_ca1_D_PP2B + ca → R_ca2_AD_PP2B	k^R_{on}
R_ca1_D_PP2B + ca → R_ca2_BD_PP2B	k^R_{on}
R_ca1_D_PP2B + ca → R_ca2_CD_PP2B	k^R_{on}
R_ca2_AB_PP2B + ca → R_ca3_ABC_PP2B	k^R_{on}
R_ca2_AB_PP2B + ca → R_ca3_ABD_PP2B	k^R_{on}
R_ca2_AC_PP2B + ca → R_ca3_ABC_PP2B	k^R_{on}
R_ca2_AC_PP2B + ca → R_ca3_ACD_PP2B	k^R_{on}
R_ca2_AD_PP2B + ca → R_ca3_ABD_PP2B	k^R_{on}
R_ca2_AD_PP2B + ca → R_ca3_ACD_PP2B	k^R_{on}
R_ca2_BC_PP2B + ca → R_ca3_ABC_PP2B	k^R_{on}
R_ca2_BC_PP2B + ca → R_ca3_BCD_PP2B	k^R_{on}
R_ca2_BD_PP2B + ca → R_ca3_ABD_PP2B	k^R_{on}
R_ca2_BD_PP2B + ca → R_ca3_BCD_PP2B	k^R_{on}
R_ca2_CD_PP2B + ca → R_ca3_ACD_PP2B	k^R_{on}

Table 10: continued

R_ca2_CD_PP2B + ca → R_ca3_BCD_PP2B	k_{on}^{R}
R_ca3_ABC_PP2B + ca → R_ca4_ABCD_PP2B	k_{on}^{R}
R_ca3_ABD_PP2B + ca → R_ca4_ABCD_PP2B	k_{on}^{R}
R_ca3_ACD_PP2B + ca → R_ca4_ABCD_PP2B	k_{on}^{R}
R_ca3_BCD_PP2B + ca → R_ca4_ABCD_PP2B	k_{on}^{R}
R_ca1_A_PP2B → R_PP2B + ca	$k_{off_A}^{R}$
R_ca1_B_PP2B → R_PP2B + ca	$k_{off_B}^{R}$
R_ca1_C_PP2B → R_PP2B + ca	$k_{off_C}^{R}$
R_ca1_D_PP2B → R_PP2B + ca	$k_{off_D}^{R}$
R_ca2_AB_PP2B → R_ca1_A_PP2B + ca	$k_{off_B}^{R}$
R_ca2_AB_PP2B → R_ca1_B_PP2B + ca	$k_{off_A}^{R}$
R_ca2_AC_PP2B → R_ca1_A_PP2B + ca	$k_{off_C}^{R}$
R_ca2_AC_PP2B → R_ca1_C_PP2B + ca	$k_{off_A}^{R}$
R_ca2_AD_PP2B → R_ca1_A_PP2B + ca	$k_{off_D}^{R}$
R_ca2_AD_PP2B → R_ca1_D_PP2B + ca	$k_{off_A}^{R}$
R_ca2_BC_PP2B → R_ca1_B_PP2B + ca	$k_{off_C}^{R}$
R_ca2_BC_PP2B → R_ca1_C_PP2B + ca	$k_{off_B}^{R}$
R_ca2_BD_PP2B → R_ca1_B_PP2B + ca	$k_{off_D}^{R}$
R_ca2_BD_PP2B → R_ca1_D_PP2B + ca	$k_{off_B}^{R}$
R_ca2_CD_PP2B → R_ca1_C_PP2B + ca	$k_{off_D}^{R}$
R_ca2_CD_PP2B → R_ca1_D_PP2B + ca	$k_{off_C}^{R}$
R_ca3_ABC_PP2B → R_ca2_AB_PP2B + ca	$k_{off_C}^{R}$
R_ca3_ABC_PP2B → R_ca2_AC_PP2B + ca	$k_{off_B}^{R}$
R_ca3_ABC_PP2B → R_ca2_BC_PP2B + ca	$k_{off_A}^{R}$
R_ca3_ABD_PP2B → R_ca2_AB_PP2B + ca	$k_{off_D}^{R}$
R_ca3_ABD_PP2B → R_ca2_AD_PP2B + ca	$k_{off_B}^{R}$
R_ca3_ABD_PP2B → R_ca2_BD_PP2B + ca	$k_{off_A}^{R}$
R_ca3_ACD_PP2B → R_ca2_AC_PP2B + ca	$k_{off_D}^{R}$
R_ca3_ACD_PP2B → R_ca2_AD_PP2B + ca	$k_{off_C}^{R}$
R_ca3_ACD_PP2B → R_ca2_CD_PP2B + ca	$k_{off_A}^{R}$
R_ca3_BCD_PP2B → R_ca2_BC_PP2B + ca	$k_{off_D}^{R}$

Table 10: continued

R_ca3_BCD_PP2B → R_ca2_BD_PP2B + ca	$k^R_{off_C}$
R_ca3_BCD_PP2B → R_ca2_CD_PP2B + ca	$k^R_{off_B}$
R_ca4_ABCD_PP2B → R_ca3_ABC_PP2B + ca	$k^R_{off_D}$
R_ca4_ABCD_PP2B → R_ca3_ABD_PP2B + ca	$k^R_{off_C}$
R_ca4_ABCD_PP2B → R_ca3_ACD_PP2B + ca	$k^R_{off_B}$
R_ca4_ABCD_PP2B → R_ca3_BCD_PP2B + ca	$k^R_{off_A}$

Table 10: List of reactions included in the model of calmodulin and their respective reaction rates.

B

MODEL OF CALMODULIN TRAPPING BY CAMKII: LIST OF REACTIONS

Table 11: List of reactions for the model of calmodulin trapping by CaMKII.

Phosphorylation of CaMKII at Thr^{286}	
Substrate:	CaMKII
Product:	CaMKII
Sets flag on neighbour:	+P286
Needs flag:	+open
Needs flags on neighbour:	+open -P286
Dephosphorylation of CaMKII at Thr^{286} by PP1	
Substrates:	CaMKII, PP1
Products:	CaMKII, PP1
Sets flag:	-P286
Needs flag:	+P286
Phosphorylation of CaMKII at Thr^{306}	
Substrate:	CaMKII
Product:	CaMKII
Sets flag:	+P306
Needs flags:	+open -P306 -calm
Dephosphorylation of CaMKII at Thr^{306} by PP1	
Substrates:	CaMKII, PP1
Products:	CaMKII, PP1
Sets flag:	-P306
Needs flag:	+P306

Table 11: continued

Calmodulin binding to CaMKII (low-affinity site)	
Substrates:	CaMKII, calmodulin
Product:	CaMKII
Sets flag:	+calm
Needs flags:	-P306 -calm -ha
Calmodulin dissociating from CaMKII (low-affinity site)	
Substrate:	CaMKII
Products:	CaMKII, calmodulin
Sets flag:	-calm
Needs flags:	+calm -ha
Calmodulin binding to CaMKII (high-affinity site)	
Substrates:	CaMKII, calmodulin
Product:	CaMKII
Sets flags:	+calm +ha
Needs flags:	+open -P306 -calm -ha
Calmodulin dissociating from CaMKII (high-affinity site)	
Substrate:	CaMKII
Products:	CaMKII, calmodulin
Sets flags:	-calm -ha
Needs flags:	+calm +ha
Opening of CaMKII (rapid equilibrium)	
Substrate:	CaMKII
Product:	CaMKII
Sets flag:	+open
Probability:	1 if +T286 or +ha
	0.004 else

Table 11: continued

"Sliding" of calmodulin to the high-affinity site	
Substrate:	CaMKII
Product:	CaMKII
Sets flag:	+ha
Probability:	0.99997 if +open and +calm

Table 11: List of reactions for the model of calmodulin trapping by CaMKII.

C

MODEL OF A CAMKII DODECAMER: LIST OF REACTIONS

Table 12: List of reactions for the model of a CaMKII dodecamer

Phosphorylation of CaMKII at Thr^{286}	
Substrate:	CaMKII
Product:	CaMKII
Sets flag on neighbour	+P286
Needs flags:	+open -coil
Needs flags on neighbour:	+open -P286 -coil
Reacting neighbour:	same ring
Dephosphorylation of CaMKII at Thr^{286} by PP1	
Substrates:	CaMKII, PP1
Products:	CaMKII, PP1
Sets flag:	-P286
Needs flag:	+P286
Phosphorylation of CaMKII at Thr^{306}	
Substrate:	CaMKII
Product:	CaMKII
Sets flag:	+P306
Needs flags:	+open -P306 -calm -coil
Dephosphorylation of CaMKII at Thr^{306} by PP1	
Substrates:	CaMKII, PP1
Products:	CaMKII, PP1
Sets flag:	-P306
Needs flag:	+P306

Table 12: continued

Binding of calmodulin (low-affinity site)	
Substrates:	CaMKII, calmodulin
Product:	CaMKII
Sets flag:	+calm
Needs flags:	-P306 -calm -ha -coil
Dissociation of calmodulin (low-affinity site)	
Substrate:	CaMKII
Products:	CaMKII, calmodulin
Sets flag:	-calm
Needs flags:	+calm -ha
Binding of calmodulin (high-affinity site)	
Substrates:	CaMKII, calmodulin
Product:	CaMKII
Sets flags:	+calm +ha
Needs flags:	+open -P306 -calm -ha -coil
Dissociation of calmodulin (low-affinity site)	
Substrate:	CaMKII
Products:	CaMKII, calmodulin
Sets flags:	-calm -ha
Needs flags:	+calm +ha
Coiled-coil formation	
Substrate:	CaMKII
Product:	CaMKII
Sets flag:	+coil
Sets flag on neighbour:	+coil
Needs flags:	-P306 -calm -ha -coil
Needs flags on neighbour:	-P306 -calm -ha
Reacting neighbour:	adjacent ring

Table 12: continued

Coiled-coil disruption	
Substrate:	CaMKII
Product:	CaMKII
Sets flag:	-coil
Sets flag on neighbour:	-coil
Needs flag:	+coil
Reacting neighbour:	adjacent ring
Opening of CaMKII (rapid equilibrium)	
Substrate:	CaMKII
Product:	CaMKII
Sets flag:	+open
Probability:	1 if +T286 or +calha
	0.004 else
"Sliding" of calmodulin to high-affinity site	
Substrate:	CaMKII
Product:	CaMKII
Sets flag:	+calha
Probability:	0.99997 if +open and +calm and -coil

Table 12: List of reactions for the model of a CaMKII dodecamer. Note that there are two kinds of neighbour-sensitive reactions: Thr^{286} phosphorylation takes place between adjacent subunits on the same ring, while the formation of a coiled-coil involves two neighbouring subunits on different rings.

D

PUBLICATIONS DURING THIS WORK

The following list details work published or submitted for publication during the course of this PhD in chronological order.

- M. I. Stefan and N. Le Novère. Molecules for memory: modelling CaMKII. *BMC Systems Biology*, 1(Suppl 1):P40, 2007.
- M. I. Stefan, S. J. Edelstein, and N. Le Novère. An allosteric model of calmodulin explains differential activation of PP2B and CaMKII. *Proc Natl Acad Sci USA*, 105(31):10768–10773, 2008.
- M. I. Stefan, S. J. Edelstein, N. Le Novère. Computing phenomenologic Adair-Klotz constants from microscopic MWC parameters. *submitted*.
- S. J. Edelstein, M. I. Stefan, N. Le Novère. Ligand depletion in vivo modulates the dynamic range of cooperative signal transduction. *submitted*.

BIBLIOGRAPHY

G. S. Adair. The hemoglobin system. IV. The oxygen dissociation curve of hemoglobin. *J Biol Chem*, 63:529–545, 1925. (Cited on pages 12, 13, 19, 43, 49, and 78.)

Y. S. Babu, C. E. Bugg, and W. J. Cook. Structure of calmodulin refined at 2.2 A resolution. *J Mol Biol*, 204(1):191–204, 1988. (Cited on pages 4, 11, 31, 33, and 51.)

Y. S. Babu, J. S. Sack, T. J. Greenhough, C. E. Bugg, A. R. Means, and W. J. Cook. Three-dimensional structure of calmodulin. *Nature*, 315(6014):37–40, 1985. (Cited on pages 4, 31, 32, and 49.)

K. U. Bayer, P. D. Koninck, A. S. Leonard, J. W. Hell, and H. Schulman. Interaction with the NMDA receptor locks CaMKII in an active conformation. *Nature*, 411(6839):801–805, 2001. doi:10.1038/35081080. (Cited on pages 126 and 127.)

K. U. Bayer, E. LeBel, G. L. McDonald, H. O'Leary, H. Schulman, and P. D. Koninck. Transition from reversible to persistent binding of CaMKII to postsynaptic sites and NR2B. *J Neurosci*, 26(4):1164–1174, 2006. doi:10.1523/JNEUROSCI.3116-05.2006. (Cited on pages 52 and 126.)

P. M. Bayley, W. A. Findlay, and S. R. Martin. Target recognition by calmodulin: dissecting the kinetics and affinity of interaction using short peptide sequences. *Protein Sci*, 5(7):1215–1228, 1996. (Cited on pages 38 and 39.)

M. F. Bear and R. C. Malenka. Synaptic plasticity: LTP and LTD. *Curr Biol*, 4(3):389–399, 1994. (Cited on page 3.)

U. S. Bhalla. Biochemical signaling networks decode temporal patterns of synaptic input. *J Comput Neurosci*, 13(1):49–62, 2002. (Cited on page 52.)

U. S. Bhalla and R. Iyengar. Emergent properties of networks of biological signaling pathways. *Science*, 283(5400):381–387, 1999. (Cited on pages 5 and 50.)

T. V. Bliss and G. L. Collingridge. A synaptic model of memory: long-term potentiation in the hippocampus. *Nature*, 361(6407):31–39, 1993. doi:10.1038/361031a0. (Cited on page 2.)

T. V. Bliss and T. Lømo. Long-lasting potentiation of synaptic transmission in the dentate area of the anaesthetized rabbit following stimulation of the perforant path. *J Physiol*, 232(2):331–356, 1973. (Cited on page 2.)

A. P. Braun and H. Schulman. The multifunctional calcium/calmodulin-dependent protein kinase: from form to function. *Annu Rev Physiol*, 57:417–445, 1995. doi:10.1146/annurev.ph.57.030195.002221. (Cited on page 6.)

D. Bray and T. Duke. Conformational spread: the propagation of allosteric states in large multiprotein complexes. *Annu Rev Biophys Biomol Struct*, 33:53–73, 2004. doi:10.1146/annurev.biophys.33.110502.132703. (Cited on page 55.)

D. Burger, J. A. Cox, M. Comte, and E. A. Stein. Sequential conformational changes in calmodulin upon binding of calcium. *Biochemistry*, 23:1966–1971, 1984. (Cited on pages 5, 43, and 49.)

D. Burger, E. A. Stein, and J. A. Cox. Free energy coupling in the interactions between Ca2+, calmodulin, and phosphorylase kinase. *J Biol Chem*, 258(23):14733–14739, 1983. (Cited on pages 5, 31, 46, 50, and 79.)

H. J. Carlisle and M. B. Kennedy. Spine architecture and synaptic plasticity. *Trends Neurosci*, 28(4):182–187, 2005. doi:10.1016/j.tins.2005.01.008. (Cited on page 42.)

D. Case, D. Pearlman, J. Caldwell, T. Cheatham III, J. Wang, W. Ross, C. Simmerling, T. Darden, K. Merz, R. Stanton, A. Cheng, J. Vincent, M. Crowley, V. Tsui, H. Gohlke, R. Radmer, Y. Duan, J. Pitera, I. Massova, G. Seibel, U. Singh, P. Weiner, and P. Kollman. *AMBER 7*. University of California, San Francisco, 2002. (Cited on page 92.)

J.-P. Changeux and S. J. Edelstein. Allosteric mechanisms of signal transduction. *Science*, 308(5727):1424–1428, 2005. doi:10.1126/science.1108595. (Cited on page 55.)

J. P. Changeux and M. M. Rubin. Allosteric interactions in aspartate transcarbamylase. 3. Interpretation of experimental data in terms of the model of Monod, Wyman, and Changeux. *Biochemistry*, 7(2):553–561, 1968. (Cited on pages 55, 56, and 63.)

R. Chattopadhyaya, W. E. Meador, A. R. Means, and F. A. Quiocho. Calmodulin structure refined at 1.7 A resolution. *J Mol Biol*, 228(4):1177–1192, 1992. (Cited on pages 4, 11, and 31.)

X. Chen, L. Vinade, R. D. Leapman, J. D. Petersen, T. Nakagawa, T. M. Phillips, M. Sheng, and T. S. Reese. Mass of the postsynaptic density and enumeration of three key molecules. *Proc Natl Acad Sci USA*, 102(32):11551–11556, 2005. doi:10.1073/pnas.0505359102. (Cited on pages 48 and 98.)

D. Cheng, C. C. Hoogenraad, J. Rush, E. Ramm, M. A. Schlager, D. M. Duong, P. Xu, S. R. Wijayawardana, J. Hanfelt, T. Nakagawa, M. Sheng, and J. Peng. Relative and absolute quantification of postsynaptic density proteome isolated from rat forebrain and cerebellum. *Mol Cell Proteomics*, 5(6):1158–1170, 2006. doi:10.1074/mcp.D500009-MCP200. (Cited on pages 48 and 78.)

D. Chin and A. R. Means. Mechanisms for regulation of calmodulin kinase IIalpha by Ca(2+)/calmodulin and autophosphorylation of threonine 286. *Biochemistry*, 41(47):14001–14009, 2002. (Cited on page 104.)

R. J. Colbran. Inactivation of Ca2+/calmodulin-dependent protein kinase II by basal autophosphorylation. *J Biol Chem*, 268(10):7163–7170, 1993. (Cited on pages 5, 87, and 91.)

R. J. Colbran. Protein phosphatases and calcium/calmodulin-dependent protein kinase II-dependent synaptic plasticity. *J Neurosci*, 24(39):8404–8409, 2004. doi:10.1523/JNEUROSCI.3602-04.2004. (Cited on page 52.)

R. J. Colbran and A. M. Brown. Calcium/calmodulin-dependent protein kinase II and synaptic plasticity. *Curr Opin Neurobiol*, 14(3):318–327, 2004. doi:10.1016/j.conb.2004.05.008. (Cited on page 128.)

M. O. Collins, H. Husi, L. Yu, J. M. Brandon, C. N. G. Anderson, W. P. Blackstock, J. S. Choudhary, and S. G. N. Grant. Molecular characterization and comparison of the components and multiprotein complexes in the postsynaptic proteome. *J Neurochem*, 97(Suppl 1):16–23, 2006. (Cited on page 48.)

S. J. Cooper. Donald O. Hebb's synapse and learning rule: a history and commentary. *Neurosci Biobehav Rev*, 28(8):851–874, 2005. doi:10.1016/j.neubiorev.2004.09.009. (Cited on pages 1, 2, and 3.)

T. H. Crouch and C. B. Klee. Positive cooperative binding of calcium to bovine brain calmodulin. *Biochemistry*, 19(16):3692–3698, 1980. (Cited on pages 5, 31, 43, 44, 49, and 79.)

G. H. Czerlinski. Allosteric competition in calmodulin. *Physiol Chem Phys Med NMR*, 16:437–447, 1984. (Cited on pages 5 and 51.)

P. d'Alcantara, S. Schiffmann, and S. Swillens. Bidirectional synaptic plasticity as a consequence of interdependent Ca2+-controlled phosphorylation and dephosphorylation pathways. *Eur J Neurosci*, 17:2521–2528, 2003. (Cited on pages 5 and 49.)

P. De Koninck and H. Schulman. Sensitivity of CaM kinase II to the frequency of Ca2+ oscillations. *Science*, 279(5348):227–230, 1998. (Cited on pages 5, 6, and 52.)

A. Dosemeci and R. W. Albers. A mechanism for synaptic frequency detection through autophosphorylation of CaM kinase II. *Biophys J*, 70(6):2493–2501, 1996. (Cited on page 52.)

C. L. Drum, S.-Z. Yan, J. Bard, Y.-Q. Shen, D. Lu, S. Soelaiman, Z. Grabarek, A. Bohm, and W.-J. Tang. Structural basis for the activation of anthrax adenylyl cyclase exotoxin by calmodulin. *Nature*, 415(6870):396–402, 2002. doi:10.1038/415396a. (Cited on page 51.)

T. A. Duke, N. L. Novère, and D. Bray. Conformational spread in a ring of proteins: a stochastic approach to allostery. *J Mol*

Biol, 308(3):541–553, 2001. doi:10.1006/jmbi.2001.4610. (Cited on page 62.)

G. Dupont, G. Houart, and P. D. Koninck. Sensitivity of CaM kinase II to the frequency of Ca2+ oscillations: a simple model. *Cell Calcium*, 34:485–497, 2003. (Cited on page 52.)

S. J. Edelstein. Extensions of the allosteric model for haemoglobin. *Nature*, 230(5291):224–227, 1971. (Cited on page 55.)

S. J. Edelstein. Cooperative interactions of hemoglobin. *Annu Rev Biochem*, 44:209–232, 1975. doi:10.1146/annurev.bi.44.070175.001233. (Cited on pages 25, 27, and 28.)

S. J. Edelstein, O. Schaad, E. Henry, D. Bertrand, and J. P. Changeux. A kinetic mechanism for nicotinic acetylcholine receptors based on multiple allosteric transitions. *Biol Cybern*, 75(5):361–379, 1996. (Cited on pages 16 and 46.)

J. L. Fallon and F. A. Quiocho. A closed compact structure of native Ca(2+)-calmodulin. *Structure*, 11(10):1303–1307, 2003. (Cited on page 51.)

L. Fetler, E. R. Kantrowitz, and P. Vachette. Direct observation in solution of a preexisting structural equilibrium for a mutant of the allosteric aspartate transcarbamoylase. *Proc Natl Acad Sci USA*, 104(2):495–500, 2007. doi:10.1073/pnas.0607641104. (Cited on page 56.)

K. M. Franks, T. M. Bartol, and T. J. Sejnowski. An MCell model of calcium dynamics and frequency-dependence of calmodulin activation in dendritic spines. *Neurocomputing*, 38-40:9–16, 2001. (Cited on pages 5, 50, and 52.)

T. R. Gaertner, S. J. Kolodziej, D. Wang, R. Kobayashi, J. M. Koomen, J. K. Stoops, and M. N. Waxham. Comparative analyses of the three-dimensional structures and enzymatic properties of alpha, beta, gamma and delta isoforms of Ca2+-calmodulin-dependent protein kinase II. *J Biol Chem*, 279(13):12484–12494, 2004. doi:10.1074/jbc.M313597200. (Cited on page 128.)

E. Gamble and C. Koch. The dynamics of free calcium in dendritic spines in response to repetitive synaptic input. *Science*, 236(4806):1311–1315, 1987. (Cited on pages 52, 68, and 74.)

J. C. Gerhart and H. K. Schachman. Allosteric interactions in aspartate transcarbamylase. II. Evidence for different conformational states of the protein in the presence and absence of specific ligands. *Biochemistry*, 7(2):538–552, 1968. (Cited on page 56.)

D. T. Gillespie. Exact stochastic simulation of coupled chemical reactions. *J Phys Chem*, 81(25):2340–2361, 1977. (Cited on page 89.)

A. Goldbeter and D. E. Koshland. An amplified sensitivity arising from covalent modification in biological systems. *Proc Natl Acad Sci USA*, 78(11):6840–6844, 1981. (Cited on page 55.)

A. Goldbeter and D. E. Koshland. Ultrasensitivity in biochemical systems controlled by covalent modification. Interplay between zero-order and multistep effects. *J Biol Chem*, 259(23):14441–14447, 1984. (Cited on page 83.)

S. Goto, Y. Matsukado, Y. Mihara, N. Inoue, and E. Miyamoto. The distribution of calcineurin in rat brain by light and electron microscopic immunohistochemistry and enzyme-immunoassay. *Brain Res*, 397(1):161–172, 1986. (Cited on pages 42 and 49.)

P. A. A. Grant, S. L. Best, N. Sanmugalingam, R. Alessio, A. M. Jama, and K. Török. A two-state model for Ca(2+)/CaM-dependent protein kinase II (alphaCaMKII) in response to persistent Ca(2+) stimulation in hippocampal neurons. *Cell Calcium*, 2008. doi: 10.1016/j.ceca.2008.03.003. (Cited on page 128.)

R. D. Groth, R. L. Dunbar, and P. G. Mermelstein. Calcineurin regulation of neuronal plasticity. *Biochem Biophys Res Commun*, 311(4):1159–1171, 2003. (Cited on pages 4 and 52.)

J. Gsponer, J. Christodoulou, A. Cavalli, J. M. Bui, B. Richter, C. M. Dobson, and M. Vendruscolo. A coupled equilibrium shift mechanism in calmodulin-mediated signal transduction. *Structure*, 16(5):736–746, 2008. doi:10.1016/j.str.2008.02.017. (Cited on page 51.)

J. Haiech, C. B. Klee, and J. G. Demaille. Effects of cations on affinity of calmodulin for calcium: ordered binding of calcium ions allows the specific activation of calmodulin-stimulated enzymes. *Biochemistry*, 20(13):3890–3897, 1981. (Cited on page 43.)

R. M. Hanley, A. R. Means, B. E. Kemp, and S. Shenolikar. Mapping of calmodulin-binding domain of Ca2+/calmodulin-dependent protein kinase II from rat brain. *Biochem Biophys Res Commun*, 152(1):122–128, 1988. (Cited on pages 5, 87, and 125.)

P. I. Hanson, T. Meyer, L. Stryer, and H. Schulman. Dual role of calmodulin in autophosphorylation of multifunctional CaM kinase may underlie decoding of calcium signals. *Neuron*, 12(5):943–956, 1994. (Cited on pages 5, 87, 90, and 126.)

Y. Hayashi, S. H. Shi, J. A. Esteban, A. Piccini, J. C. Poncer, and R. Malinow. Driving AMPA receptors into synapses by LTP and CaMKII: requirement for GluR1 and PDZ domain interaction. *Science*, 287(5461):2262–2267, 2000. (Cited on page 4.)

D. O. Hebb. *The organization of behavior; a neuropsychological theory.* Wiley, 1949. (Cited on page 1.)

A. V. Hill. The possible effects of the aggregation of the molecules of haemoglobin on its dissociation curves. *J Physiol*, 40:iv–vii, 1910. (Cited on pages 12 and 55.)

A. V. Hill. The combinations of haemoglobin with oxygen and with carbon monoxide. I. *Biochem J*, 7(5):471–480, 1913. (Cited on page 49.)

W. S. Hlavacek, J. R. Faeder, M. L. Blinov, A. S. Perelson, and B. Goldstein. The complexity of complexes in signal transduction. *Biotechnol Bioeng*, 84(7):783–794, 2003. doi:10.1002/bit.10842. (Cited on page 87.)

W. S. Hlavacek, J. R. Faeder, M. L. Blinov, R. G. Posner, M. Hucka, and W. Fontana. Rules for modeling signal-transduction systems. *Sci STKE*, 2006(344):re6, 2006. doi:10.1126/stke.3442006re6. (Cited on page 88.)

S. S. Hook and A. R. Means. Ca(2+)/CaM-dependent kinases: from activation to function. *Annu Rev Pharmacol Toxicol*, 41:471–505, 2001. doi:10.1146/annurev.pharmtox.41.1.471. (Cited on page 52.)

S. Hoops, S. Sahle, R. Gauges, C. Lee, J. Pahle, N. Simus, M. Singhal, L. Xu, P. Mendes, and U. Kummer. COPASI–a COmplex PAthway SImulator. *Bioinformatics*, 22(24):3067–3074, 2006. doi: 10.1093/bioinformatics/btl485. (Cited on pages 41 and 96.)

C. Y. Huang, V. Chau, P. B. Chock, J. H. Wang, and R. K. Sharma. Mechanism of activation of cyclic nucleotide phosphodiesterase: requirement of the binding of four Ca2+ to calmodulin for activation. *Proc Natl Acad Sci USA*, 78(2):871–874, 1981. (Cited on pages 4, 5, 31, 50, 51, and 79.)

A. Hudmon, J. Aronowski, S. J. Kolb, and M. N. Waxham. Inactivation and self-association of Ca2+/calmodulin-dependent protein kinase II during autophosphorylation. *J Biol Chem*, 271(15):8800–8808, 1996. (Cited on page 128.)

A. Hudmon and H. Schulman. Structure-function of the multifunctional Ca2+/calmodulin-dependent protein kinase II. *Biochem J*, 364(Pt 3):593–611, 2002. doi:10.1042/BJ20020228. (Cited on pages 6, 119, 121, and 130.)

W. H. Jefferys and J. O. Berger. Sharpening Ockham's Razor on a Bayesian strop. Technical Report 91-44C, Department of Statistics, Purdue University, 1991. (Cited on page 81.)

S. Kakiuchi, S. Yasuda, R. Yamazaki, Y. Teshima, K. Kanda, R. Kakiuchi, and K. Sobue. Quantitative determinations of calmodulin in the supernatant and particulate fractions of mammalian tissues. *J Biochem (Tokyo)*, 92(4):1041–1048, 1982. (Cited on pages 48, 52, and 99.)

E. R. Kantrowitz and W. N. Lipscomb. Escherichia coli aspartate transcarbamoylase: the molecular basis for a concerted allosteric transition. *Trends Biochem Sci*, 15(2):53–59, 1990. (Cited on page 56.)

A. Karlin. On the application of "a plausible model" of allosteric proteins to the receptor for acetylcholine. *J Theor Biol*, 16(2):306–320, 1967. (Cited on page 60.)

R. L. Kincaid and M. Vaughan. Direct comparison of Ca2+ requirements for calmodulin interaction with and activation of protein phosphatase. *Proc Natl Acad Sci USA*, 83(5):1193–1197, 1986. (Cited on pages 4, 31, 50, and 79.)

H. Kitano. Systems biology: a brief overview. *Science*, 295(5560):1662–1664, 2002. doi:10.1126/science.1069492. (Cited on page 78.)

I. M. Klotz. The application of the law of mass action to binding by proteins. Interactions with calcium. *Arch Biochem*, 9:109–117, 1946. (Cited on pages 12, 13, 19, 28, 43, 49, and 78.)

I. M. Klotz. Ligand-receptor complexes: origin and development of the concept. *J Biol Chem*, 279(1):1–12, 2004. doi:10.1074/jbc.X300006200. (Cited on page 12.)

S. J. Kolodziej, A. Hudmon, M. N. Waxham, and J. K. Stoops. Three-dimensional reconstructions of calcium/calmodulin-dependent (CaM) kinase II alpha and truncated CaM kinase II alpha reveal a unique organization for its structural core and functional domains. *J Biol Chem*, 275(19):14354–14359, 2000. (Cited on page 5.)

D. E. Koshland. Application of a theory of enzyme specificity to protein synthesis. *Proc Natl Acad Sci U SA*, 44(2):98–104, 1958. (Cited on page 13.)

D. E. Koshland, A. Goldbeter, and J. B. Stock. Amplification and adaptation in regulatory and sensory systems. *Science*, 217(4556):220–225, 1982. (Cited on page 83.)

D. E. Koshland, G. Némethy, and D. Filmer. Comparison of experimental binding data and theoretical models in proteins containing subunits. *Biochemistry*, 5(1):365–385, 1966. (Cited on page 13.)

R. Kötter. Postsynaptic integration of glutamatergic and dopaminergic signals in the striatum. *Prog Neurobiol*, 44(2):163–196, 1994. (Cited on pages 99 and 117.)

H. Kuboniwa, N. Tjandra, S. Grzesiek, H. Ren, C. B. Klee, and A. Bax. Solution structure of calcium-free calmodulin. *Nat Struct Biol*, 2(9):768–776, 1995. (Cited on pages 4, 31, 32, 33, 49, and 51.)

N. Le Novère, B. Bornstein, A. Broicher, M. Courtot, M. Donizelli, H. Dharuri, L. Li, H. Sauro, M. Schilstra, B. Shapiro, J. L. Snoep, and M. Hucka. BioModels Database: a free, centralized database of curated, published, quantitative kinetic models of biochemical and cellular systems. *Nucleic Acids Res*, 34(Database issue):D689–D691, 2006. doi:10.1093/nar/gkj092. (Cited on pages 41 and 81.)

N. Le Novère and T. S. Shimizu. STOCHSIM: modelling of stochastic biomolecular processes. *Bioinformatics*, 17(6):575–576, 2001. (Cited on pages 88, 89, 94, and 117.)

H. K. Lee, M. Barbarosie, K. Kameyama, M. F. Bear, and R. L. Huganir. Regulation of distinct AMPA receptor phosphorylation sites during bidirectional synaptic plasticity. *Nature*, 405(6789):955–959, 2000. doi:10.1038/35016089. (Cited on page 4.)

S. Linse, A. Helmersson, and S. Forsén. Calcium binding to calmodulin and its globular domains. *J Biol Chem*, 266(13):8050–8054, 1991. (Cited on pages 49 and 66.)

J. Lisman. A mechanism for the Hebb and the anti-Hebb processes underlying learning and memory. *Proc Natl Acad Sci USA*, 86(23):9574–9578, 1989. (Cited on pages 1, 2, 3, 52, and 130.)

J. Lisman, H. Schulman, and H. Cline. The molecular basis of CaMKII function in synaptic and behavioural memory. *Nat Rev Neurosci*, 3:175–190, 2002. (Cited on page 3.)

J. E. Lisman and A. M. Zhabotinsky. A model of synaptic memory: a CaMKII/PP1 switch that potentiates transmission by organizing an AMPA receptor anchoring assembly. *Neuron*, 31(2):191–201, 2001. (Cited on pages 6, 123, and 130.)

V. Lučić, G. Greif, and M. Kennedy. Detailed state model of CaMKII activation and autophosphorylation. *Eur Biophys J*, 2008. doi:10.1007/s00249-008-0362-4. (Cited on pages 98 and 116.)

G. S. Lynch, T. Dunwiddie, and V. Gribkoff. Heterosynaptic depression: a postsynaptic correlate of long-term potentiation. *Nature*, 266(5604):737–739, 1977. (Cited on page 2.)

R. C. Malenka and R. A. Nicoll. Long-term potentiation–a decade of progress? *Science*, 285(5435):1870–1874, 1999. (Cited on page 2.)

A. Malmendal, J. Evenäs, S. Forsén, and M. Akke. Structural dynamics in the C-terminal domain of calmodulin at low calcium levels. *J Mol Biol*, 293(4):883–899, 1999. doi:10.1006/jmbi.1999.3188. (Cited on page 50.)

S. J. Martin, P. D. Grimwood, and R. G. Morris. Synaptic plasticity and memory: an evaluation of the hypothesis. *Annu Rev Neurosci*, 23:649–711, 2000. doi:10.1146/annurev.neuro.23.1.649. (Cited on pages 2 and 3.)

M. L. Mayer and G. L. Westbrook. The action of N-methyl-D-aspartic acid on mouse spinal neurones in culture. *J Physiol*, 361:65–90, 1985. (Cited on page 3.)

M. L. Mayer and G. L. Westbrook. Permeation and block of N-methyl-D-aspartic acid receptor channels by divalent cations in mouse cultured central neurones. *J Physiol*, 394:501–527, 1987. (Cited on page 3.)

T. Meyer, P. I. Hanson, L. Stryer, and H. Schulman. Calmodulin trapping by calcium-calmodulin-dependent protein kinase. *Science*, 256(5060):1199–1202, 1992. (Cited on pages 5, 87, 90, 91, 96, 99, 100, 101, 102, 105, and 116.)

P. V. Migues, I. T. Lehmann, L. Fluechter, M. Cammarota, J. W. Gurd, A. T. R. Sim, P. W. Dickson, and J. A. P. Rostas. Phosphorylation of CaMKII at Thr253 occurs in vivo and enhances binding to isolated postsynaptic densities. *J Neurochem*, 98(1):289–299, 2006. doi:10.1111/j.1471-4159.2006.03876.x. (Cited on page 128.)

S. Mirzoeva, S. Weigand, T. J. Lukas, L. Shuvalova, W. F. Anderson, and D. M. Watterson. Analysis of the functional coupling between calmodulin's calcium binding and peptide recognition properties. *Biochemistry*, 38(13):3936–3947, 1999. doi:10.1021/bi9821263. (Cited on pages 5 and 49.)

J. Monod, J. Wyman, and J. P. Changeux. On the nature of allosteric transitions: A plausible model. *J Mol Biol*, 12:88–118, 1965. (Cited on pages 7, 14, 17, 19, 20, 21, 55, 62, and 77.)

S. Mukherji and T. R. Soderling. Regulation of Ca2+/calmodulin-dependent protein kinase II by inter- and intrasubunit-catalyzed autophosphorylations. *J Biol Chem*, 269(19):13744–13747, 1994. (Cited on pages 5 and 90.)

P. Mullasseril, A. Dosemeci, J. E. Lisman, and L. C. Griffith. A structural mechanism for maintaining the 'on-state' of the CaMKII memory switch in the post-synaptic density. *J Neurochem*, 103(1):357–364, 2007. doi:10.1111/j.1471-4159.2007.04744.x. (Cited on page 127.)

H. Naoki, Y. Sakumura, and S. Ishii. Local signaling with molecular diffusion as a decoder of Ca2+ signals in synaptic plasticity. *Mol Syst Biol*, 1:2005.0027, 2005. doi:10.1038/msb4100035. (Cited on pages 5 and 50.)

B. B. Olwin, A. M. Edelman, E. G. Krebs, and D. R. Storm. Quantitation of energy coupling between Ca2+, calmodulin, skeletal muscle myosin light chain kinase, and kinase substrates. *J Biol Chem*, 259(17):10949–10955, 1984. (Cited on pages 5, 31, 46, 50, and 79.)

B. L. Patton, S. G. Miller, and M. B. Kennedy. Activation of type II calcium/calmodulin-dependent protein kinase by Ca2+/calmodulin is inhibited by autophosphorylation of threonine within the calmodulin-binding domain. *J Biol Chem*, 265(19):11204–11212, 1990. (Cited on pages 5, 87, and 91.)

M. E. Payne, Y. L. Fong, T. Ono, R. J. Colbran, B. E. Kemp, T. R. Soderling, and A. R. Means. Calcium/calmodulin-dependent protein kinase II. Characterization of distinct calmodulin binding and inhibitory domains. *J Biol Chem*, 263(15):7190–7195, 1988. (Cited on pages 5, 109, and 125.)

O. B. Peersen, T. S. Madsen, and J. J. Falke. Intermolecular tuning of calmodulin by target peptides and proteins: differential effects on Ca2+ binding and implications for kinase activation. *Protein Sci*, 6(4):794–807, 1997. (Cited on pages 35, 38, 40, 43, and 44.)

J. D. Petersen, X. Chen, L. Vinade, A. Dosemeci, J. E. Lisman, and T. S. Reese. Distribution of postsynaptic density (PSD)-95 and Ca2+/calmodulin-dependent protein kinase II at the PSD. *J Neu-*

rosci, 23(35):11270–11278, 2003. (Cited on pages 42, 49, 98, 99, 117, and 126.)

C. Pifl, B. Plank, W. Wyskovsky, O. Bertel, G. Hellmann, and J. Suko. Calmodulin X (Ca2+)4 is the active calmodulin-calcium species activating the calcium-, calmodulin-dependent protein kinase of cardiac sarcoplasmic reticulum in the regulation of the calcium pump. *Biochim Biophys Acta*, 773(2):197–206, 1984. (Cited on pages 5 and 49.)

T. Porumb. Determination of calcium-binding constants by flow dialysis. *Anal Biochem*, 220(2):227–237, 1994. doi:10.1006/abio.1994.1332. (Cited on pages 43 and 44.)

A. R. Quintana, D. Wang, J. E. Forbes, and M. N. Waxham. Kinetics of calmodulin binding to calcineurin. *Biochem Biophys Res Commun*, 334(2):674–680, 2005. doi:10.1016/j.bbrc.2005.06.152. (Cited on pages 42, 48, and 49.)

O. S. Rosenberg, S. Deindl, R.-J. Sung, A. C. Nairn, and J. Kuriyan. Structure of the autoinhibited kinase domain of CaMKII and SAXS analysis of the holoenzyme. *Cell*, 123(5):849–860, 2005. doi:10.1016/j.cell.2005.10.029. (Cited on pages 5, 6, 7, 90, 92, 109, 110, 111, 115, and 130.)

M. M. Rubin and J. P. Changeux. On the nature of allosteric transitions: implications of non-exclusive ligand binding. *J Mol Biol*, 21(2):265–274, 1966. (Cited on pages 17, 35, and 55.)

J. R. Sanes and J. W. Lichtman. Can molecules explain long-term potentiation? *Nat Neurosci*, 2(7):597–604, 1999. (Cited on page 4.)

H. Schulman and P. Greengard. Ca2+-dependent protein phosphorylation system in membranes from various tissues, and its activation by "calcium-dependent regulator". *Proc Natl Acad Sci USA*, 75(11):5432–5436, 1978a. (Cited on page 3.)

H. Schulman and P. Greengard. Stimulation of brain membrane protein phosphorylation by calcium and an endogenous heat-stable protein. *Nature*, 271(5644):478–479, 1978b. (Cited on page 3.)

M. A. Schumacher, A. F. Rivard, H. P. Bächinger, and J. P. Adelman. Structure of the gating domain of a Ca2+-activated K+ channel complexed with Ca2+/calmodulin. *Nature*, 410(6832):1120–1124, 2001. doi:10.1038/35074145. (Cited on page 50.)

K. Shen and T. Meyer. Dynamic control of CaMKII translocation and localization in hippocampal neurons by NMDA receptor stimulation. *Science*, 284(5411):162–166, 1999. (Cited on page 127.)

K. Shen, M. N. Teruel, J. H. Connor, S. Shenolikar, and T. Meyer. Molecular memory by reversible translocation of calcium/calmodulin-dependent protein kinase II. *Nat Neurosci*, 3(9):881–886, 2000. doi:10.1038/78783. (Cited on page 127.)

J. M. Shifman, M. H. Choi, S. Mihalas, S. L. Mayo, and M. B. Kennedy. Ca2+/calmodulin-dependent protein kinase II (CaMKII) is activated by calmodulin with two bound calciums. *Proc Natl Acad Sci USA*, 103(38):13968–13973, 2006. doi:10.1073/pnas.0606433103. (Cited on pages 4, 5, 31, 38, 39, 43, 46, 49, 50, 51, and 79.)

T. J. Shors and L. D. Matzel. Long-term potentiation: what's learning got to do with it? *Behav Brain Sci*, 20(4):597–614; discussion 614–55, 1997. (Cited on page 2.)

A. J. Silva, R. Paylor, J. M. Wehner, and S. Tonegawa. Impaired spatial learning in alpha-calcium-calmodulin kinase II mutant mice. *Science*, 257(5067):206–211, 1992a. (Cited on pages 3 and 5.)

A. J. Silva, C. F. Stevens, S. Tonegawa, and Y. Wang. Deficient hippocampal long-term potentiation in alpha-calcium-calmodulin kinase II mutant mice. *Science*, 257(5067):201–206, 1992b. (Cited on pages 3 and 5.)

S. I. Singla, A. Hudmon, J. M. Goldberg, J. L. Smith, and H. Schulman. Molecular characterization of calmodulin trapping by calcium/calmodulin-dependent protein kinase II. *J Biol Chem*, 276(31):29353–29360, 2001. doi:10.1074/jbc.M101744200. (Cited on page 94.)

T. R. Soderling, B. Chang, and D. Brickey. Cellular signaling through multifunctional Ca2+/calmodulin-dependent protein kinase II. *J*

Biol Chem, 276(6):3719–3722, 2001. doi:10.1074/jbc.R000013200. (Cited on page 127.)

M. I. Stefan, S. J. Edelstein, and N. L. Novère. An allosteric model of calmodulin explains differential activation of PP2B and CaMKII. *Proc Natl Acad Sci USA*, 105(31):10768–10773, 2008. doi: 10.1073/pnas.0804672105. (Cited on pages 28, 53, 64, and 68.)

G. S. Stent. A physiological mechanism for Hebb's postulate of learning. *Proc Natl Acad Sci USA*, 70(4):997–1001, 1973. (Cited on page 1.)

S. Strack, M. A. Barban, B. E. Wadzinski, and R. J. Colbran. Differential inactivation of postsynaptic density-associated and soluble Ca2+/calmodulin-dependent protein kinase II by protein phosphatases 1 and 2A. *J Neurochem*, 68(5):2119–2128, 1997a. (Cited on pages 98, 99, and 116.)

S. Strack, S. Choi, D. M. Lovinger, and R. J. Colbran. Translocation of autophosphorylated calcium/calmodulin-dependent protein kinase II to the postsynaptic density. *J Biol Chem*, 272(21):13467–13470, 1997b. (Cited on page 127.)

A. Thalhammer, Y. Rudhard, C. M. Tigaret, K. E. Volynski, D. A. Rusakov, and R. Schoepfer. CaMKII translocation requires local NMDA receptor-mediated Ca2+ signaling. *EMBO J*, 25(24):5873–5883, 2006. doi:10.1038/sj.emboj.7601420. (Cited on page 127.)

N. Tjandra, H. Kuboniwa, H. Ren, and A. Bax. Rotational dynamics of calcium-free calmodulin studied by 15N-NMR relaxation measurements. *Eur J Biochem*, 230(3):1014–1024, 1995. (Cited on page 50.)

D. P. Tolle and N. Le Novère. Particle-based stochastic simulation in systems biology. *Curr Bioinformatics*, 1:315–320, 2006. (Cited on page 89.)

J. K. Y. Tse, A. M. Giannetti, and J. M. Bradshaw. Thermodynamics of calmodulin trapping by Ca2+/calmodulin-dependent protein kinase II: subpicomolar Kd determined using competition titration calorimetry. *Biochemistry*, 46(13):4017–4027, 2007. doi: 10.1021/bi700013y. (Cited on pages 90, 91, 92, 96, 97, 99, 104, and 116.)

J. Z. Tsien. Linking Hebb's coincidence-detection to memory formation. *Curr Opin Neurobiol*, 10(2):266–273, 2000. (Cited on page 3.)

J. Z. Tsien, P. T. Huerta, and S. Tonegawa. The essential role of hippocampal CA1 NMDA receptor-dependent synaptic plasticity in spatial memory. *Cell*, 87(7):1327–1338, 1996. (Cited on page 3.)

A. Tzortzopoulos and K. Török. Mechanism of the T286A-mutant alphaCaMKII interactions with Ca2+/calmodulin and ATP. *Biochemistry*, 43(21):6404–6414, 2004. doi:10.1021/bi036224m. (Cited on pages 42, 48, 49, and 98.)

A. Šali and T. L. Blundell. Comparative protein modelling by satisfaction of spatial restraints. *J Mol Biol*, 234(3):779–815, 1993. doi:10.1006/jmbi.1993.1626. (Cited on page 92.)

R. S. Walikonis, A. Oguni, E. M. Khorosheva, C. J. Jeng, F. J. Asuncion, and M. B. Kennedy. Densin-180 forms a ternary complex with the (alpha)-subunit of Ca2+/calmodulin-dependent protein kinase II and (alpha)-actinin. *J Neurosci*, 21(2):423–433, 2001. (Cited on page 128.)

M. E. Wall, J. B. Clarage, and G. N. Phillips. Motions of calmodulin characterized using both Bragg and diffuse X-ray scattering. *Structure*, 5(12):1599–1612, 1997. (Cited on page 92.)

J. T. Warren, Q. Guo, and W.-J. Tang. A 1.3-A structure of zinc-bound N-terminal domain of calmodulin elucidates potential early ion-binding step. *J Mol Biol*, 374(2):517–527, 2007. doi:10.1016/j.jmb.2007.09.048. (Cited on pages 33 and 51.)

D. M. Watterson, F. Sharief, and T. C. Vanaman. The complete amino acid sequence of the Ca2+-dependent modulator protein (calmodulin) of bovine brain. *J Biol Chem*, 255(3):962–975, 1980. (Cited on page 31.)

K. Weber. New structural model of E. coli aspartate transcarbamylase and the amino-acid sequence of the regulatory polypeptide chain. *Nature*, 218(5147):1116–1119, 1968. (Cited on page 56.)

J. R. Whitlock, A. J. Heynen, M. G. Shuler, and M. F. Bear. Learning induces long-term potentiation in the hippocampus. *Science*,

313(5790):1093–1097, 2006. doi:10.1126/science.1128134. (Cited on page 3.)

D. C. Wiley and W. N. Lipscomb. Crystallographic determination of symmetry of aspartate transcarbamylase. *Nature*, 218(5147):1119–1121, 1968. (Cited on page 56.)

J. Wyman and S. J. Gill. *Binding and linkage. Functional chemistry of biological molecules*. University Science Books, 1990. (Cited on page 12.)

T. Yamauchi. Neuronal Ca2+/calmodulin-dependent protein kinase II–discovery, progress in a quarter of a century, and perspective: implication for learning and memory. *Biol Pharm Bull*, 28(8):1342–1354, 2005. (Cited on page 104.)

T. Yonetani, S.-I. Park, A. Tsuneshige, K. Imai, and K. Kanaori. Global allostery model of hemoglobin. Modulation of O(2) affinity, cooperativity, and Bohr effect by heterotropic allosteric effectors. *J Biol Chem*, 277(37):34508–34520, 2002. doi:10.1074/jbc.M203135200. (Cited on pages 27 and 28.)

A. M. Zhabotinsky. Bistability in the Ca(2+)/calmodulin-dependent protein kinase-phosphatase system. *Biophys J*, 79(5):2211–2221, 2000. (Cited on pages 6, 123, and 130.)

LIST OF FIGURES

LIST OF TABLES

LIST OF ACRONYMS

AMPA	α-amino-3-hydroxy-5-methyl-4-isoxazolepropionic acid
ATCase	aspartate transcarbamylase
C-terminal	carboxy-terminal
CaATPase	Ca^{2+}-ATPase
CaMKII	calcium/calmodulin-dependent protein kinase II
COPASI	Complex Pathway Simulator
Glu^{120}	glutamate residue 120
HFS	high frequency stimulation
KNF	Koshland-Némethy-Filmer
LTD	long-term depression
LTP	long-term potentiation
Met^{124}	methionine residue 124
mRNA	messenger RNA
MWC	Monod-Wyman-Changeux
N-terminal	amino-terminal
NMDA	*N*-methyl-D-aspartate
NR1	subunit 1 of the NMDA receptor
NR2B	subunit 2B of the NMDA receptor
Phe^{293}	phenylalanine residue 293
PhK5	phosphorylase kinase
PP1	protein phosphatase 1

PP2B ..... protein phosphatase 2B, also called calcineurin

PSD ..... postsynaptic density

R ..... relaxed

SBML ..... Systems Biology Markup Language

skMLCK ..... skeletal myosin light chain kinase

T ..... tense

T286A ..... threonine residue 286 to alanine

Thr^{253} ..... threonine residue 253

Thr^{286} ..... threonine residue 286

Thr^{306} ..... threonine residue 306

Colophon

This thesis was typeset with LaTeX 2ε on the basis of André Miede's style `classicthesis`, which is available for LaTeX via CTAN as "`classicthesis`".

Final version as of 17 July 2009